SECURITY CLASSIFICATION OF THIS PAGE

MENTATION PAGE

Form Approved
OMB No. 0704-0188

AD-A214 424

1b. RESTRICTIVE MARKINGS

2a. S

2b. DECLASSIFICATION/DOWNGRADING SCHEDULE

3 DISTRIBUTION/AVAILABILITY OF REPORT

Approved for public release,
distribution unlimited

4. PERFORMING ORGANIZATION REPORT NUMBER(S)

5. MONITORING ORGANIZATION REPORT NUMBER(S)

6a. NAME OF PERFORMING ORGANIZATION	6b. OFFICE SYMBOL (If applicable)	7a. NAME OF MONITORING ORGANIZATION
CARNEGIE MELLON UNIVERSITY	MEMS	

6c. ADDRESS (City, State, and ZIP Code)	7b. ADDRESS (City, State, and ZIP Code)
PITTSBURGH, PA 15213-3890	

8a. NAME OF FUNDING/SPONSORING ORGANIZATION	8b. OFFICE SYMBOL (If applicable)	9 PROCUREMENT INSTRUMENT IDENTIFICATION NUMBER
AFOSR	NE	AFOSR-84-0303

8c. ADDRESS (City, State, and ZIP Code)	10 SOURCE OF FUNDING NUMBERS			
	PROGRAM ELEMENT NO.	PROJECT NO.	TASK NO	WORK UNIT ACCESSION NO
BUILDING 410 BOLLING AFB DC 20332-6448	61102F	2306	A1	

11. TITLE (Include Security Classification)

(U)
FUNDAMENTAL STUDIES OF BETA PHASE DECOMPOSITION MODES IN TITANIUM ALLOYS

12. PERSONAL AUTHOR(S)

PROFESSOR HUBERT I. AARONSON

13a. TYPE OF REPORT	13b. TIME COVERED	14. DATE OF REPORT (Year, Month, Day)	15. PAGE COUNT
FINAL	FROM 01Oct88 TO 30Sep89	89 Oct 31	75

16. SUPPLEMENTARY NOTATION

17. COSATI CODES			18. SUBJECT TERMS (Continue on reverse if necessary and identify by block number)
FIELD	GROUP	SUB-GROUP	
11.06			Ti ALLOYS, PHASE TRANSFORMATIONS, BETA PHASE DECOMPOSITION

19. ABSTRACT (Continue on reverse if necessary and identify by block number)

AN EXPERIMENTAL INVESTIGATION OF THE INTERFACIAL STRUCTURE OF THE BROAD FACES OF WIDMANSTATTEN ALPHA PLATES AND OF GRAIN BOUNDARY ALPHA ALLOTRIOMORPHS FORMED IN A Ti-7.15 W/O (6.62 A/O) Cr ALLOY HAS BEEN COMPLETED. A SUPPORTING MODELING STUDY WAS ALSO MADE OF THE STRUCTURE OF THESE BCC:HCP INTERFACES, USING BOTH A COMPUTER MODELING TECHNIQUE AND THE BOLLMANN O-LATTICE METHOD. NO MISFIT DISLOCATIONS WERE FOUND AT ANY OF THE INTERFACES EXAMINED ON EITHER MORPHOLOGY. INSTEAD, c- OR (c+a)-TYPE MISFIT-COMPENSATING LEDGES OF VARIABLE HEIGHT ELIMINATED THE NEED FOR ONE SET OF MISFIT DISLOCATIONS; STRUCTURUAL LEDGES REMOVED THE REQUIREMENT FOR THE OTHER SET. THE FORMER LEDGES WERE READILY IMAGED WITH CONVENTIONAL TEM; THEY ARE STRAIGHT AND UNIFORMLY SPACED. DIRECT OBSERVATION OF STRUCTURAL LEDGES REQUIRED THE USE OF ATOMIC RESOLUTION TEM. HOT-STAGE TEM CONFIRMED THE MOBILITY OF GROWTH LEDGES AND THE IMMOBILITY OF c-TYPE LEDGES.

20 DISTRIBUTION/AVAILABILITY OF ABSTRACT	21 ABSTRACT SECURITY CLASSIFICATION
☒ UNCLASSIFIED/UNLIMITED ☐ SAME AS RPT ☐ DTIC USERS	UNCLASSIFIED

22a NAME OF RESPONSIBLE INDIVIDUAL	22b TELEPHONE (Include Area Code)	22c OFFICE SYMBOL
DR ALAN H. ROSENSTEIN	(202) 767-4933	NE

DD Form 1473, JUN 86 *Previous editions are obsolete.* SECURITY CLASSIFICATION OF THIS PAGE

Interim Technical Report

from

Department of Metallurgical Engineering
and Materials Science
Carnegie Mellon University

to

Air Force Office of Scientific Research
Electronic and Solid State Sciences
Bolling Air Force Base
Washington, DC 20332

on

Fundamental Studies of Beta Phase Decomposition Modes In Titanium Alloys

by

H. I. Aaronson, Principal Investigator
T. Furuhara, Graduate Student
Y. Mou, Graduate Student

for the period
1 October 1988 - 30 September 1989

31 October 1989

TABLE OF CONTENTS

Fundamental Studies of Beta Phase Decomposition Modes in Titanium Alloys

ABSTRACT

An experimental investigation of the interfacial structure of the broad faces of Widmanstatten alpha plates and of grain boundary alpha allotriomorphs formed in a Ti-7.15 W/O (6.62 A/O) Cr alloy has been completed. A supporting modeling study was also made of the structure of these bcc:hcp interfaces, using both a computer modeling technique and the Bollmann O-lattice method. No misfit dislocations were found at any of the α:β interfaces examined on either morphology. Instead, c- or (c+a)-type misfit-compensating ledges of variable height eliminated the need for one set of misfit dislocations; structural ledges removed the requirement for the other set. The former ledges were readily imaged with conventional TEM; they are straight and uniformly spaced. Direct observation of structural ledges required the use of atomic resolution TEM. The presence of structural ledges was usually accomplished upon the basis of indirect crystallographic evidence. Growth ledges appear to have formed through fortuitous local amalgamation of c- or (c+a)-type misfit-compensating ledges; they are characteristically high and irregular in both path and spacing. Hot-stage TEM confirmed the mobility of growth ledges and the immobility of c-type ledges. The inability of c- and (c+a)-type ledges to participate in growth arises from dislocation-like elastic interactions with adjacent parallel ledges of the same type. Migration of both misfit compensating ledges and structural ledges would require the highly improbable formation of equivalent densities and distributions of kinks on the risers of all ledges in a given array. Insofar as could be ascertained from the direct and indirect evidence gathered on the structure of α:β boundaries, good agreement obtained between the modeled and the observed structures--after account was taken of the replacement of one set of misfit dislocations be either c- or (c+a)-type misfit compensating ledges. A parallel study of the interfacial structure and the growth kinetics and mechanisms of massive:matrix boundaries is now making rapid progress. The (bcc) → (hcp) massive transformation of $\beta \rightarrow \xi_m$ in a Ag-26 A/O Al alloy is being used as a model transformation because, unlike its Ti-X counterparts, β matrix not transformed massively can be retained at room temperature (provided that a cold-stage is employed during TEM examination). All $\beta:\xi_m$ boundaries so far observed are partially coherent. As in the Ti-Cr alloy investigated, however, partial coherency between misfitting habit planes of the two crystal structures appears to be obtained through one.

and more likely two sets of misfit-compensating ledges rather than by equivalent arrays of misfit dislocations. Growth ledges, also similar to those seen at α:β boundaries in Ti-Cr, evidently are the source of the mobility of β:ξ_m boundaries. Back-calculation of inter-ledge spacing to height rations from the published data of Perepezko and Massalski on $\beta \rightarrow \xi_m$ growth kinetics in Ag-24.4 A/O Al yields results in approximate agreement with the ratios (15-20) experimentally observed during the present investigation.

1. INTRODUCTION

This program consists of inter-related fundamental studies on the crystallography, morphology and kinetics of the proeutectoid alpha and the massive alpha transformations in Ti-X alloys. Because that portion of the beta matrix which is not transformed to massive alpha is converted to martensite during quenching to room temperature in the Ti-X systems in which the $\beta \rightarrow \alpha_m$ reaction has been observed (1), however, the crystallographically equivalent massive transformation in a Ag-26 A/O Al alloy has been (2) and is currently being employed as a surrogate model massive transformation.

The experimental portions of the present program are centered about studies of interphase boundary structure. The interphase boundaries being examined are generated during the precipitation of grain boundary alpha allotriomorphs at beta grain faces in a Ti-7.15 W/O Cr alloy and during the $\beta \rightarrow \xi_m$ massive transformation in an Ag-26 A/O Al alloy. as well as during the formation of Widmanstatten α plates in the former material.

2. CRYSTALLOGRAPHY, INTERFACIAL STRUCTURE AND GROWTH KINETICS OF GRAIN BOUNDARY ALPHA ALLOTRIOMORPHS IN A Ti-7.15 W/O Cr ALLOY

2.1 Introduction

Studies of the nucleation kinetics of grain boundary allotriomorphs of proeutectoid ferrite during the proeutectoid ferrite reaction in Fe-C (3) and in Fe-C-X (4) alloys and during the proeutectoid alpha reaction in Ti-X alloys (5) have provided indirect but nonetheless rather convincing evidence that grain boundary allotriomorphs ought to be as coherent as possible during their nucleation stage (6). On the considerations of van der Merwe (7), during the early stages of growth, most coherent interfaces--unless the misfit across them is very small indeed

and/or mechanisms for acquisition of misfit dislocations are scarce or operating very slowly--should become partially coherent (6). This view contravenes earlier wisdom on grain boundary nucleated precipitates (8,9), according to which the allotriomorph:matrix interface is likely to be partially coherent with respect to only one of the matrix grains forming a grain face. A disordered structure was considered likely to form the interface between the allotriomorph and the adjacent matrix grain, since the orientation relationship between the allotriomorph and the latter grain was presumed to be irrational and thus incapable of supporting a partial coherent interfacial structure. However, measurements of the thickening kinetics of ferrite allotriomorphs in Fe-C alloys, wherein the collector/rejector plate mechanism (10) is unlikely to interfere, yielded rates somewhat less than those allowed by volume diffusion control (11), suggesting that partial coherency might reign on both broad faces of grain boundary allotriomorphs. Further, even though experimental observations indicate that ferrite allotriomorphs have a rational orientation relationship with respect to only one austenite grain, facets are readily observed on both the interface of the allotriomorph with this austenite grain as well as the interface with the austenite grain toward which the allotriomorphs are irrationally oriented (12). A similar observation was later made on grain boundary allotriomorphs of ξ_m formed during the $\beta \rightarrow \xi_m$ massive transformation in a Ag-26 A/O Al alloy (2,13). Hence the available indirect evidence on both nucleation and growth suggests that allotriomorphs are probably partially coherent with respect to both matrix grains forming grain faces. Except for a preliminary report of the present investigation (14), however, no direct evidence is available in the literature on the interfacial structure of grain boundary allotriomorphs. The present investigation was undertaken to fill this important gap in our knowledge and has served as a portion of the Ph.D. thesis of Dr. Tadashi Furuhara.

Although it might have been preferable to have conducted this investigation on the proeutectoid ferrite reaction, since this is by far the most widely known and studied reaction in solid metallic alloys, conversion of effectively all of the austenite untransformed during isothermal reaction to martensite during quenching to room temperature makes observation of the interphase boundary structure of ferrite allotriomorphs in hypoeutectoid steels impossible with room temperature techniques. (Use of hot-stage TEM could circumvent this problem, but the loss of resolution attending observations made at elevated temperatures would have even more serious consequences). On the other hand, in numerous hypoeutectoid Ti-X alloy

systems it is possible to retain all of the beta matrix upon quenching to room temperature, even in thin foils, once a critical composition is exceeded. We chose a hypoeutectoid Ti-7.15 W/O Cr alloy for the present study because we have used the same alloy in several previous investigations and have found it quite satisfactory for the purposes of the present study. Some very small precipitates of the transitional omega phase form in the beta matrix during quenching to room temperature, but they do not seriously interfere with TEM observations.

In our previous Interim Technical Report, we have shown that grain boundary alpha allotriomorphs in a Ti - 7.15 W/O Cr alloy have an exact or near-Burgers orientation relationship (13) with respect to one of its parent β grains but an irrational one with respect to the other beta grain (14). All of the Burgers-related interfaces examined were found to contain one or more sets of growth ledges as well as one set of what are originally thought to be structural ledges.* At the non-Burgers related interfaces, when the OR exhibits a relatively small deviation from the Burgers OR, both growth and the supposed structural ledges are again observed. Even when the deviation from the Burgers OR is large and ledge structures can no longer be observed with our Philips EM 420, planar facets are present, implying that a partially coherent interfacial structure exists at these interface as well. Curiously, no misfit dislocations were observed at either Burgers or non-Burgers α:β boundaries. During the present report period, emphasis was accordingly placed upon attempting to understand the observed ledge structures by a combination of TEM and modeling studies, and also why misfit dislocations were not seen. Additionally efforts were made to broaden our "data base" of interfacial structure observations by extending these studies to intragranular alpha plates in the same Ti-Cr alloy. This effort permitted interfacial structure studies to be made in a simpler crystallographic situation. One of the advantages provided by this simplification was that brief access gained to the JEOL 4000 EX electron microscope at Case Western Reserve University proved sufficient to yield atomic resolution TEM evidence for the existence of structural ledges at the interphase boundaries of these plates. Finally, a cooperative study with Dr. Masato Enomoto, at the National Research Institute for Metals in Tokyo (a former, NSF-supported graduate student of the P.I.), permitted re-analysis of experimental data on the growth kinetics of grain boundary alpha allotriomorphs in the present alloy, reported by Menon and Aaronson (5), in terms of the ledge mechanism.

---

*Structural ledges compensate misfit by causing areas of good matching to repeat on their terraces and thereby markedly raise the average level of coherency at the interfaces (15). Although there is dispute about the mobility of these ledges, it seems unlikely at this time that their risers are able to migrate to a significant extent (16).

Dr. Furuhara defended his Ph.D. thesis with much success on September 26, 1989, before a committee consisting of Professors Subhash Mahajan and James Howe of CMU and Professor George Weatherly of the University of Toronto. The papers derived from this thesis are now being prepared for publication. Hence, after a brief recounting of the experimental procedures utilized, the three major components of his thesis, plus the joint work with Dr. Enomoto, will be summarized with the aim of emphasizing the most important additions to our understanding of interphase boundary structure.

2.2. Experimental Procedures

The Ti-7.15 W/O Cr alloy was obtained from Titanium Metals Corporation of America, Henderson, NV. It was homogenized for 3 days at 1000°C. The homogenized alloy was then hot rolled by TIMET and the product was given the same homogenization treatment. It was immediately recognized that the coarse beta grain size characteristic of this alloy (and most other Ti-X alloys capable of being converted 100% to the beta phase) would make a TEM study of grain boundary alpha allotriomorphs infeasible. Dr. Donald Kroger of the Oak Ridge National Laboratory solved this problem for us by rapidly solidifying small portions of the homogenized alloy by means of the hammer and anvil technique. This yielded a beta grain size a few tens of microns in diameter and ensured that most thin areas, prepared for TEM, would contain portions of at least a few beta grain boundaries. Specimens cut from the rapidly quenched material were wrapped in Ta foil and encapsulated in Vycor under a vacuum $<10^{-5}$ torr. They were transformed by upquenching directly to the intended isothermal reaction temperature. During this process, the omega phase precipitates must have dissolved prior to allotriomorph nucleation and growth, since it is a long familiar observation that in the presence of omega the alpna phase nucleates preferentially at omega:beta interfaces, yielding an ultra-fine dispersion of minute alpha crystals. TEM specimens were prepared by means of ion milling, since electropolishing has been convincingly shown to produce the "interface phase" (17), which grows allotriomorphically along alpha:beta boundaries and hence would entirely prevent this investigation from being conducted. The orientation relationships between alpha allotriomorphs and their bounding beta grains were determined by analyzing the Kikuchi pattern obtained from each phase. At least two different tilting conditions were used for a given phase. The error associated with this procedure was less than 1°.

2.3. Results and Discussion of Modeling Studies on the Structure of Partially Coherent bcc:hcp Interfaces

Both the computer-based graphical technique originally employed by Rigsbee and Aaronson (18) for fcc:bcc interfaces and the Bollmann (19) O-lattice method were used to determine the structure of partially coherent bcc:hcp boundaries. These analyses were conducted on several pairs of parallel planes in the two lattices for the three different orientation relationships described in Table I. Additionally, small co-planar rotations away from these orientation relationships were introduced as well as variations in the ratios of the lattice parameters of the hcp to the bcc phases. However, base values of these ratios were chosen so as to correspond to those appropriate to a Ti-7.15 W/O Cr alloy reacted within the temperature range experimentally employed.

Consider first the interfacial structures predicted for planar interfaces by the computer graphical method. Figs. 1a-d show the structure of the $(0001)_\alpha // (0\bar{1}1)_\beta$ interface at four rotations about $[0001]_\alpha$ of one plane relative to the other, from $\Theta = 0°$, the Burgers relationship, to $\Theta = 5.26°$, the Pitsch-Schrader relationship, where Θ is the angle through which the $[11\bar{2}0]_\alpha$ direction was rotated counter-clockwise from the $[111]_\beta$ direction. As Θ increases, the coherent patches become more elongated in shape and larger in size but the proportion of the interface which is coherent is little changed. Two sets of misfit dislocations are seen to be predicted at these interfaces. O-lattice analysis placed O-points, i.e., the points of optimum matching between the two interfacial planes at the boundary, at the center of each coherent patch, and yielded identical misfit dislocation structures. This result, and analogous results on other interfaces, further supports the correctness of the graphical technique, as previously demonstrated by Hall et al (22) for fcc:bcc interfaces.

O-lattice analysis shows that the misfit dislocations in both sets in Fig. 1 are of a-type and are of mixed edge and screw character. An equivalent study of $(1\bar{1}00)_\alpha // (2\bar{1}\bar{1}0)_\beta$ interfaces yielded one set of $\underline{a}/3[11\bar{2}0]_\alpha$ dislocations and one set of $\underline{c}[0001]_\alpha$ dislocations. At the Burgers relationship, both are pure edges. When $\Theta \neq 0°$, each set of dislocations becomes more closely spaced and develops a mixed character.

When interfacial structures associated with two other pairs of conjugate habit planes,

$(1\bar{1}01)_\alpha//(1\bar{1}0)_\beta$ and $(0\bar{1}10)_\alpha//(011)_\beta$, were investigated, the graphical technique yielded additional coherent areas of the boundary which could not be predicted from O-lattice analysis. This difference arose because the atoms located half-way "up" the c-axis in the hcp unit cell could not be included in the O-lattice analyses when the procedure of previous investigations (2,19,22) was followed. Figs. 2a and b show the graphically determined interfacial structures produced by these planes for $\Theta = 0°$ (the Potter orientation relationship) and $\Theta = 1°$ and $-1°$. Fig. 3 shows the structure of two of these interfaces as evaluated through O-lattice calculations. Comparison of Figs. 2 and 3 demonstrates that an extra coherent patch is present in the graphically constructed interfaces midway between the O-point at the origin and its neighboring O-point related to that at the origin by the Burgers vector described as $\underline{b}_2$ in Fig. 3, i.e., $\underline{a}/3[\bar{2}113]_\alpha$. Hence, the actual Burgers vector for misfit dislocations lying between these patches should be $a/6[\bar{2}113]_\alpha$. This is nearly equal to the Burgers vector of a perfect dislocation in the bcc lattice, i.e., $\underline{a}/2[111]_\beta$.

Interfacial structures for two other pairs of parallel planes, $(11\bar{2}0)_\alpha//(111)_\beta$ and $(2\bar{1}1\ 0)_\alpha//(100)_\beta$, were also analyzed. However, interfacial coherency was found to be limited to good directional matching, leading to the conclusion that these habit planes are unlikely to form a partially coherent structure.

Variations in lattice parameter ratio and of the lattice orientation relationship, the latter by small co-planar rotations, did not produce significant changes in the proportion of coherent areas, even though the size, shape and spatial distribution of these areas was shown to change continuously. The individual identities of the coherent patches were retained throughout these manipulations. Also, a more restrictive definition of what constitutes coherency was shown to introduce no fundamental changes in the results obtained, as was previously demonstrated for fcc:bcc interfaces (15).

These interfaces were then re-examined when structural ledges of monatomic and greater height were introduced in order to ascertain whether or not an increase was secured in the proportion of coherent interfacial area. No such increase obtained when monatomic ledges were incorporated in $(0001)_\alpha//(0\bar{1}1)_\beta$ interfaces because both the hcp and the bcc lattices have an ABAB-type stacking sequence normal to this interface. In the fcc:bcc case, parallel close

packed planes, i.e., $(111)_{fcc}//(110)_{bcc}$, have an ABCABC-sequence on the fcc side and an A'B'A'B'-sequence on the bcc side of the interface, thereby permitting structural ledges to change (and in this instance to improve) the level of coherency on the terraces of the structural ledges (15, 18). At $(1\bar{1}00)_\alpha//(2\bar{1}\bar{1}0)_\beta$ interfaces, however, while there is again an ABAB-sequence normal to the interface on both sides of the boundary, $d_{1\bar{1}00_\alpha}$ is nearly equal to $2d_{2\bar{1}\bar{1}_\beta}$, resulting in a different effective stacking sequence on opposite sides of the boundary. Hence Fig. 4a, showing the interfacial structure resulting from the introduction of biatomic structural ledges, exhibits 13.5% coherency whereas at planar $(1\bar{1}00)_\alpha//(2\bar{1}\bar{1}0)_\beta$ interfaces (Fig. 5a), only 5% coherency obtains. At the structurally ledged interface, there is a more frequent recurrence of coherent patches along the $[11\bar{2}0]_\alpha//[111]_\beta$ direction, with a regular spacing of only about 1 nm. Comparison of Figs. 4a and 5a shows that one set of misfit dislocations, whose Burgers vector is $\underline{a}/2[11\bar{2}0]_\alpha$, is eliminated by the structural ledges; only one set of misfit dislocations, of $\underline{b} = \underline{c}[0001]_\alpha$, spaced 22.3 nm. apart, is now required. Figs. 4b and 4c show that structural ledges 4 and 6 atomic planes high successfully compensate misfit in the same direction as the biatomic ledges, while the spacing between the c-type misfit dislocations remains the same.

Rotation of the terrace planes with respect to one another through the angle Θ changes the spacings between the structural ledges and c-type misfit dislocations as well as the directions of both sets of defects, while maintaining the regular repetition of coherent patches and the elimination of a-type dislocations. Figs. 6a and b show the variation in the spacings of parallel biatomic structural ledges and of misfit dislocations, respectively, as a function of Θ. Fig. 7 shows how the apparent habit plane of structurally ledges interfaces varies with Θ, together with the directions of structural ledge risers and of c-type misfit dislocations. The apparent habit plane is seen to rotate toward the $(0001)_\alpha$ pole as Θ becomes larger.

Structural ledges were also found to increase the pct. coherency for $(1\bar{1}01)_\alpha//(1\bar{1}\bar{1}0)_\beta$ terrace planes when the Potter orientation relationship (Table I) is operative, with $\underline{b} = \underline{a}/3[11\bar{2}0]_\alpha$ misfit dislocations being eliminated. An interledge spacing of 0.40 nm and a riser height of 0.23 nm were also predicted. However $(0\bar{1}10)_\alpha//(011)_\beta$ interfaces show no repetition of coherent patches in the presence of monatomic structural ledges, making unlikely the presence of such ledges at this interface.

The ability of structural ledges to eliminate a set of misfit dislocations must mean that they

have a Burgers vector parallel to their terrace plane. Fig. 8 is a $(0001)_\alpha$ projection of a bcc:hcp interface containing a biatomic structural ledge when the terrace planes are $(1\bar{1}00)_\alpha//(2\bar{1}\bar{1}0)_\beta$ and a Burgers orientation relationship obtains. This structural ledge is seen to have a $\underline{b} = \underline{a}/12[111]_\beta$, equivalent to $\underline{a}/18[11\bar{2}0]_\alpha$, parallel to the terrace plane. Shockley partial dislocations at $(111)_{fcc}//(0001)_{hcp}$ interfaces also have their Burgers vector parallel to these (terrace) planes, and serve as both misfit dislocations and growth ledges. However, structural ledges become such an integral part of a partially coherent interphase boundary that the flexibility in their arrangement is much more restricted than is that of Shockley partials at fcc:hcp interfaces. The spacing and direction of structural ledges must thus be maintained approximately constant. Hence structural ledges must migrate laterally in essentially synchronous fashion. However, since the risers of structural ledges are partially coherent, they can only be displaced by kinks on their risers (16). Hence parallel structural ledges must have approximately the same kink density and distribution. This is unlikely. Thus one predicts that structural ledges should be essentially immobile (16,25). This prediction has been experimentally confirmed for structural ledges on fcc:bcc interfaces (16,26).

Fig. 9 summarizes the results of the present study in pictorial fashion, showing that a structurally ledged interface requires only one set of parallel misfit dislocations instead of the usual two sets. This interfacial structure is equivalent to that previously sketched (18,27) and then experimentally demonstrated (28) for fcc:bcc interfaces.

2.4. Results and Discussion of Interfacial Structure Studies on Intragranular Alpha Plates

Previous studies on the structure of the broad faces of hcp plates precipitated from a bcc matrix consist of the observations of Weatherly and co-workers (29,30) on hcp alpha plates precipitated from bcc beta Zr-Nb alloys and of Menon and Aaronson (31) on hcp alpha plates precipitated from the present bcc beta Ti-Cr alloy. There are several conflicts between these two sets of results and also among these results and those of the present study. The underlying reason for these differences is probably that the resolution of the electron microscopes previously used was insufficient to resolve the principal features of the interfacial structures present. In particular, Weatherly and co-workers described as misfit dislocations linear defects at their plate broad faces which are probably ledges 1-2 nm. high.

Confirming the preliminary results described in last year's Interim Technical Report to AFOSR, no misfit dislocations were observed on any Widmanstatten alpha plates (or grain boundary alpha allotriomorphs) examined. Instead, three different types of defect were observed. In descending order of riser height, these were:

(i) growth ledges
(ii) c-type, essentially immobile, misfit-compensating ledges
(iii) structural ledges

It turns out to be simplest to describe these results by beginning with c-type ledges. On "normal alpha" plates--irregularly formed and relatively thick plates to whose lengthening edge-to-edge sympathetic nucleation (32,33) extensively contributes (34,35)--the spacing between parallel c-type ledges is typically 12 nm. and the height of these ledges is 6 nm. On "black" alpha plates--well formed, thin, more rapidly lengthening plates (31,34)--c-type ledges are usually 10-13 nm. apart, though in some instances a spacing of c. 23 nm. was observed. Analysis with the g·b technique demonstrated that the Burgers vector of these ledges lies parallel to their terraces, rather than normal to them as is customarily the case (36). Usually, $\underline{b} = \underline{c}/2[0001]_\alpha$, but in some instances $\underline{b} = \underline{c}[0001]_\alpha$.

The arrows in the micrograph of Fig. 10 point out three c-type ledges. The SAD pattern indicates that the electron beam is parallel to $[0001]_\alpha // [0\bar{1}1]_\beta$. However, on the basis of this information, the sketch in this Figure shows that the ledge terrace is approximately 16° away from the expected terrace habit planes, $(1\bar{1}00)_\alpha // (2\bar{1}\bar{1}0)_\beta$. This angle, on the other hand, is less than 2° from the apparent habit plane for this interface assuming that the interface is structurally ledged. Similarly, the spacing between c-type ledges is in good agreement with the inter-dislocation spacing expected for the one set of misfit dislocations predicted on structurally ledged interfaces in the modeling study summarized in section 2.3 of this Report.

Structural ledges predicted on the interphase boundary in Fig. 10 cannot be observed with conventional TEM because their spacing is only c. 1.0 nm. and their height is c. 0.25 nm. Hence, high-resolution TEM was performed with a JEOL 4000EX microscope. Fig. 11 shows an edge-on view of the columns of atoms comprising the atomic structure of structural ledges. The hexagonal arrangement of columns of atoms cut by a $(0001)_\alpha$ plane can be resolved within the α phase, but only $(011)_\beta$ fringes are fully resolved in the β phase. Along the interface, atomic steps, whose height, equal to $d_{1\bar{1}00}$ (c. 0.25 nm), can be seen to have a very uniform

spacing of c. 1 nm. The atomic habit plane of the terrace is $(\bar{1}100)_\alpha // (\bar{2}11)_\beta$. These characteristics fit almost perfectly those of the structural ledges described in Fig. 4a. It is of particular interest to note that one-to-one matching of atoms obtains across the interface outlined with white lines; evidently this interface is fully coherent. However, elastic strains can be discerned in association with the structural ledges. Evaluation of the average misfit strain per ledge from measurements on atomic resolution micrographs confirms the prediction of the modeling study that this vector is approximately $\underline{a}/18[11\bar{2}0]_\alpha = \underline{a}/12[111]_\beta$, again in agreement with the modeling result (Fig. 8).

Fig. 12 is an isometric sketch showing schematically how structural ledges and c-type ledges coexist. Recall that structural ledges compensate misfit by reducing it through more frequent repetition of coherent areas whereas c-type ledges compensate misfit in just the style of misfit dislocations, i.e., by means of extra half-planes perpendicular to $(0001)_\alpha$.

Fig. 13 shows c-type ledges (one of which is indicated by a pair of thin, parallel arrows) and growth ledges--appearing as dark, wiggly lines, irregularly spaced, on this micrograph and pointed out by heavy single arrows. Presumably kinks in the risers of these ledges account for their highly variable paths and permit the risers to form a marked angle with respect to those of the uniformly spaced c-type ledges. Growth ledges are also significantly higher than c-type ledges. Since growth ledges apparently have the same habit plane as c-type ledges, the irregular risers are essential to the mobility of growth ledges.

Hot-stage TEM experiments were performed in order to test the deduction that c-type ledges are immobile whereas growth ledges can migrate readily. (The resolution available in such experiments is insufficient to permit direct observation of structural ledges.) A Ti foil was attached to the Ti-Cr thin foils in order to getter oxygen and nitrogen in the microscope atmosphere. The irregularly spaced ledges with a larger height were indeed mobile, through the kink-on-ledge mechanism (37) whereas the uniformly spaced c-type ledges exhibited only small wiggles. However, it was unfortunately not feasible to secure satisfactory micrographs documenting these statements.

Immobility of c-type ledges may be ascribed to the dislocation-like elastic interactions

between adjacent ledges. Unless all ledges in a parallel array move simultaneously as a consequence of highly improbable equivalent densities and distributions of kinks in their risers, these elastic interactions should quickly overcome the chemical driving force for growth and prevent any more movement other than that required to remove accidentally introducted irregularities in their paths.

One may suggest, however, that under occasional unusual circumstances adjacent c-type ledges may be able to grow into contact with one another. Doubling the height of one ledge and eliminating the other should reduce the ability of elastic interactions with their neighbors to restore equal spacings between adjacent ledges. The irregularities in the path of the doubled c-type ledge arising from the growth-together process should provide additional local mobility and thus shorten the time required for tripling of this ledge. The relatively large and unequal distances between adjacent growth ledges thus generated should minimize elastic interaction between them and ought thus to permit these ledges to migrate laterally as long as they have an adequate density of kinks.

It should finally be noted that the interfacial structure of the broad faces of alpha plates in our Ti-Cr alloy is of sessile character. Hence thickening of these plates by a shear mechanism should be mechanistically infeasible. This is consistent with the finding that c. 80% of monocrystalline alpha plates in the present alloy exhibit a tent-shaped rather than a martensitic invariant plane strain surface relief effect (38). Lengthening kinetics of alpha plates are essentially those permitted by volume diffusion-control (39). And recently, Enomoto and Fujita (40) have shown that the composition of alpha plates closely approximates their equilibrium composition from the earliest stage of thickening at which analytical electron microscopy can successfully accomplish such measurements. Hence the Ti-Cr system has become a good model system upon which to test views on the controversy about shear vs. the ledgewise diffusional mechanisms of precipitate growth.

2.5 Results and Discussion of Interfacial Structure Studies on Grain Boundary Alpha Allotriomorphs

Orientation relationship data with respect to both beta grains were acquired for 40 grain boundary alpha allotriomorphs nucleated at beta grain faces. Fig. 14 shows the results obtained for the alpha allotriomorphs which were nearly Burgers-related with respect to a beta

grain; these beta grains are designated as β_B. Beta grains to which allotriomorphs were non-Burgers oriented are designated β_N. Fig. 15 presents the orientation relationships for allotriomorphs with respect to their β_N grains. Dots near the $(0001)_\alpha$ pole in these two Figures represent the $(011)_\beta$ planes nearest to the $(0001)_\alpha$ plane while dotes near the $(11\bar{2}0)_\alpha$ pole represents the $<111>_\beta$ directions nearest to the $<11\bar{2}0>_\alpha$ direction. Alpha allotriomorphs are seen to have orientation relationships with a scatter of less than c. 5° from parallelisms of the close packed directions and planes given by a Burgers relationship. On the other hand, the deviations of the relationships of the allotriomorphs with respect to their β_N grains are larger than 25° in both close packed planes and directions; these relationships appear, in fact, to be nearly random. These findings are in essential agreement with those of previous investigations performed on a wide range of alloy systems (41-49).

As in the case of Widmanstatten alpha plates in the present alloy, both growth ledges and misfit-compensating ledges were found. Because of deviations from exact Burgers orientation relationships and the extreme sensitivity of atomic resolution TEM to precise alignment with a low index direction in the interface, no high resolution TEM experiments were performed on alpha allotriomorphs. Hence evidence for structural ledges on their interfaces could only be secured by indirect means.

Fig. 16 is a set of TEM micrographs of the same area of a β_B interface, taken with different diffraction vectors, showing both growth ledges (thick, wiggly dark lines whose spacing changes with boundary orientation) and c-type misfit-compensating ledges (narrower, straight, closely and uniformly spaced lines). The c-type ledges are here spaced only 5 nm. apart. Fig. 17 is a similar set of micrographs of another β_B interphase boundary, which demonstrates that these misfit-compensating ledges are of c+a type, i.e., $\underline{a}/3[\bar{1}2\bar{1}3]_\alpha$. Their height is c. 40 nm and inter-ledge spacing is c. 60 nm. These ledges are formed by the agglomeration of 6 or 7 individual ledges--each of which now exhibits somewhat different contrast behavior. Note the hexagonal arrays of ledges visible in Fig. 17a especially; this behavior is similar to that often displayed by misfit dislocations. Finally, Fig. 18 shows occasional growth ledges and uniformly spaced (c. 12 nm.) c-type misfit-compensating ledges. The direction of these ledges is almost identical to that of the c-type misfit dislocations at the Burgers related interface with structural ledges and $(1\bar{1}00)_\alpha//(2\bar{1}\bar{1}0)_\beta$ terraces modeled in Fig. 9. The experimentally determined apparent habit plane

is less than 2° from the apparent habit plane of the structure shown in Fig. 9. This is good indirect evidence for the presence of structural ledges at the interface shown in Fig. 18.

An example was found of an allotriomorph with a near-Potter instead of a near-Burgers orientation relationship. In this case, misfit compensating ledges were only 2 nm. apart and were of the (c+a)-type.

As to interfaces with β_N grains, Fig. 19 shows (c+a) misfit-compensating ledges, i.e., with $\underline{b} = \underline{a}/3[1\bar{2}13]_\alpha$ at one such boundary, again viewed with various reflections. Fig. 19h displays kinks in the risers of these ledges. Yet another set of ledges, on too fine a scale to be identified, can be discerned in Figs. 19f, g and h. At other β_N interfaces, c-type ledges were observed. When the angles between close packed planes and close packed directions of the alpha allotriomorph and the β_N grain deviate by more than c. 15° from those applicable at the Burgers orientation relationship, ledge structures were no longer visible. However, Fig. 20 shows that even in the absence of clearly defined ledges, a planar facet can still develop when close packed planes are rotated 26° apart and close packed directions are 23° apart. Hence a barrier to growth must also have been present at this interface in the form of a partially coherent structure. Presumably misfit-compensating ledges are again involved, but in this situation are spaced too close to one another to be resolved with conventional TEM.

Clearly, the results of this investigation have provided strong support for the deduction made from nucleation theory as to the type of interfacial structure associated with allotriomorphs (3,6). However, the details of this structure were in part unexpected. The finding of misfit-compensating ledges which play no role in growth, i.e., the c-type and the (c+a)-type ledges, is both new (for any alloy system) and unexpected. As will be discussed in more detail in an overview paper on the role of ledges in diffusional phase transformations now in preparation, a number of categories of both ledges and misfit dislocations have now been recognized which do not fit into the original "extremum" categories of pure growth ledges (playing no role in misfit compensation) and pure misfit dislocations (which have no role to play in respect of growth). The present investigation, through the discovery of c- and (c+a)-type ledges, has added another intermediate category to this still developing generic classification system.

2.6 Results and Discussion of Analysis of Growth Kinetics of Grain Boundary

Alpha Allotriomorphs by the Ledge Mechanism

This investigation was performed in collaboration with Dr. Masato Enomoto of the National Research Institute of Metals in Tokyo, Japan. Graduate Student Tadashi Furuhara provided the data used on growth ledge configurations, ledge heights and inter-ledge spacings, together with the recognition that the involvement of two systems of growth ledges on the broad faces of some allotriomorphs required the development of a more advanced analysis of ledgewise growth. Dr. Enomoto had previously published a sophisticated, and now widely recognized and approved, computerized finite difference model for the growth kinetics of single sets of straight, parallel ledges arrayed in trains of both infinite (50) and finite (51) length. Because of the extreme complexity of the diffusion field associated with the growth of even a single, diffusionally isolated ledge (52,53) and the much greater intricacy of the diffusion field geometry when the diffusion fields of adjacent, straight, parallel ledges overlap (54,55), there is increasing evidence that analytic solutions to ledgewise growth problems are difficult to the point of becoming self-defeating (56). At the recent symposium on "The Role of Ledges in Phase Transformations", in which nearly all of the Western theoreticians who are or have been involved in analytical studies of ledgewise growth participated, including Profs. Rohit Trivedi (Iowa State), Colin Atkinson (Imperial College), John Hirth (Washington State) and William Mullins (Carnegie Mellon), Dr. Enomoto's finite difference analysis appeared to receive the most attention and deference from all of the other theoretical "players".

Although the finding of multiple growth ledges on allotriomorphs, reported in a short paper in Scripta Metallurgica (57) and in a previous Interim Report, was the immediate factor shaping Dr. Enomoto's current computer analysis, another circumstance underlay this investigation. In research previously supported by the present Grant, Menon and Aaronson measured the thickening kinetics of grain boundary alpha allotriomorphs in the present Ti-Cr alloy. They found that these kinetics are moderately more rapid than those predicted by direct volume diffusion-control of growth. They therefore proposed that the growth of allotriomorphs is accelerated by the "rejector plate" mechanism (10). On this mechanism, Cr being rejected from the allotriomorphs diffuses along the supposedly disordered broad faces of the allotriomorphs into the surrounding grain boundary. Final disposition of the rejected solute takes place by volume diffusion into the untransformed beta matrix normal to the surrounding grain boundary.

Because the area of grain boundary from which solute is rejected is about an order of magnitude or more larger than the area of interphase boundary available, despite the indirect and longer transport route now required, the kinetics with which solute is dispersed into the surrounding matrix can be much increased provided that the product of the interphase boundary diffusivity and the thickness of the interphase boundary is much greater than the product of the volume diffusivity and the length of an allotriomorph broad face. When the crystal structure of the matrix phase is fcc, the kinetic advantage conferred by the rejector plate mechanism, and its solute-rich precipitate counterpart, the collector plate mechanism, is very large indeed. Below c. $0.9T_m$, this mechanism tends to dominate both growth (58) and dissolution (59,60) of grain boundary allotriomorphs in substitutional alloys. In view of the lower ratio of grain boundary to volume diffusivities at a given homologous temperature in bcc substitutional alloys (61), however, the suggestion has been made that the rejector/collector plate mechanism will be a considerably less prominent contributor to growth when the matrix has a bcc structure (58). The findings of Menon and Aaronson (5) on alpha allotriomorph thickening kinetics in the present Ti-Cr alloy appeared to confirm this prediction.

However, as soon as the presence of partial coherency on both broad faces of alpha allotriomorphs in this alloy was recognized, the following possibility was considered. Experimental studies have shown that during the early stages of plate thickening the overall kinetics are sometimes more rapid than those calculated assuming that the broad faces are formed by planar, disordered boundaries (37). This finding was originally rationalized through application of the Jones-Trivedi (52) analysis of the growth kinetics of diffusionally isolated ledges (62). Christian (63) has disputed this rationalization on the ground that the Jones-Trivedi analysis does not take account of the prior passage of growth ledges across a given fiducial line and the resultant diminution in driving force for subsequent ledgewise growth. However, Enomoto (50) used his finite difference method to re-examine the problem, taking account of "prior passage" and concluded that, before extensive diffusional interaction amongst adjacent ledges occurs, a densely ledged boundary can indeed grow initially more rapidly than a planar disordered one provided that the diffusion distance associated with each ledge is short. Hence we were led to worry that ledgewise thickening, particularly by double sets of growth ledges, of alpha allotriomorphs might also have led to faster than disordered boundary thickening of allotriomorphs even though effectively all mass transport might be taking place by volume

diffusion. We accordingly asked Dr. Enomoto to develop his finite element program still further in order to study the thickening kinetics of alpha allotriomorphs via volume diffusion when two sets of growth ledges are operative. He presented the resulting paper whose results are now summarized at the symposium on "The Role of Ledges in Phase Transformations".

Enomoto assumed that two sets of growth ledges were oriented orthogonal to one another. The inter-ledge spacing in each set was taken as a variable; the heights of the ledges in the two sets were assumed to be the same. The DuFort-Frankel (64) finite difference equation for the diffusion field associated with each grid point and growth time was then derived. The solute concentration in the matrix in contact with the bottom of each riser was again taken to be a constant; supersaturation at successively higher points on the risers was then reduced sufficiently to ensure that each ledge migrated laterally at a uniform rate. Fig. 21 shows the variation of the (laterial) velocity of two orthogonal sets of ledges whose inter-ledge spacing to ledge height ratio is the same, i.e., $(\lambda/h)_X = (\lambda/h)_Y = 10$, curve 2, with reduced time, $T = Dt/h^2$, where D = diffusivity in the matrix phase, t = growth time and h = riser height. This result is compared with the velocity vs. reduced time curve for a single set of ledges when $\lambda/h = 10$ (Curve 1) and when $\lambda/h = 5$ (Curve 3), respectively. Thus the variation of velocity with time for a double set of ledges is seen to be little different than that for a single set of ledges with half the inter-ledge spacing. The result that velocity at a given reduced time diminishes with decreasing λ/h must be due to overlapping of diffusion fields. In support of this deduction, note that as reduced time approaches zero, the lateral velocity of all three ledge configurations approaches a constant value.

Fig 22 shows how ledge velocity varies with reduced time for a double set of ledges in which λ/h in the X-direction is 50 but is only 10 in the Y-direction. These results are compared with those for single sets of ledges with the same values of λ/h. Contrary to initial expectation, the velocity of the more widely spaced set of ledges is seen to be reduced much more, relative to a single set of ledges, than is that of the more closely spaced ledges. This difference may be ascribed to a more severe effect of diffusion field overlap associated with the closely spaced ledges upon the growth kinetics of the more widely spaced ledges than vice versa. Fig. 23 shows that when λ/h is kept constant for the more widely spaced ledges but is reduced in successive steps for the more closely spaced ledges, the ratio of the velocity of the widely

spaced to the closely spaced ledges increases more with reduced time the closer together are the latter ledges.

The overall growth rate of a ledged interface at a particular growth time is given by the sum of the growth rates associated with the two individual sets of ledges. Fig. 24 compares the total growth rate, G_1, with the two individual growth rates, G_X and G_Y, and the growth rate of a planar, disordered boundary, G_d, all as a function of reduced time at the same supersaturation, Ω for the same configuration of ledges as was used to construct Fig. 22. It is immediately seen that G_X is much smaller than G_Y at all T, and that G_1 is largely determined by G_Y, i.e., by the set of ledges with the smaller λ/h. The dashed curve in Fig. 24 applies to a single set of ledges with $\lambda/h = 50$. Note that this curve is approaching G_d with increasing time; Enomoto (50,51) has repeatedly found this to be the case for single sets of parallel ledges. In the presence of two sets of ledges, however, the contribution to G_1 of the more widely spaced ledges is much decreased by diffusional interaction with the more closely spaced ledges, even at very long reduced times. Further, it was shown in another investigation, by Enomoto and Aaronson (65), that when $\lambda/h = 50$, a constant growth rate is achieved when T = c. 20 - 100. However, no such regime occurs for either set of ledges or for both combined in the two-sets-of-ledges situation; G_X (for $\lambda/h = 50$) is seen to decrease monotonically with time.

Consideration was also given to the problems of non-orthogonal sets of ledges and to situations in which the height of one set differs from that of the other. Although calculations were not performed to test mathematically either of these cases, qualitative reasoning was employed to show that neither is likely to affect importantly the conclusions drawn from the orthogonal, equal-height pairs of arrays. In the non-orthogonality situation, the more extensive overlap of diffusion fields in the matrix region where the angle between ledges is less than 90° ought to be compensated by the less extensive overlap at the other two more-than-90° apecies of the parallelograms formed by intersecting non-orthogonal arrays of ledges. While smaller ledges should grow more rapidly, their contribution to the overall growth rate of the ledged interface in the direction normal to the terraces should be proportionately diminished, thereby leaving only differential overlap in diffusion fields as a possible source of incomplete compensation of the difference in height of two sets of ledges.

Table II shows the data from the experimental studies on the interfacial structure of grain

boundary alpha allotriomorphs in our Ti-Cr alloy provided to the analytical effort on the growth of these precipitates by the ledge mechanism. Fig. 25 plots allotriomorph half-thickness in this alloy as a function of the logarithm of the isothermal reaction time at 715°C. The "Menon and Aaronson" curve is the trend line obtained from the experimental data plot at this temperature. The curves denoted by "p" and "e" are respectively those calculated for a planar, disordered boundary and an ellipsoidal, disordered boundary at this reaction temperature and for the alloy composition employed. As a reasonable approximation to the experimental data, two sets of growth ledges were assumed to make a 90° angle with respect to one another and to have λ/h ratios of 50 and 10, respectively. Curves 1 and 2 in this Figure were calculated for single ledge systems with ratios of 50 and 10, respectively. The curve lying above "1" was computed for the two sets of growth ledges. The thickening kinetics produced by either set of single ledges or by two sets of ledges simultaneously are seen to approximate those of a planar, disordered boundary considerably more closely than those of an ellipsoid with the experimentally observed aspect ratio. Hence the conclusion of Menon and Aaronson (5) that the rejector plate mechanism is moderately accerating the thickening of grain boundary alpha allotriomorphs in our Ti-Cr alloy is seen to be reenforced by Enomoto's new ledge growth kinetics calculations.

3. MASSIVE TRANSFORMATION IN A Ag-26 A/O Al ALLOY

3.1 Introduction

This is the Ph.D. thesis research of Mr. Yiwen Mou. As noted in the Introduction section of this Report, its objectives are to ascertain whether or not massive:matrix boundaries are partially coherent, as we predicted more than 20 years ago from elementary considerations of nucleation theory (66), and to correlate the growth kinetics reported by Perepezko and Massalski (67) in an alloy with nearly the same composition with those predicted by the experimentally observed interfacial structure. TEM is the principal experimental tool being employed in this investigation.

3.2 Alloy Preparation

An ingot of Ag-24.4 A/O Al was prepared for us by the ALCOA Research Laboratories in ALCOA Center, PA. However, this alloy proved to be too brittle to roll, quite possibly because of rapid formation of the μ_m phase. The ingot was then remelted as a Ag-26 A/O Al alloy,

comparable to the one previously employed. Little difficulty was now encountered in rolling sheets of alloy 0.3 mm. thick. We would have preferred the 24.4 A/O Al composition because this one is exactly the congruent composition in this system and thus there could be no complaints about part of the transformation with the bcc + hcp region; however, this proved impractical and we do not think that such complaints will be serious.

3.3 Heat Treatment of Specimens

In order to obtain samples suitable for TEM observation of interphase boundary structure produced by the massive transformation, we must have both massive crystals and retained β matrix in the samples, and also ensure that the two phases have appropriate proportions and distributions. An ideal microstructure would be many very small massive crystals formed on grain boundaries within a retained β matrix. Due to the very fast kinetics of massive transformations, however, microstructures of this type are difficult to secure. Another problem arises from the very large β grain size due to the great proclivity for grain growth in the Ag-26 A/O Al alloy. This situation further complicates TEM sample preparation; in most samples we cannot find any grain boundaries within the thin areas.

We tried many different ways to heat treat specimens prepared by the ALCOA Research Laboratory. We found that quenching rate played an important role in determining the microstructure of this alloy. With faster quenching rates, the transformation favored is changed from equilibrium ξ precipitation to massive ξ_m and finally to martensite. The quenching rate depends upon both the quenching medium and the specimen thickness. With many combinations of these two factors we always obtained big massive crystals, sometimes connected with each other along the grain boundaries as networks; in some samples, no retained β was observed. When very thin specimens were quenched into iced brine, the size and distribution of massive crystals were sometimes improved, but martensite formed in many cases.

We have finally incorporated plastic deformation and recrystallization in our heat treatment cycle, and have thereby obtained much better microstructures and also reduced the β grain size. Specimens 0.3 mm. thick are heated in a salt bath to 700°C for 10 minutes, followed by iced brine quenching. Then they are rolled to 0.2 mm. thickness (33% reduction) and once

again heated to 700°C or a little higher, but in some instances for only 5 seconds, and are finally quenched into room temperature water. With these treatments we obtained microstructures with very small massive crystals separately formed along grain boundaries in a matrix of retained β phase. The grain size of the specimens is also reduced from larger than 1 mm. to about 0.1 mm. We further found that a slightly higher temperature than 700°C can lead to a smaller quantity of massive ξ_m and more retained β phase.

Although an even smaller grain size would be useful in TEM samples, massive transformations become difficult to control in specimens with too small a grain size. This was observed during heat treatment of thin ribbon specimens made by splat quenching directly from liquid state. These ribbons have a composition of Ag-24.4 A/O Al and a grain size less than 0.05 mm. Even with iced brine quenching, all of the high temperature β phase in almost all specimens transformed into massive ξ_m crystals without retained β phase. A possible explanation for this result is that a much higher nucleation rate per unit specimen volume of ξ_m obtains due to the larger number densities of grain faces, and especially of grain edges and corners, in the small grained specimens, and a much shorter time is required for growing nuclei to impinge upon their neighbors. These two effects greatly accelerate overall transformation kinetics.

3.4 TEM Sample Preparation and Use

In order to increase the probability that electron transparent areas in a sample will appear in microstructural regions containing small massive crystals on grain boundaries with retained β as the matrix phase, we first grind, polish and etch a specimen, and then observe its microstructure with a light microscope. The specimen is next lightly marked at the most favorable areas and then trimmed so that the best of these areas lie in the middle of the sample.

Two methods were used for TEM sample preparation: twin-jet electropolishing and ion milling. The following electrolyte and polishing conditions were found fairly suitable for twin-jet electropolishing: 5% perchloric acid, 10% glycerine and balance ethanol, held at -15°C, with the current range 10-15mA and voltage 20-25V. A problem arising with this method is that some massive crystals disappear from thin areas due to preferred electropolishing of interphase boundaries. Further modifications of this procedure may thus be required.

Ion milling is also being employed to make TEM samples. The initial sample thickness used is about 0.03 mm. Conditions utilized for milling are current - 0.3 mA, voltage - 5kV, and an incident angle of 15° for the first 2 hours and then 10° until perforation (requiring 3-5 more hours). Due to the different characteristics of electropolishing and ion milling, the concept of combining these two methods, i.e. first electropolishing almost to perforation and then ion milling, may be helpful for sample preparation.

All observations were performed on a Philips 420 TEM operating at 120 kV. A cold-stage specimen holder was always used to avoid occurrence of μ_m phase formation while observations were being made. For the same purpose, a cold stage was used during ion milling of TEM samples. Both TEM samples and as-quenched specimens are saved in a vacuum container floated on a bath of liquid nitrogen.

3.5 Results

3.5.1 Optical Microstructure

Fig. 26 shows a typical optical microstructure of massive ξ_m crystals formed in a retained β matrix. It is clear that almost all the massive crystals (white) nucleated at matrix grain boundaries. Some massive crystals preferentially grew into only one matrix grain, and some others grew into both bounding matrix grains. Even under so low a magnification (100x), the massive crystals are clearly seen to be pronouncedly faceted. This feature was mentioned by Aaronson, Laird and Kinsman (66) as the earliest evidence supporting the presence of partially coherent massive:matrix interphase boundaries.

3.5.2 Orientation relationship

Fig. 27a shows a massive ξ_m (hcp) crystal formed at a retained β (bcc) matrix grain boundary. The orientation relationship between the ξ_m crystal and the upper β matrix grain was determined to be the Burgers (13) orientation relationship:

$$(0001)_{\xi_m} // (\bar{1}10)_{\beta}$$

$$(\bar{1}010)_{\xi_m} // (\bar{1}\bar{1}2)_{\beta}$$

$$(1\bar{2}10)_{\xi_m} // [111]_{\beta}$$

This is demonstrated in the selected area diffraction pattern in Fig. 27b. The orientation relationship between the ξ_m crystal and the lower β matrix grain was found to be irrational and not of the Burgers type, but a detailed analysis was not completed.

3.5.3 Massive:Matrix Interfacial Structure

Fig. 28 is an enlarged image of the same ξ_m crystal shown in Fig. 27. Two sets of linear interfacial defects are found in the upper interface with a Burgers orientation relationship between the two phases. The first set, pointed by big arrowheads, is relatively thick and irregularly distributed in both direction and spacing. The second set, indicated by small arrowheads, is relatively thin and regularly distributed in both direction and spacing. The thick and irregular lines are clearly seen to deflect the thin and regular lines when they intersect each other. This feature shows that the thick lines are ledges with relatively high risers. If their irregular direction and interledge spacing are also taken into account, these thick ledges can be described, with some assurance, as growth ledges. The thin and uniformly-spaced lines are found to deflect extinction contours (thickness fringes), and also the growth ledges if careful attention is paid to some intersections between the two sets of lines. The thin lines, therefore, are also ledges, which thereafter will be (temporarily) called uniformly-spaced ledges.

At the lower interface in Fig. 28, which has a non-Burgers orientation relationship with its β grain, there exists a set of lines irregularly distributed but roughly parallel lines which are most probably growth ledges. A second set of lines, whose nature is not yet clear, is also present.

Fig. 29 shows another Burgers-related massive ξ_m:β boundary, imaged with a (0002) ξ_m reflection. The ledges pointed by big arrowheads are growth ledges; the huge deflections of the uniformly spaced ledges again indicate these growth ledges have very high risers. As a special feature of this interface, a third set of lines, pointed out by small arrowheads, was also observed. Although a Burgers vector analysis was found to be difficult because of their very weak contrast, we imaged these lines also with another reflection, i.e. $(\bar{1}0\bar{1}1)_{\xi_m}$. As a result, we may conclude that they are not Moire fringes, but presumably are still another set of ledges.

3.5.4 Burgers vector analysis

Fig. 30 shows five micrographs obtained by using different reflections from the massive ξ_m crystal in Fig. 28. The reason that ξ_m (hcp) reflections are always employed in this analysis and also in the habit plane analysis reported next is that Kikuchi lines can be easily obtained from the ξ_m phase. The uniformly-spaced ledges exhibit the contrast behavior summarized in Table III. These results indicate that the uniformly-spaced ledges have an effective Burgers vector of $a/3[\bar{1}2\bar{1}3]_{\xi_m}$.

3.5.5 Habit plane analysis

A habit plane analysis was completed for the same Burgers-related massive:matrix interface as was used in the Burgers vector analysis. Fig. 31 shows two micrographs taken for this purpose. The same reflection, namely $(0002)_{\xi_m}$, was employed but with two different zone axes ($[1\bar{2}10]_{\xi_m}$ and $[1\bar{1}00]_{\xi_m}$). Table IV summarizes the data measured from the two micrographs. From these data a stereographic projection can be constructed as shown in Fig. 32. The results indicate that the habit plane is between the $(0001)_{\xi_m}$ and $(\bar{1}010)_{\xi_m}$ planes, about 10° away from the latter, and the uniformly-spaced ledges have a direction 18° away from $[1\bar{2}10]_{\xi_m}$, though they are actually curved. Also shown in this figure is the effective Burger vector of the same ledges analyzed in the previous sub-section.

3.5.6 Growth ledge measurements

A typical growth ledge morphology is shown in Fig. 33. The steps shown by two big arrowheads are evidence that these ledges have high risers and are of the growth type. Another set of ledges also can be seen with almost uniform spacing.

An even more prominently stepped morphology of growth ledges along the intersection line of the interface and the sample surface is shown in Fig. 34. Big arrowheads point out the growth ledges with riser heights which can be easily measured. A geometry determined by the sample tilting position, the interface orientation, and the angle between the interface and the sample surface is employed to calculate true ledge heights from the apparent heights. Growth ledge heights measured by this method range from 5 to 8 nm. Inter-ledge spacings for growth ledges were also measured and corrected with a similar, though simpler geometry; they range from 80 to 150 nm.

3.5.7 Composition Invariance

From the Ag-Al phase diagram shown in Fig. 35 (68) it is clear that over a very large undercooling range (more than 250°C), reactions occurring in a specimen quenched from the β phase field involve transformation from one single-phase region to another. The only possibility in this case is a massive transformation--without a change in composition. To make sure that the hcp phase observed in this work is massive, however, the composition of ξ_m crystals and their retained β matrix were determined with energy dispersive spectroscopy. Fig. 36 shows typical results. All measurements indicated that there are no statistically significant differences between the compositions of the ξ_m crystals and their β matrix.

3.6 Discussion

3.6.1 Nature of massive:matrix interfaces

The results of TEM observations in the present work show that there are two or three sets of ledges at ξ_m:β interfaces. This provides the first direct experimental evidence for the presence of partially coherent massive:matrix interphase boundaries.

Fig. 37 shows schematically the Burgers-related massive:matrix interface constructed by using the results of this investigation. For simplicity, only one set of uniformly-spaced ledges has been included. From experimental determinations, the conjugate habit planes of the terraces in this case were $(\bar{1}010)_{\xi_m}//(\bar{1}1\ 2)_{\beta}$. The ledge height for the uniformly-spaced ledges was about 1.9 nm, corresponding to eight atom layers. Because their effective Burgers vector is parallel to the conjugate habit plane, these uniformly-spaced ledges appear to be misfit-compensating ledges as discussed in Sections 2.4 and 2.5. Bearing in mind that there evidently exists a second set of uniformly-spaced ledges at least at some interfaces, it seems likely that they too are able to compensate misfit, thereby completing the task of making these interfaces partially coherent.

3.6.2 Ledge growth kinetics

Menon, Plichta and Aaronson (69) wrote the following equation for the growth rate, V, of a massive phase by the ledge mechanism:

$$V = \frac{h}{\lambda} \frac{D_o}{a_o} \left(-\frac{\Delta G}{RT}\right) \exp\left(-\frac{\Delta H_{D_b}}{RT}\right) \quad (1)$$

where h = ledge height; λ = interledge spacing; D_o = pre-exponential term of the trans-interphase boundary diffusivity; a_o = lattice parameter; ΔG = chemical free energy change; ΔH_{D_b} = activation enthalpy for trans-interphase boundary diffusion; R = gas constant; and T = absolute temperature. Rearranging and taking logarithms gives:

$$ln = \left(\frac{RTVa_o}{-\Delta G D_o}\right) = ln\left(\frac{h}{\lambda}\right) - \frac{\Delta H_{D_b}}{R} \frac{1}{T} \quad (2)$$

Plots of this equation give straight lines, from which $\frac{h}{\lambda}$ can be evaluated. The kinetic data of Perepezko and Massalski (66), measured in a Ag-24.5 at % Al alloy, and the Zener range of acceptable values of D_o, 10^{-5} to 10^{-3} m^2/s (70) were employed and the results were λ/h = 0.2 - 20. The experimental measurements of ledge heights and interledge spacings during this investigation yielded λ/h = 15 - 20. This agreement provides further support for the control of growth during the $\beta \rightarrow \xi_m$ massive transformation by the ledge mechanism.

4. FUTURE PLANS

Some minor changes are being made in three papers (summarized in sections 2.3, 2.4 and 2.5) on modeling the interphase boundary structure of partially coherent bcc:hcp interfaces, and on experimental studies of the structure of the interfaces of Widmanstatten alpha plates and of grain boundary alpha allotriomorphs, respectively, in a Ti-7.15 W/O Cr alloy. These papers will soon be submitted together to Acta Metallurgica. The paper on modeling growth by two sets of growth ledges will be submitted to Metallurgical Transactions A, to be published as part of the proceedings of the recent symposium on "The Role of Ledges in Phase Transformations, for which AFOSR provided substantial travel support for foreign participants.

The investigation now in progress on the massive transformation in a Ag-26 A/O Al alloy will be completed by the end of the next Report Year, i.e., by September 30, 1990. Because we are scheduled to publish the results of the growth kinetics studies in the aforementioned proceedings of the Ledges Symposium, we plan to complete these studies first. Hot-stage TEM is being employed to measure the lengthening kinetics of individual ledges. These data will

then be used to analyze both the motion of the risers and of the overall interfaces. For the latter, we shall continue to use the excellent data of Perepezko and Massalski (66), secured on a nearly identical alloy. The remainder of the investigation will be focussed upon a considerably more detailed evaluation of the structure of β:ξ_m boundaries. For this purpose, we plan to use this Department's recently acquired JEOL 4000EX electron microscope, with which atomic resolution TEM studies can be made. We hope in this manner to acquire more definitive information on the "uniformly spaced" misfit-compensating ledges and also on the third, still smaller set of ledges. These results will then be evaluated against the computer models of bcc:hcp interfaces discussed in section 2.3 of this Report.

The P.I. has already begun to switch over into the "generic overview paper-writing" mode planned for the next two years of this Grant. A very large review has been written and submitted for publication as part of the proceedings of a symposium on interfaces; this review deals with discrimination between shear and diffusional mechanisms of growth at the atomic level. A major overview of the bainite reaction is also nearing completion and will shortly be submitted for publication. Both of these reviews are "aimed" at Metallurgical Transactions A symposium proceedings.

Writeup of an overview of ledgewise growth from vapor, liquid and solid matrices will shortly commence; this will be the introductory paper for the proceedings of the symposium on "The Role of Ledges in Phase Transformations". During this Report year, an overview was also completed and accepted for publication on interphase boundary structure in Ti-base alloys; this, also, will appear in Metallurgical Transactions A as the introductory paper of a symposium proceedings. Later this year, the P.I. will commence writing his Institute of Metals Division Lecture, to be presented at the February, 1990 Annual Meeting of TMS. This lecture, on "Atomic Mechanisms of Diffusional Nucleation and Growth", will become the basis for a paper with the same title.

In the way of individual research papers, five papers on the bainite reaction in steel have already been submitted (from three Ph.D. theses, supported in part by ARO and an NSF-MRL) for publication as part of the proceedings of the Bainite Reaction symposium (organized and edited by Prof. Morris Cohen). A sixth paper, also on steel, is nearing completion.

All of the papers we have so far published on steel have dealt with Fe-C or Fe-C-X alloys (where X is a substitutional alloying element). During the forthcoming year, at least one paper on nucleation and growth kinetics of ferrite at austenite grain boundaries in an Fe-C-Mn-Si alloy should be submitted for publication. Either this year or next, a second paper, dealing with the same topic in Fe-C-Mn-X_i alloys (the bulk of a Ph.D. thesis whose writeup is being delayed by the candidate's employment by hard-driving Nippon Steel Corporation) ought also to be published.

A variety of other papers on various fundamental topics in diffusional nucleation and growth is also projected for the next two years. But the foregoing should keep the P.I. well occupied for most of the coming year--as will also the editorial duties connected with the approximately three dozen papers being received for the Ledges Symposium.

REFERENCES

1. M. R. Plichta, J. C. Williams and H. I. Aaronson: Met. Trans., 8A, 1885 (1977).
2. M. R. Plichta and H. I. Aaronson: Acta Met., 28, 1041 (1980).
3. W. F. Lange III, M. Enomoto and H. I. Aaronson: Met. Trans., 19A, 427 (1988).
4. M. Enomoto and H. I. Aaronson: Met. Trans., 17A, 1385 (1986).
5. E. S. K. Menon and H. I. Aaronson: Met. Trans., 17A, 1703 (1986).
6. H. I. Aaronson and K. C. Russell: Proc. of an International Conf. on Solid-Solid Phase Transformations, p. 371, TMS, Warrendale, PA (1986).
7. J. H. van der Merwe: Jnl. App. Phys., 34, 117, 123 (1963).
8. C. S. Smith: Trans. ASM, 45, 533 (1953).
9. H. I. Aaronson: Decomposition of Austenite by Diffusional Processes, p. 387, Interscience, NY (1962).
10. H. B. Aaron and H. I. Aaronson: Acta Met., 16, 789 (1968).
11. J. R. Bradley, J. M. Rigsbee and H. I. Aaronson: Met. Trans., 8A, 323 (1977).
12. A. D. King and T. Bell: Met. Trans., 6A, 1428 (1975).
13. W. G. Burgers: Physica, 1, 561 (1934).
14. T. Furuhara, A. M. Dalley and H. I. Aaronson: Scripta Met., 22, 1509 (1988).
15. M. G. Hall, H. I. Aaronson and K. R. Kinsman: Surf. Sci., 31, 257 (1972).
16. J. M. Rigsbee, E. S. K. Menon, H. J. Lee and H. I. Aaronson: Scripta Met., 17, 1465 (1983).
17. D. Banerjee, C. G. Shelton, B. Ralph and J. C. Williams: Acta Met., 36, 125 (1988).
18. J. M. Rigsbee and H. I. Aaronson: Acta Met., 27, 351 (1979).

19. W. Bollmann: Crystal Defects and Crystalline Interfaces, Springer Verlag, Berline (1970).

20. D. I. Potter: Jnl. Lee Common Metals, 31, 299 (1973).

21. W. Pitsch and A. Schrader: Arch. Eisenhuttenwesen, 29, 715 (1958).

22. M. G. Hall, J. M. Rigsbee and H. I. Aaronson: Acta Met., 34, 1419 (1986).

23. Wang Rong, G. L. Dunlop and K. H. Kuo: Acta Met., 34, 681 (1986).

24. H. K. Lee and H. I. Aaronson: unpublished research, CMU, 1989.

25. M. G. Hall, H. I. Aaronson and K. R. Kinsman: Surface Sci., 31, 257 (1972).

26. J. M. Rigsbee: private communication, Univ. of Illinois (1980).

27. H. I. Aaronson, G. Spanos, E. S. K. Menon, M. G. Hall, W. F. Lange III and K. Chattopadhyay, Structure and Deformation of Boundaries, TMS, Warrendale, PA, p.3 (1986).

28. J. M. Rigsbee and H. I. Aaronson: Acta Met., 27, 365 (1979).

29. V. Perovic, G. C. Weatherly and C. J. Simpson: Acta Met., 31, 1381 (1983).

30. V. Perovic and G. C. Weatherly: Acta Met., 37, 813 (1989).

31. E. S. K. Menon and H. I. Aaronson: Acta Met., 34, 1975 (1986).

32. H. I. Aaronson and C. Wells: Trans. AIME, 206, 1216 (1956).

33. E. S. K. Menon and H. I. Aaronson: Acta Met., 35, 549 (1987).

34. H. I. Aaronson, W. B. Triplett and G. M. Andes: Trans. AIME, 209, 1227 (1957).

35. E. S. K. Menon and H. I. Aaronson: Acta Met., 34, 1963 (1986).

36. G. C. Weatherly and C. M. Sargent: Phil. Mag., 22, 1049 (1970).

37. H. I. Aaronson, C. Laird and K. R. Kinsman: Phase Transformations, ASM, Metals Park, OH, p. 313 (1970).

38. H. J. Lee and H. I. Aaronson: Acta Met., 36, 787 (1987).

39. H. I. Aaronson: Trans. AIME, 224, 693 (1962).

40. M. Enomoto and M. Fujita: submitted to Met. Trans.

41. R. F. Mehl and O. T. Marzke: Trans. AIME, 93, 123 (1931).

42. M. Hillert: Decomposition of Austenite by Diffusional Processes, Interscience, NY, p. 197 (1962).

43. P. L. Ryder and W. Pitsch: Acta Met., 14, 1437 (1966).

44. P. L. Ryder, W. Pitsch and R. F. Mehl: Acta Met., 16, 563 (1968).

45. D. Vaughan: Acta Met., 16, 563 (1968).

46. D. Vaughan: Acta Met., 18, 183 (1970).

47. A. D. King and T. Bell: Met. Trans., 6A, 1419 (1975).

48. J. K. Park and A. J. Ardell: Acta Met., 34, 2399 (1986).

49. K. Ameyama, T. Maki and I. Tamura: Jnl. Japan Inst. Metals, 50, 602 (1986).

50. M. Enomoto: Acta Met., 35, 935 (1987).

51. M. Enomoto: Acta Met., 35, 947 (1987).

52. G. J. Jones and R. Trivedi: Jnl. App. Phys., 42, 4299 (1971).

53. C. Atkinson: Proc. Roy. Soc., A378, 351 (1981).

54. G. J. Jones and R. Trivedi: Jnl. Crystal Growth, 29, 155 (1975).

55. C. Atkinson: Proc. Roy. Soc., A384, 167 (1982).

56. M. Enomoto, H. I. Aaronson, J. Avila and C. Atkinson: Proc. Int. Conf. on Solid-Solid Phase Transformation, TMS, Warrendale, PA, p. 567 (1983).

57. T. Furuhara, A. M. Dalley and H. I. Aaronson: Scripta Met., 22, 1509 (1988).

58. J. Goldman, H. I. Aaronson and H. B. Aaron: Met. Trans., 1, 1805 (1970).

59. A. Pasparakis, D. E. Coates and L. C. Brown: Acta Met., 21, 991 (1973).

60. A. Pasparakis and L. C. Brown: Acta Met., 21, 1259 (1973).

61. N. A. Gjostein: Diffusion, ASM, Metals Park, OH, p. 241 (1974).

62. C. Atkinson, K. R. Kinsman, H. I. Aaronson: Scripta Met., 7, 1105 (1973).

63. J. W. Christian, The Theory of Transformations in Metals and Alloys, Part I, 2nd Ed., Pergamon Press, Oxford, p. 502, (1975).

64. E. C. DuFort and S. P. Frankel: Math. Tabl. Natn. Res. Council, Washington, 7, 43 (1953).

65. M. Enomoto and H. I. Aaronson: Scripta Met., in press.

66. H. I. Aaronson, C. Laird and K. R. Kinsman: Scripta Met., 2, 259 (1968).

67. J. H. Perepezko and T. B. Massalski: Acta Met., 23, 621 (1975).

68. T. B. Massalski: Binary Alloy Phase Diagrams, vol. 1, ASM, Metals Park, OH, p. 3 (1986).

69. E. S. K. Menon, M. R. Plichta and H. I. Aaronson: Acta Met., 36, 321 (1988).

70. C. Zener: Imperfections in Nearly Perfect Crystals, John Wiley, NY, p. 289 (1952).

FIGURE CAPTIONS

Fig. 1 Computer plot of coherent patches and misfit dislocation structures on $(0001)_\alpha//(01\bar{1}1)_\beta$ interfaces: (a) $\Theta = 0°$ (the Burgers orientation relationship); (b) $\Theta = 2°$; (c) $\Theta = 4°$; (d) $\Theta = 5.26°$ (*the Pitsch-Schrader orientation* relationship); o -- hcp atoms. + -- bcc atoms.

Fig. 2 Computer plot of coherent patches and misfit dislocation structures on $(1\bar{1}01)_\alpha//(1\bar{1}10)_\beta$ interfaces: (a) $\Theta = 0°$ (the Potter orientation relationship); (b) $\Theta = 1°$; (c) $\Theta = -1°$. o -- hcp atoms. + -- bcc atoms.

Fig. 3 Computer plots of O-points and misfit dislocation structures on $(1\bar{1}01)_\alpha//(1\bar{1}10)_\beta$ interfaces. $\mathbf{b}_1$ and $\mathbf{b}_2$ are the Burgers vectors for the two sets of parallel dislocations, respectively. (a) $\Theta = 0°$ (the Potter orientation relationship); (b) $\Theta = 1°$.

Fig. 4 Computer plot of coherent patches and misfit dislocation structures with structural ledges of which the terrace is the $(1\bar{1}00)_\alpha//(2\bar{1}\bar{1}0)_\beta$, $[11\bar{2}0]_\alpha//[111]_\beta$ interface; the Burgers orientation relationship assumed: (a) biatomic (b) 4-atomic and (c) 6-atomic height ledges. o, , -- hcp atoms. +, • -- bcc atoms.

Fig. 5 Computer plot of coherent patches and misfit dislocation structures on the $(1\bar{1}00)_\alpha//(2\bar{1}\bar{1}0)_\beta$ interfaces: (a) $\Theta = 0°$ (the Burgers orientation relationship); (b) $\Theta = 2°$; (c) $\Theta = -4°$. o -- hcp atoms. + -- bcc atoms.

Fig. 6 (a) Interledge spacing and (b) misfit dislocation spacing as a function of rotation angle Θ on the interfaces with biatomic structural ledges with $(1\bar{1}00)_\alpha//(2\bar{1}\bar{1}0)_\beta$ terraces.

Fig. 7 $(11\bar{2}0)_{hcp}$ stereographic projection, on which are plotted the overall habit plane and the directions of ledge risers and of misfit dislocations on the terraces of structural ledges as a function of rotation angle Θ.

Fig. 8 Schematic of a Burgers-related bcc:hcp interface projected onto an $(0001)_\alpha//(01\bar{1}1)_\beta$ plane, containing one biatomic structural ledge of which the terrace is parallel to the $(1\bar{1}00)_\alpha//(2\bar{1}\bar{1}0)_\beta$ plane, showing that the structural ledge is associated with a Burgers vector of $\mathbf{a}/12[111]_\beta$, equivalent to $\mathbf{a}/18[11\bar{2}0]_\alpha$.

Fig. 9 Isometric sketch of a Burgers-related bcc:hcp interface with structural ledges, of which the terrace plane is $(\bar{1}100)_\alpha//(\bar{2}11)_\beta$, and with misfit dislocations.

Fig. 10 Edge-on view of the broad face of a normal α plate. Note the steps corresponding to **c**-type ledges (indicated by arrowheads). The attached diffraction pattern shows the incident beam direction is parallel to $[0001]_\alpha//[01\bar{1}1]_\beta$. The drawing indicates schematically that the ledge terrace plane is rotated 16° away from $(1\bar{1}00)_\alpha//(2\bar{1}\bar{1}0)_\beta$.

Fig. 11 High-resolution image of the broad face of a normal α plate. The foil orientation is parallel to $[0001]_\alpha//[0\bar{1}1]_\beta$. α:β interface is indicated by the white line drawn in the micrograph.

Fig. 12 Isometric sketch of the structure actually observed on the broad faces of normal α plates.

Fig. 13 The broad face of a normal α plate showing irregular growth ledges (large arrowheads) as well as **c**-type ledges, uniformly spaced (indicated by a pair of arrowheads).

Fig. 14 A $[0001]_\alpha$ stereographic projection for the near-Burgers orientation relationships on which the $<011>_\beta$ poles nearest to $[0001]_\alpha$ and the $<111>_\beta$ poles nearest to $[11\bar{2}0]_\alpha$ are plotted with respect to $[0001]_\alpha$ for the 40 α grain boundary α allotriomorphs examined.

Fig. 15 A $[0001]_\alpha$ stereographic projection for the non-Burgers orientation relationships on which the $<011>_\beta$ poles nearest to $[0001]_\alpha$ and the $<111>_\beta$ poles nearest to $[11\bar{2}0]_\alpha$ are plotted with respect to $[0001]_\alpha$ for the 40 α grain boundary α allotriomorphs examined.

Fig. 16 Dark-field micrographs showing the interfacial structure of an α allotriomorph with its β_B grain. (a) $(0002)_\alpha$; (b) $[\bar{1}011]_\alpha$; (c) $[10\bar{1}1]_\alpha$; (d) $[\bar{2}020]_\alpha$; (e) $[\bar{2}110]_\alpha$.

Fig. 17 Dark-field micrographs showing the interfacial structure of an α allotriomorph with its β_B grain. (a) $(000\bar{2})_\alpha$; (b) $[20\bar{2}0]_\alpha$; (c) $[101\bar{1}]_\alpha$; (d) $[10\bar{1}1]_\alpha$; (e) $[\bar{1}101]_\alpha$; (f) $[\bar{1}101]_\alpha$; (g) $[\bar{2}200]_\alpha$; (h) $[\bar{2}110]_\alpha$.

Fig. 18 Dark-field micrographs showing the β_B interfacial structure of an α allotriomorph whose orientation relationship permits $[1\bar{1}00]_\alpha // [2\bar{1}\bar{1}]_\beta$. (a) Weak-beam dark-field, $(0002)_\alpha$; (b) $[1\bar{2}10]_\alpha$; (c) $[0\bar{1}11]_\alpha$; (d) $[0\bar{1}11]_\alpha$; (e) $[0\bar{1}10]_\alpha$.

Fig. 19 Dark-field micrographs showing the interfacial structure of an α allotriomorph formed at a β grain face in a Ti-6.62 at% Cr alloy reacted for 1200 s at 973 K with its β_N grain. (a) ; $(0002)_\alpha$; (b) $(000\bar{2})_\alpha$, weak-beam; (c) $(01\bar{1}1)_\alpha$; (e) $(11\bar{2}0)_\alpha$; (f) $(\bar{2}020)_\alpha$; (g) $(101\bar{1})_\alpha$; (h) $(\bar{1}011)_\alpha$.

Fig. 20 An example of an α allotriomorph, whose non-Burgers orientation relationship deviates far from the Burgers one, formed at a β grain face; reacted for 1200 s at 973 K. Dark-field TEM micrograph showing a planar facet on the β_N interface of the α allotriomorph; $\mathbf{g} = (10\bar{1}1)_\alpha$.

Fig. 21 Comparison of the (dimensionless) ledge velocity of two orthogonal sets with that of a single set of the same interledge spacing (curve 1) and of the same ledge density (curve 3).

Fig. 22 Comparison of the velocity of two orthogonal sets of ledges of $(\lambda/h)_X=50$ and $(\lambda/h)_Y=10$ with the velocity of a single set of the same ledge spacing.

Fig. 23 Variation of the V_X/V_Y ratio with time for three $(\lambda/h)_Y$ values. The $(\lambda/h)_X$ value is fixed at 50.

Fig. 24 Variation of the (dimensionless) growth rate of two orthogonal sets of ledges with $(\lambda/h)_X=50$ and $(\lambda/h)_Y=10$ with time. Dashed curve is the growth rate of a single set of $\lambda/h=50$. $\Omega=0.5$.

Fig. 25 Comparison of measured (5) and calculated half-thickness of α - allotriomorphs isothermally formed from the β matrix in a Ti-6.6 A/O Cr alloy. The reaction temperature is 715°C. Curves 1 and 2 are calculated with $(\lambda/h)_X$=50 and $(\lambda/h)_Y$=10, respectively. Dashed lines e and p are the variation of half-thickness with time by ellipsoidal and planar disordered growth.

Fig. 26 Optical micrograph showing massive ξ_m crystals (white) formed at β matrix grain boundaries.

Fig. 27 An example of massive ξ_m crystals formed at a β matrix grain boundary: (a) bright-field micrograph, and (b) selected area diffraction pattern for a Burgers orientation relationship.

Fig. 28 TEM micrograph showing ledged massive:matrix interphase boundaries.

Fig. 29 TEM micrograph showing a massive:matrix interface with three sets of ledges.

Fig. 30 Dark-field micrographs of a Burgers-related massive:matrix interphase boundary, imaged with five different reflections from the ξ_m phase: (a) $(0002)_{\xi_m}$, (b) $(\bar{1}\bar{1}20)_{\xi_m}$, (c) $(10\bar{1}0)_{\xi_m}$, (d) $(\bar{1}011)_{\xi_m}$, and (e) $(\bar{1}011)_{\xi_m}$.

Fig. 31 Bright-field micrographs taken for the same interface as shown in Fig. 29, imaged with two different zone axes: (a) 4° from $[1\bar{1}00]_{\xi_m}$, and (b) 6° from $[1\bar{2}10]_{\xi_m}$.

Fig. 32 A $(0001)_{\xi_m}$ stereographic projection showing the construction and results of a habit plane analysis using the data listed in Table 4.

Fig. 33 A typical growth ledge morphology: (a) bright-field, and (b) dark-field micrographs.

Fig. 34 A portion of the Ag-Al phase diagram.

Fig. 35 TEM micrograph showing risers of growth ledges, used for ledge height measurements.

Fig. 36 Energy dispersive spectra obtained from a massive ξ_m crystal and its retained matrix grain.

Fig. 37 A schematic indicating a Burgers-related massive:matrix interface with a set of uniformly-spaced ledges.

Table 1: Well-known Orientation Relationships between the BCC and HCP Phases

Orientation relationship	Conjugate planes hcp	bcc
Burgers (13)	(0001)	$(0\bar{1}1)$
	$(1\bar{1}00)$	$(2\bar{1}\bar{1})$
	$(11\bar{2}0)$	(111)
Pitsch-Schrader (21)	(0001)	$(0\bar{1}1)$
	$(0\bar{1}10)$	(011)
	$(2\bar{1}\bar{1}0)$	(100)
Potter (20)	$(1\bar{1}01)$	$(1\bar{1}0)$
	$(11\bar{2}0)$	(111)

Table 2: Data on Ledge Configurations on Interfaces of Alpha Allotriomorphs in a Ti-6.6 A/O Cr alloy.

heat-treatment	Diffusivity cm^2/sec	Allot. No.	Single or Dbl. sets	λ, nm	h, nm	λ/h	Angle	REMARKS
700°C-20min	1.87×10^{-11}	A1	Single	50-100	7-10	5-14		Burgers side At facets
				40-50	4	10-13		Non-Burger side λ≈13nm
		A2	Double	50-70	7	7-10	90°	
				50-60	7	7-9		
		A3	Single	120-150	4	30-38		At facets λ≈30-40nm
		A4	Double	45	11	≈4		
				45	5	9		
725°C-1hr	3.11×10^{-11}	A5	Single	70-90	5-6	12-18	60°	
		A6	Single	50-100	5-11	4.5-20		

Table 3 Observed and Theoretical Contrast Behavior for the Ledges in Figure 29

g	Observed Contrast	**g · b** for $\frac{1}{3}[\bar{1}2\bar{1}3]$
0002	Strong	2
$\bar{1}\bar{1}20$	Weak	- 1
$10\bar{1}0$	No	0
$\bar{1}01\bar{1}$	Weak	- 1
$\bar{1}011$	Weak	1

Table 4 Data for the Habit Plane Analysis, Extracted from the Micrograph in Fig. 30

Zone axis	g	Feature	Rotation angle	Symbol
4° to (1100)	(0002)	Regular ledge	-50°	L1
		Surface/habit	25°	S1
		Growth ledge	52°	G1
6° to (1210)	(0002)	Regular ledge	-10°	L2
		Surface/habit	15°	S2
		Growth ledge	25°	G2

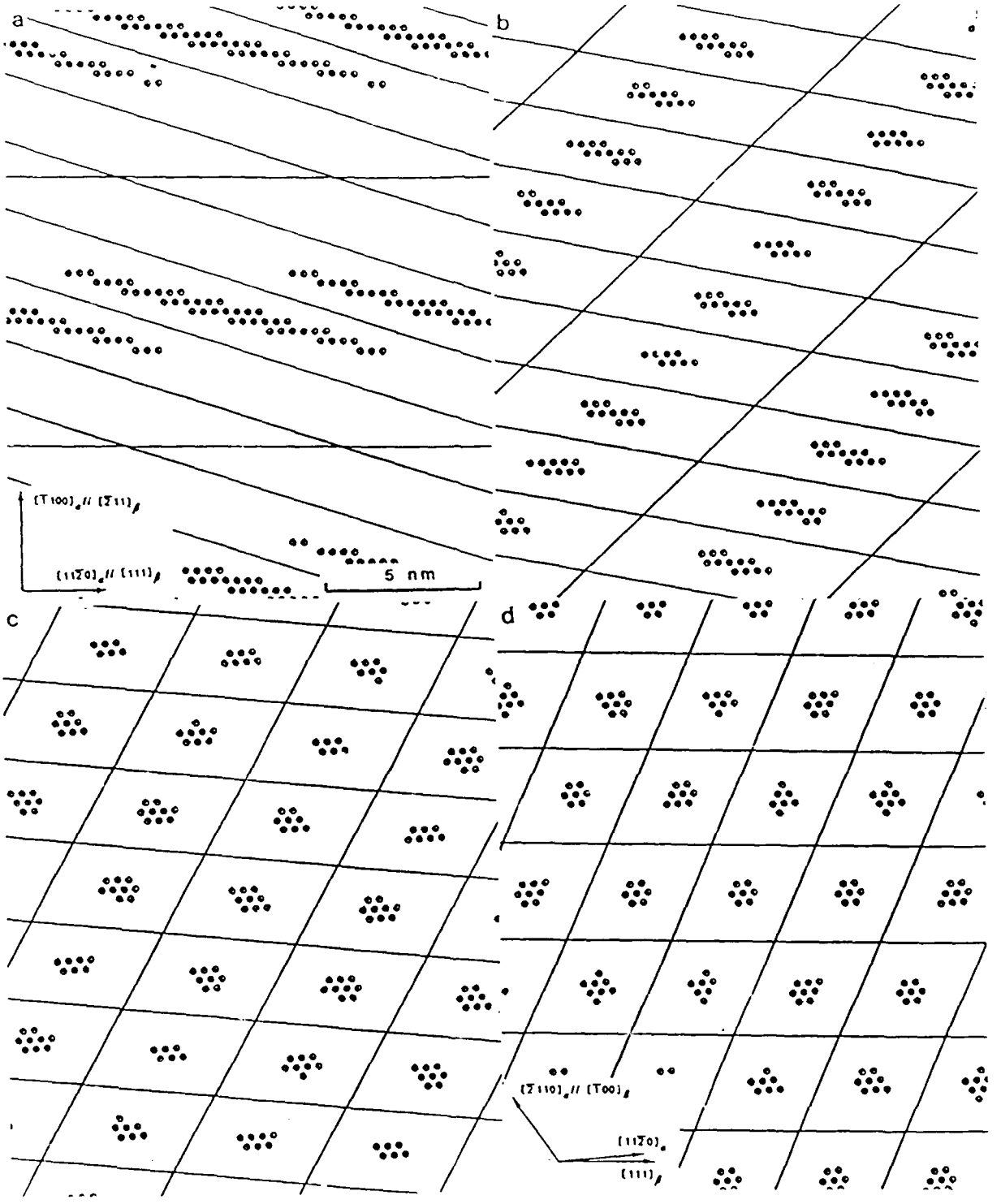
a
b
c
d
$[\bar{1}100]_\alpha // [\bar{2}11]_\beta$
$[11\bar{2}0]_\alpha // [111]_\beta$
5 nm
$[\bar{2}110]_\alpha // [\bar{1}00]_\beta$
$[11\bar{2}0]_\alpha$
$[111]_\beta$

Figure 1

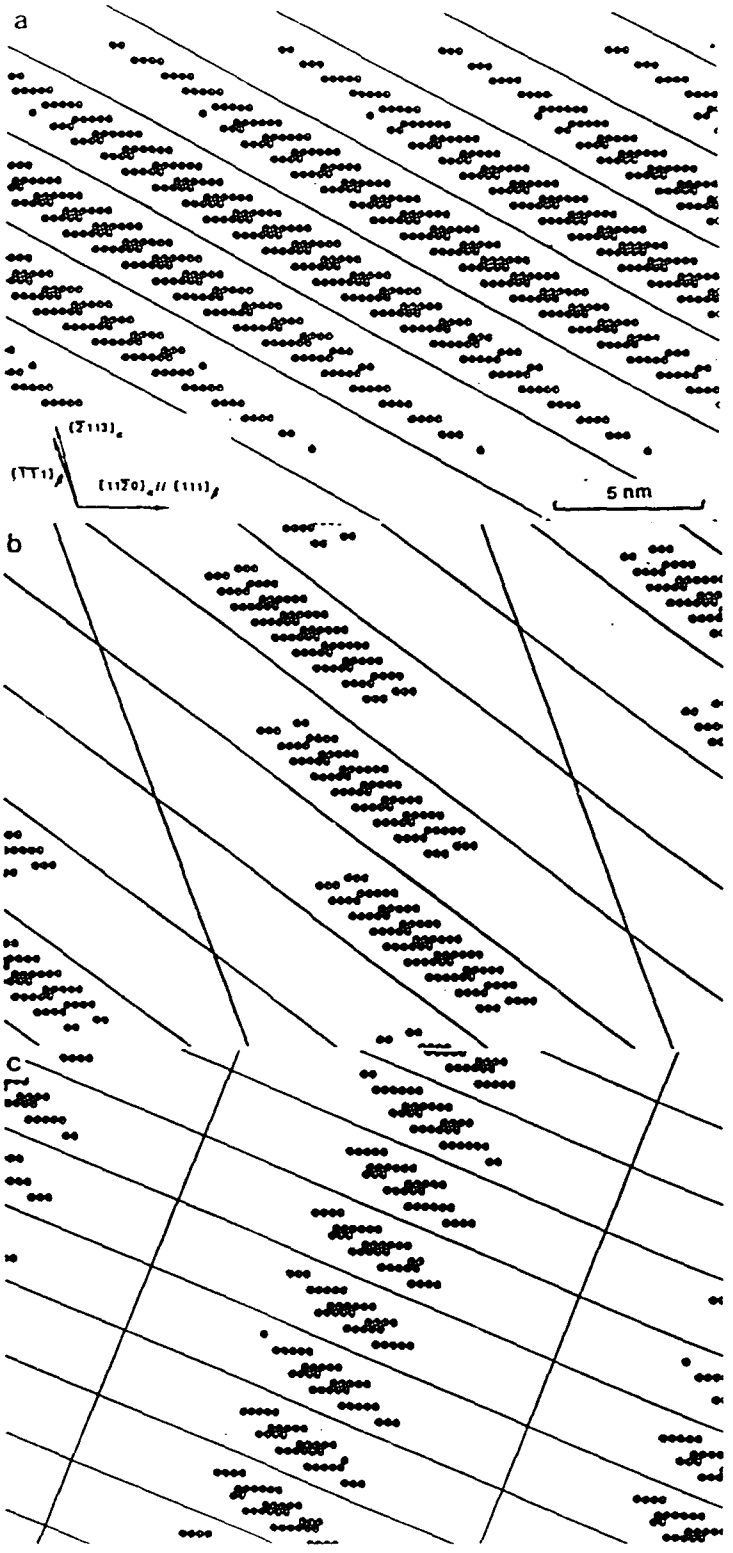

Figure 2

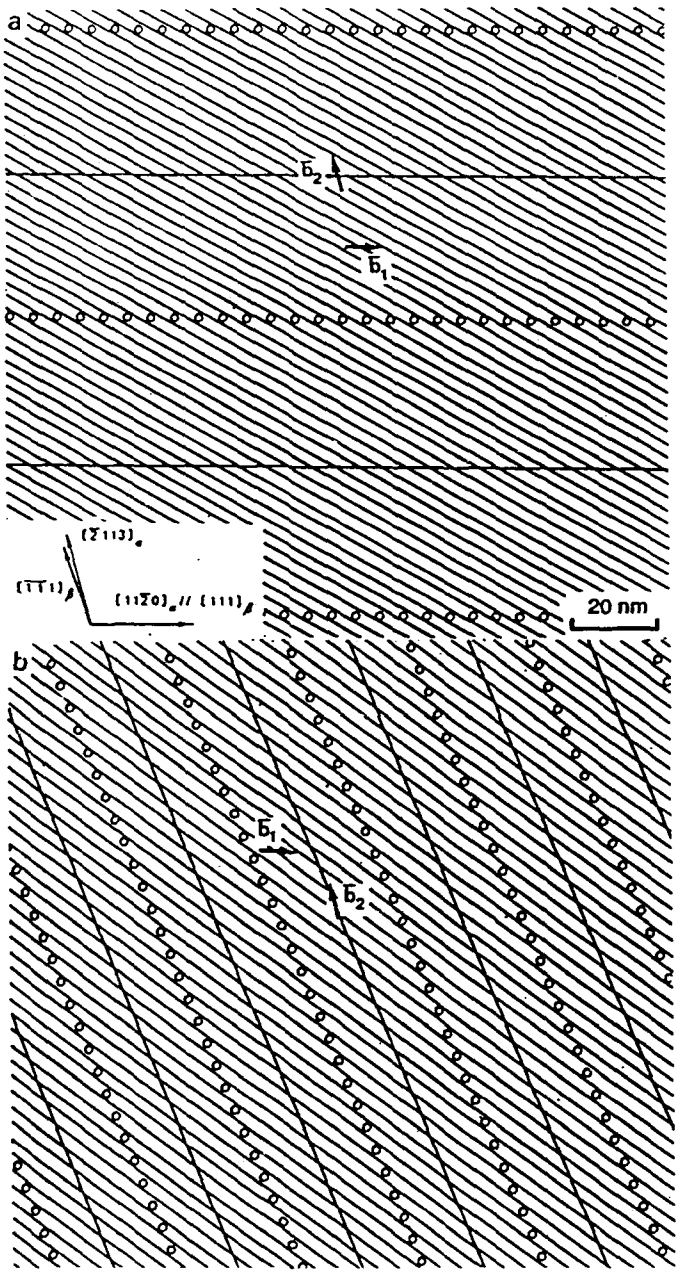
a
$\vec{b}_2$
$\vec{b}_1$
$(\bar{2}113)_\alpha$
$(\bar{1}\bar{1}1)_\beta$
$(11\bar{2}0)_\alpha // (111)_\beta$
20 nm
b
$\vec{b}_1$
$\vec{b}_2$

Figure 3

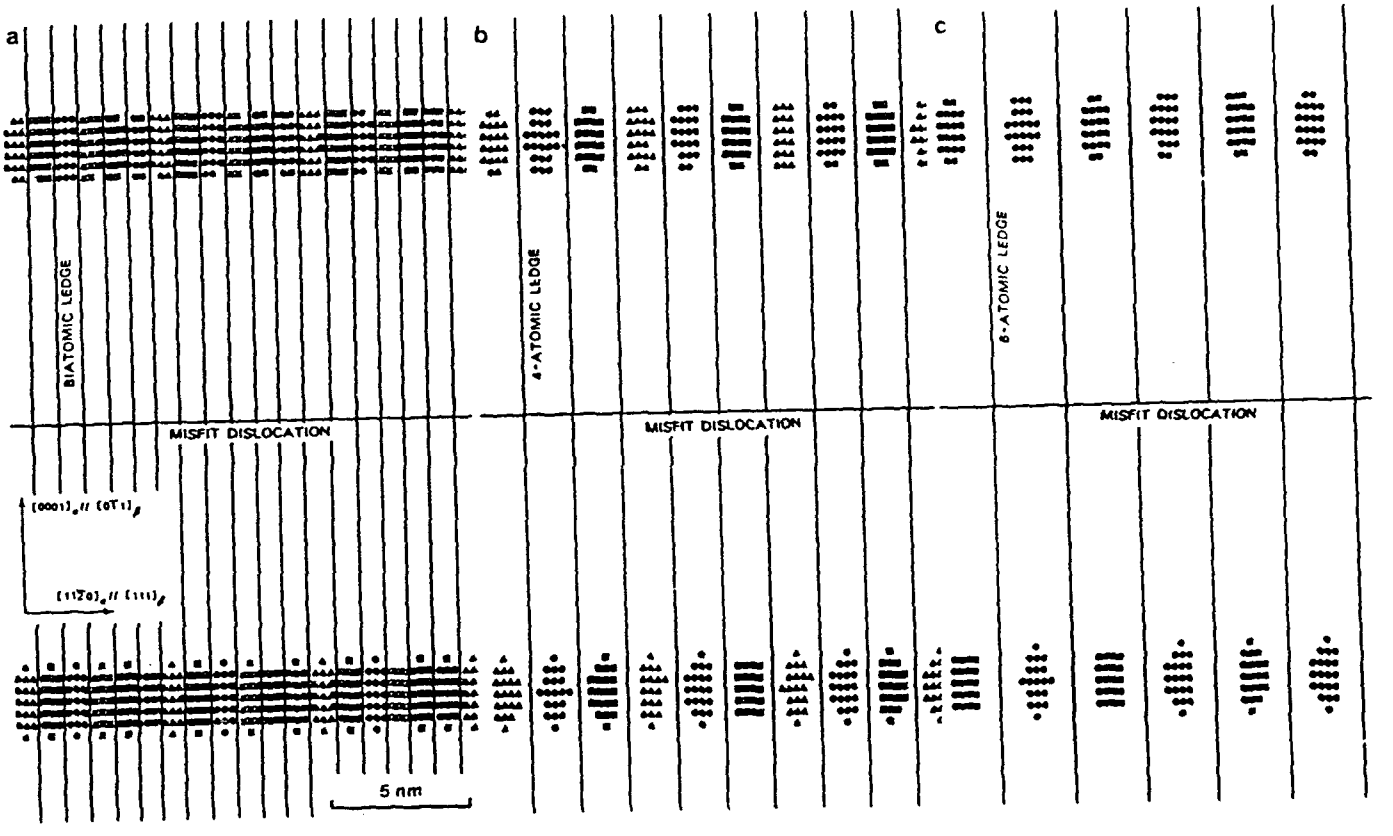
a
b
c
BIATOMIC LEDGE
4-ATOMIC LEDGE
6-ATOMIC LEDGE
MISFIT DISLOCATION
MISFIT DISLOCATION
MISFIT DISLOCATION
5 nm

Figure 4

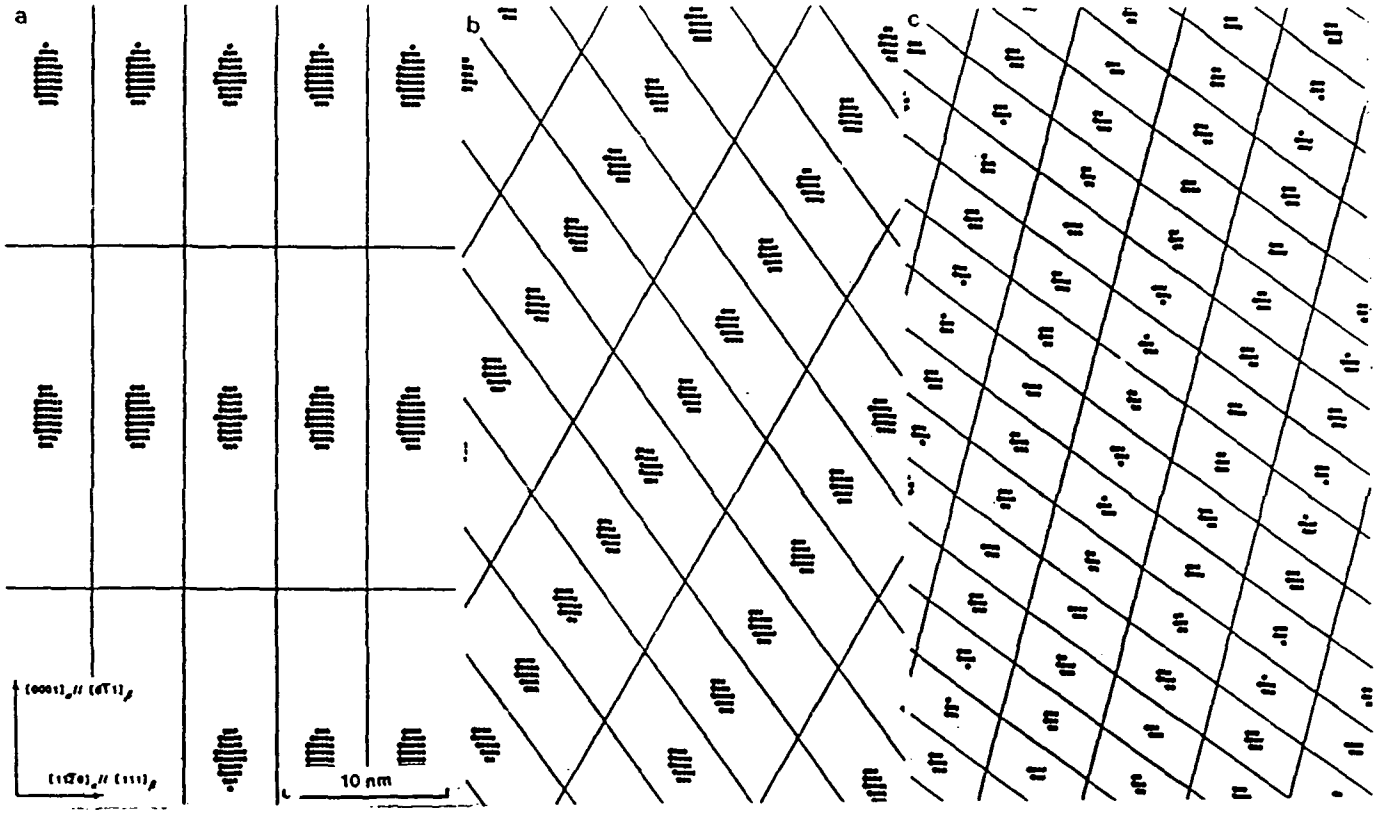

Figure 5

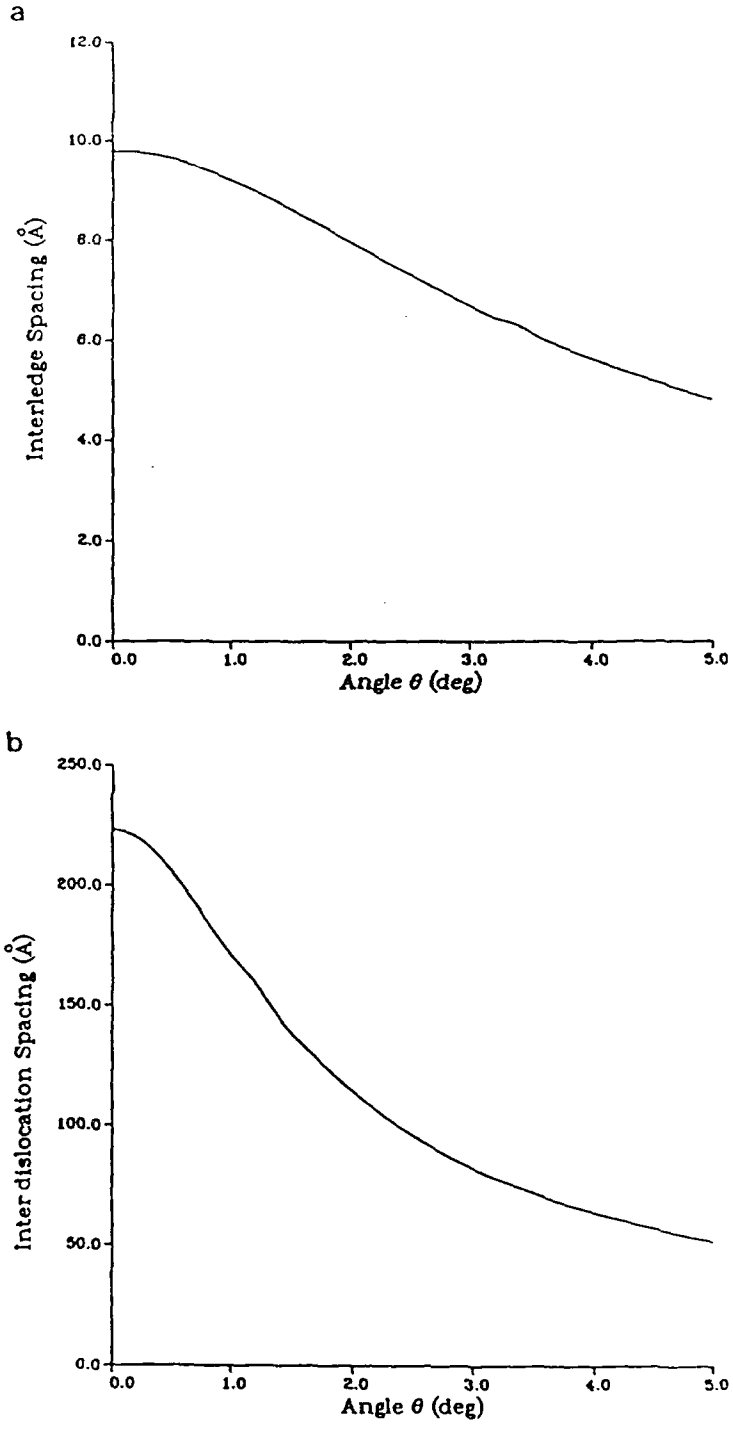
a
12.0
10.0
8.0
6.0
4.0
2.0
0.0
Interledge Spacing (Å)
0.0
1.0
2.0
3.0
4.0
5.0
Angle θ (deg)
b
250.0
200.0
150.0
100.0
50.0
0.0
Inter dislocation Spacing (Å)
0.0
1.0
2.0
3.0
4.0
5.0
Angle θ (deg)

Figure 6

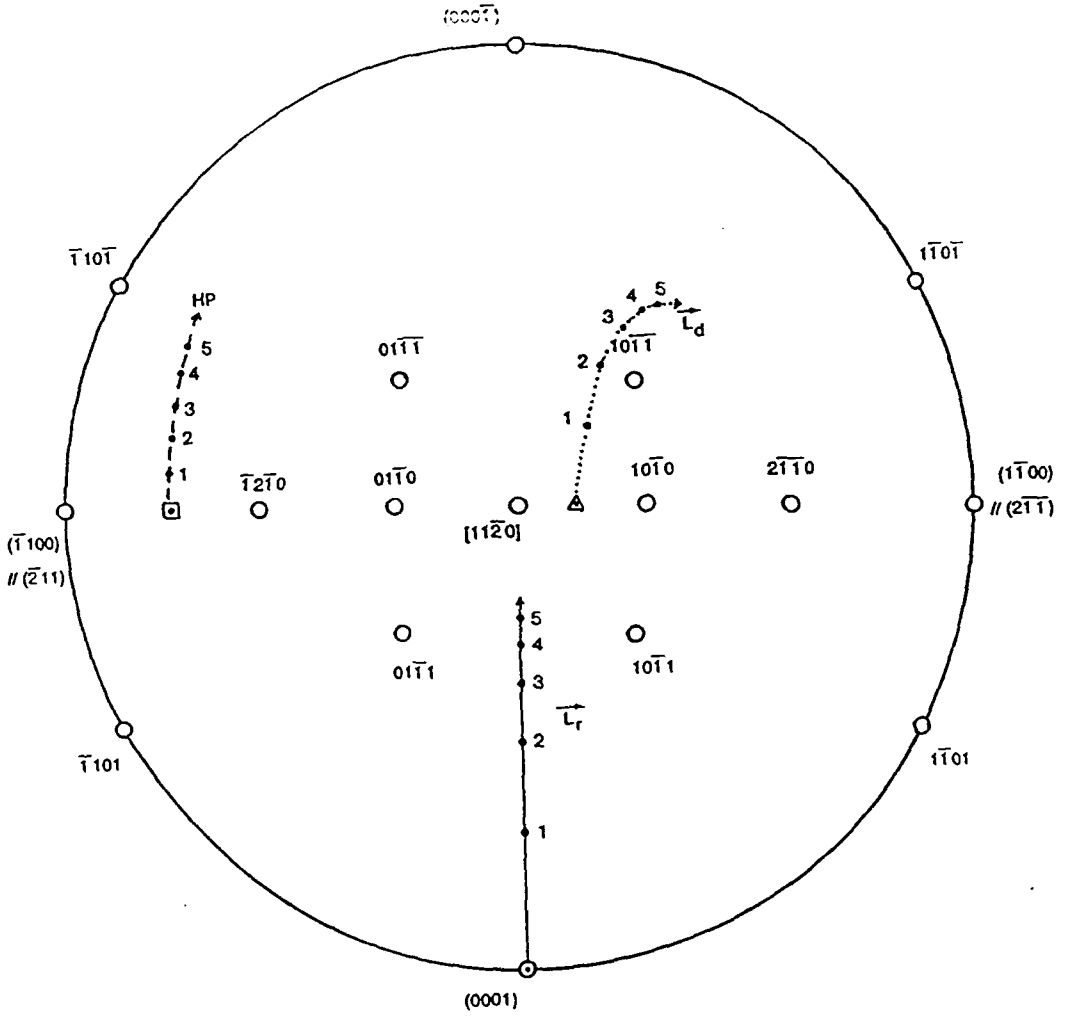
(0001)
$\bar{1}10\bar{1}$
$1\bar{1}0\bar{1}$
HP
5
4
3
2
1
$01\bar{1}\bar{1}$
$10\bar{1}\bar{1}$
$\vec{L}_d$
$\bar{1}2\bar{1}0$
$01\bar{1}0$
$10\bar{1}0$
$2\bar{1}\bar{1}0$
$[11\bar{2}0]$
$(1\bar{1}00)$
$//(2\bar{1}\bar{1})$
$(\bar{1}100)$
$//(\bar{2}11)$
$01\bar{1}1$
$10\bar{1}1$
$\vec{L}_r$
$\bar{1}101$
$1\bar{1}01$
(0001)

Figure 7

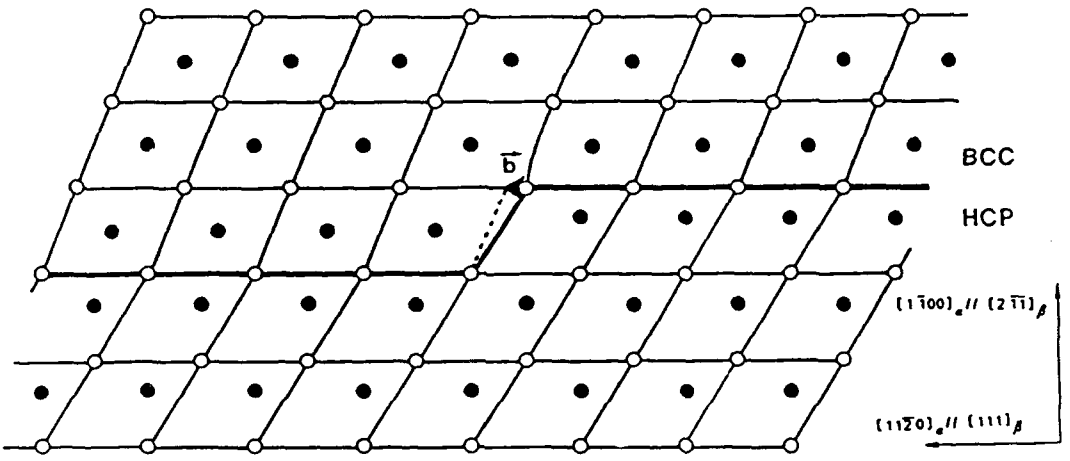
b
BCC
HCP
[1$\bar{1}$00]$_\alpha$ // [2$\bar{1}\bar{1}$]$_\beta$
[11$\bar{2}$0]$_\alpha$ // [111]$_\beta$

Figure 8

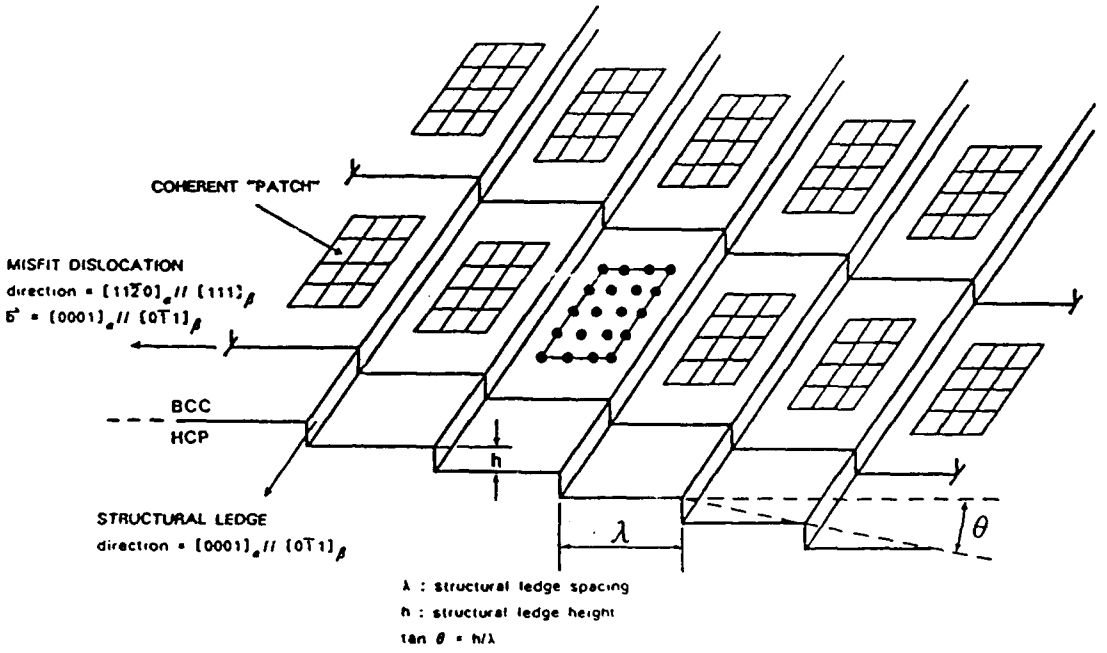
COHERENT "PATCH"
MISFIT DISLOCATION
direction = [11$\bar{2}$0]$_\alpha$ // [111]$_\beta$
$\vec{b}$ = [0001]$_\alpha$ // [0$\bar{1}$1]$_\beta$
BCC
HCP
h
STRUCTURAL LEDGE
direction = [0001]$_\alpha$ // [0$\bar{1}$1]$_\beta$
λ
θ
λ : structural ledge spacing
h : structural ledge height
tan θ = h/λ

Figure 9

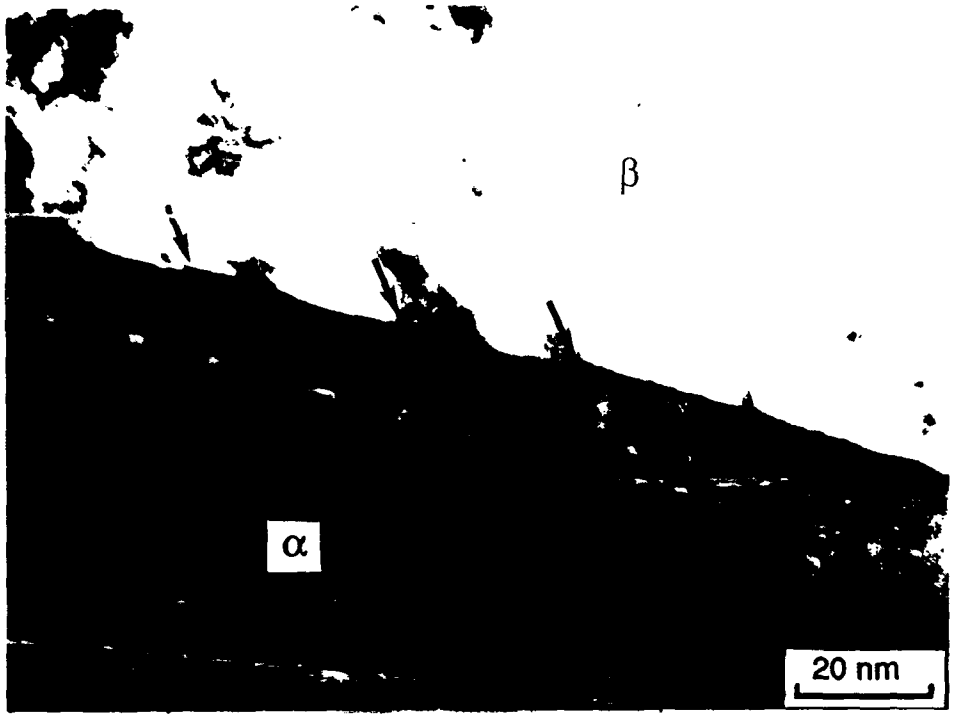

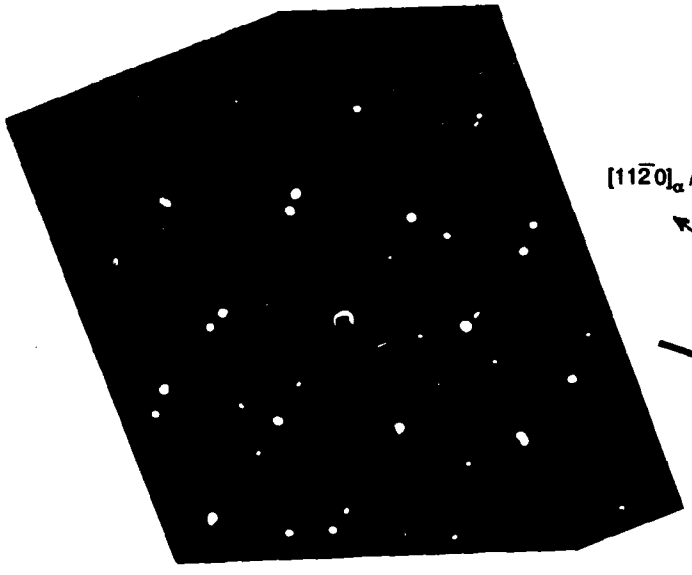

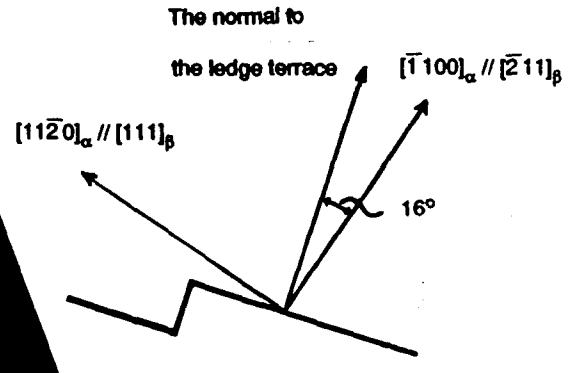

$Z = [0001]_\alpha$ // $[0\bar{1}1]_\beta$

Figure 10

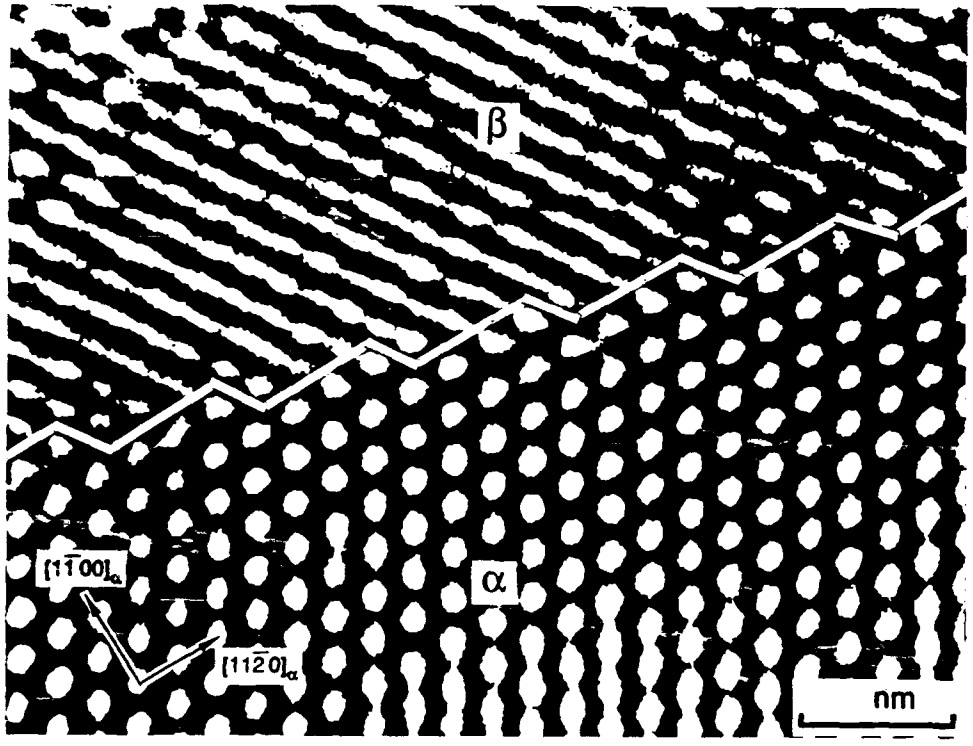

Figure 11

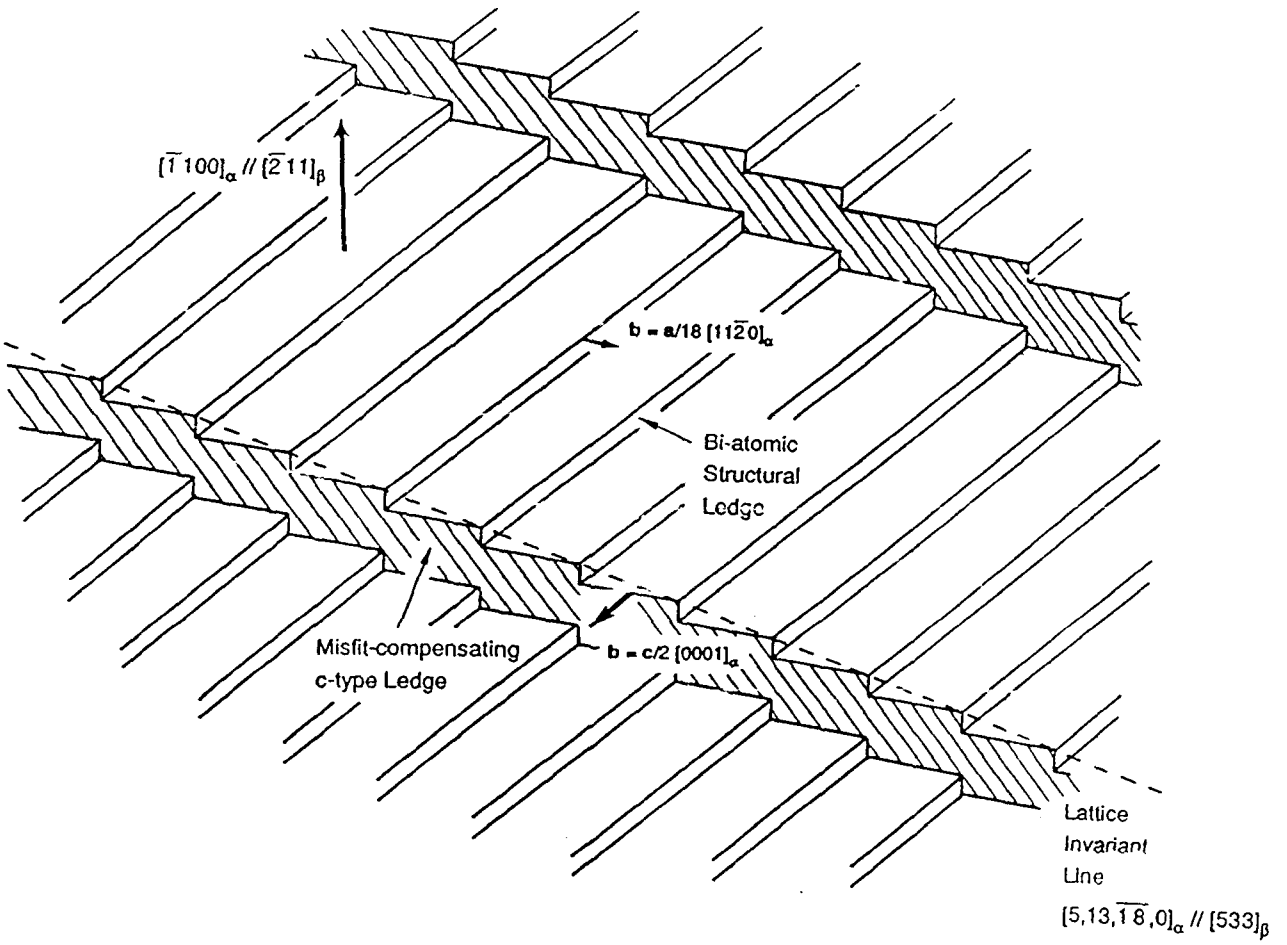
$[\bar{1}100]_\alpha // [\bar{2}11]_\beta$
$b = a/18\,[11\bar{2}0]_\alpha$
Bi-atomic
Structural
Ledge
Misfit-compensating
c-type Ledge
$b = c/2\,[0001]_\alpha$
Lattice
Invariant
Line
$[5,13,\overline{18},0]_\alpha // [533]_\beta$

Figure 12

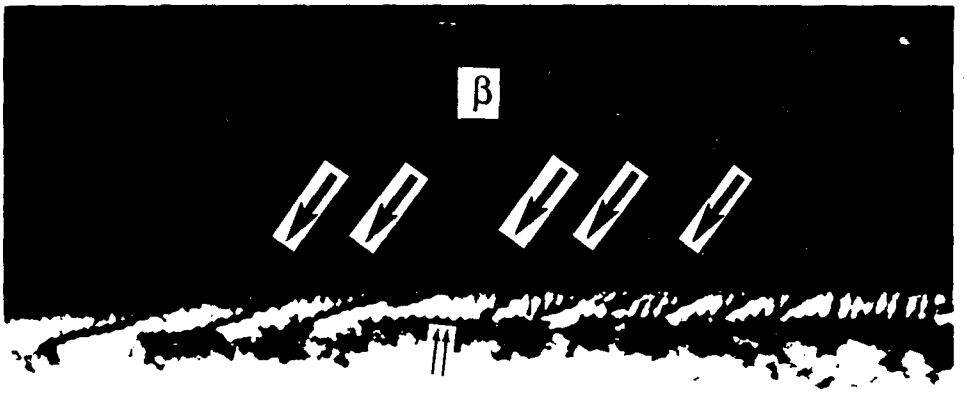

Figure 13

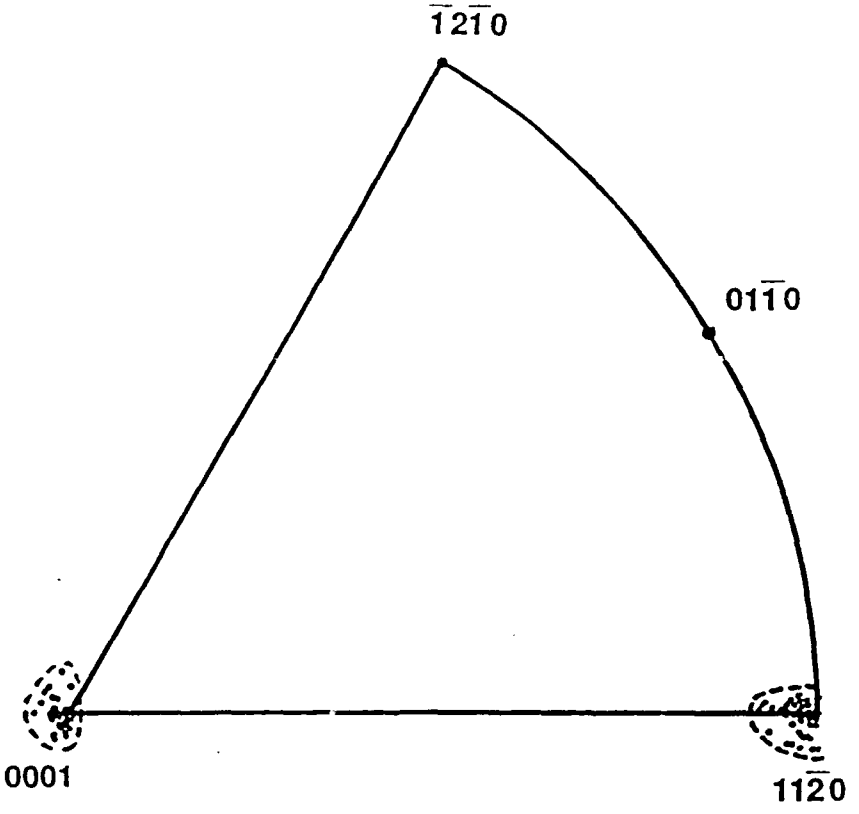

Figure 14

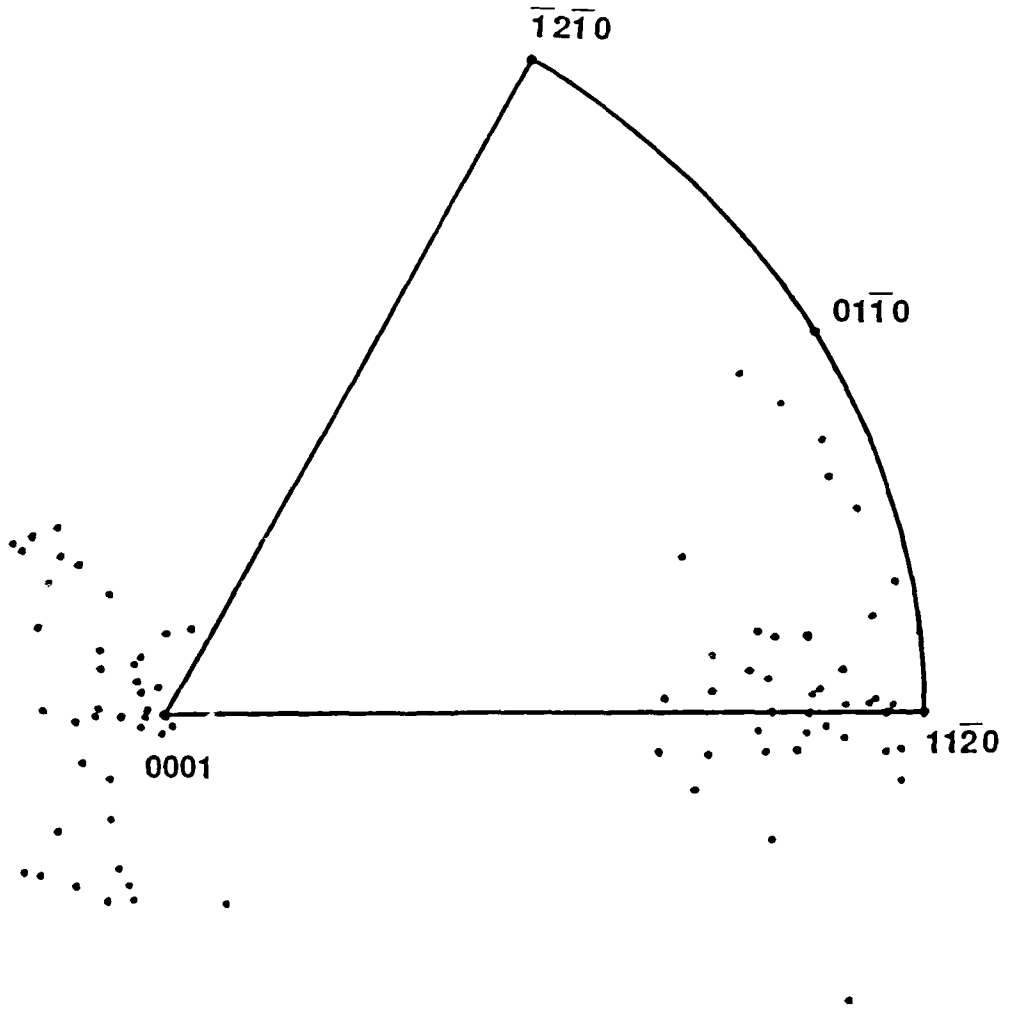

Figure 15

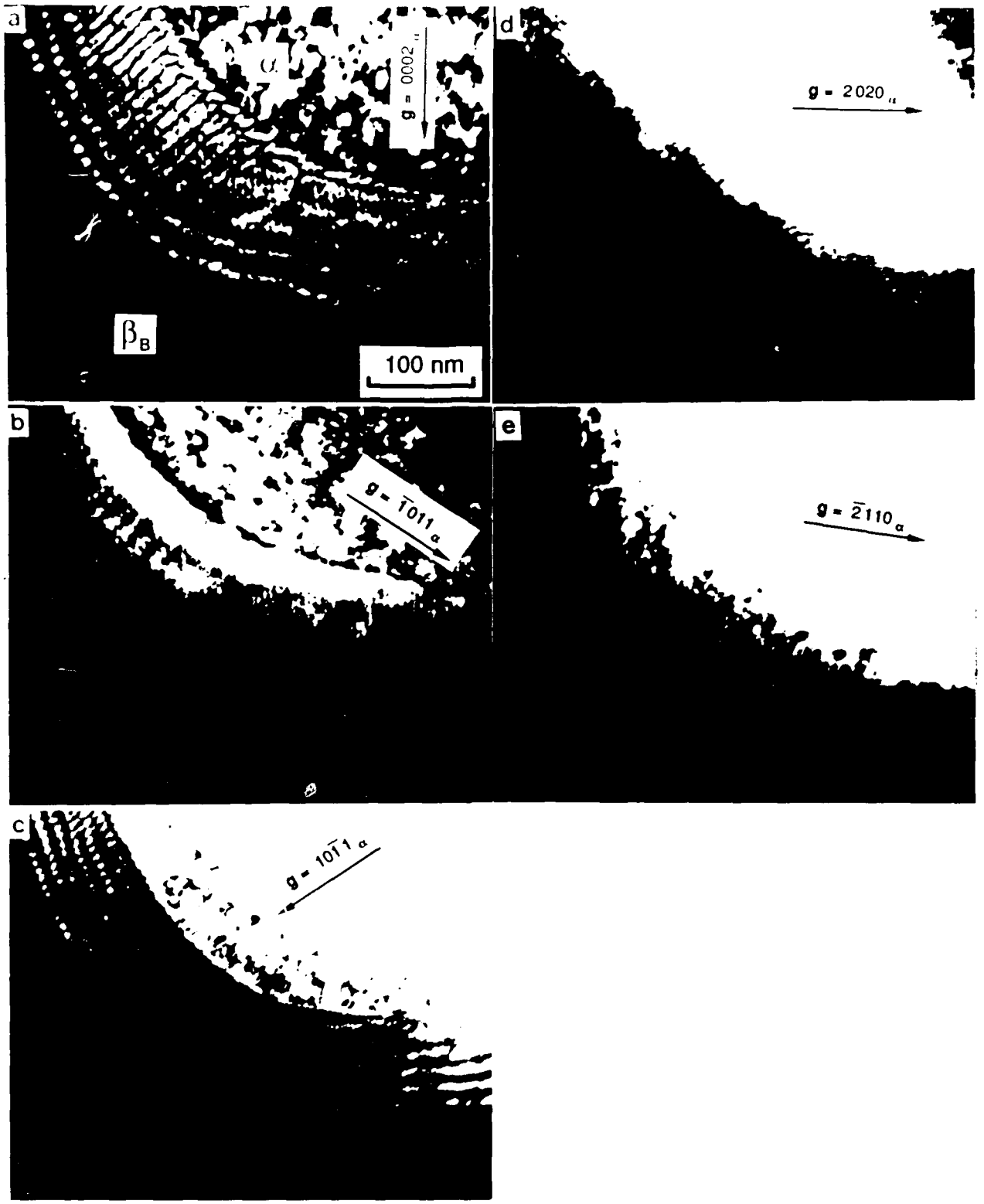

Figure 16

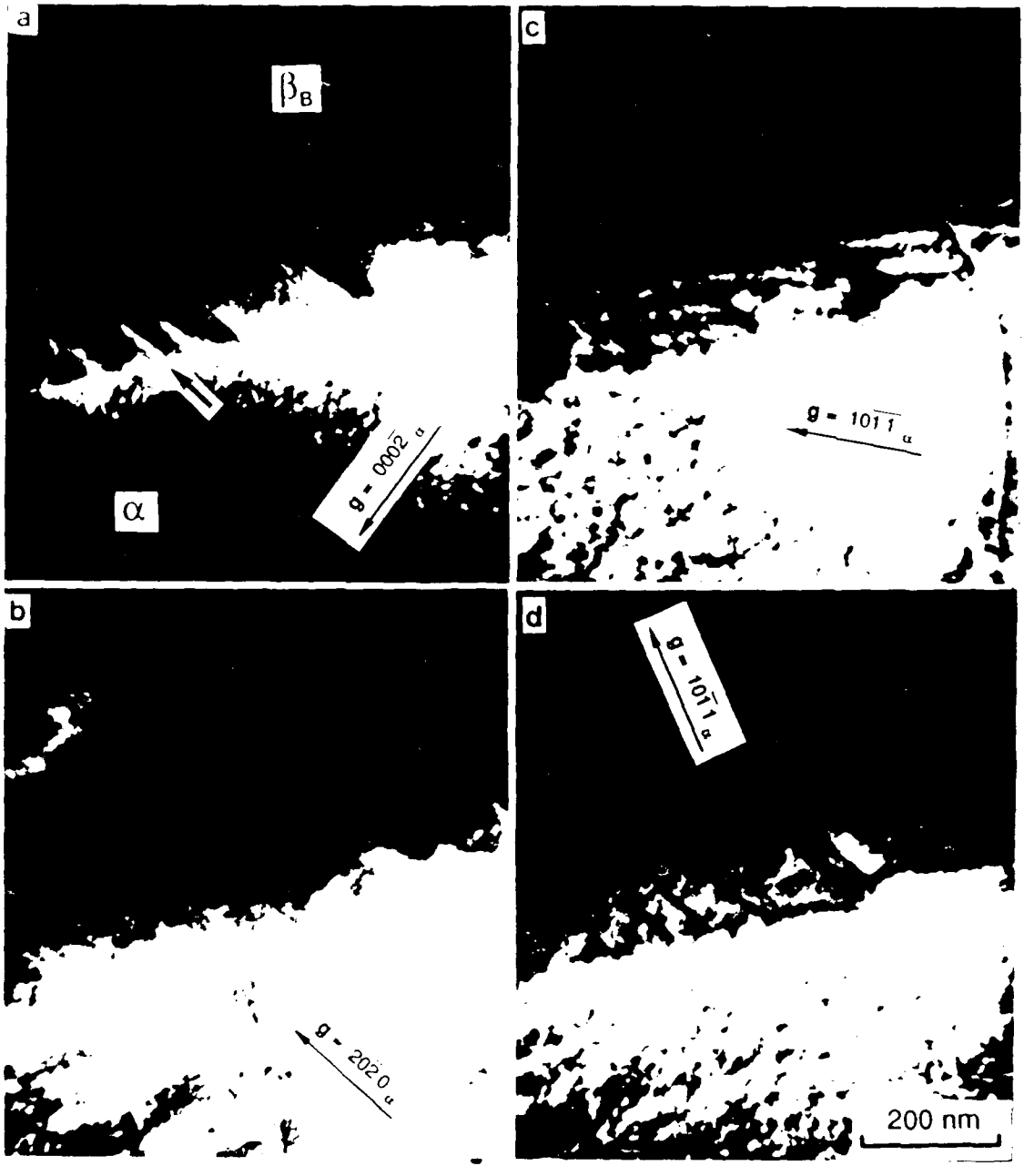

Figure 17

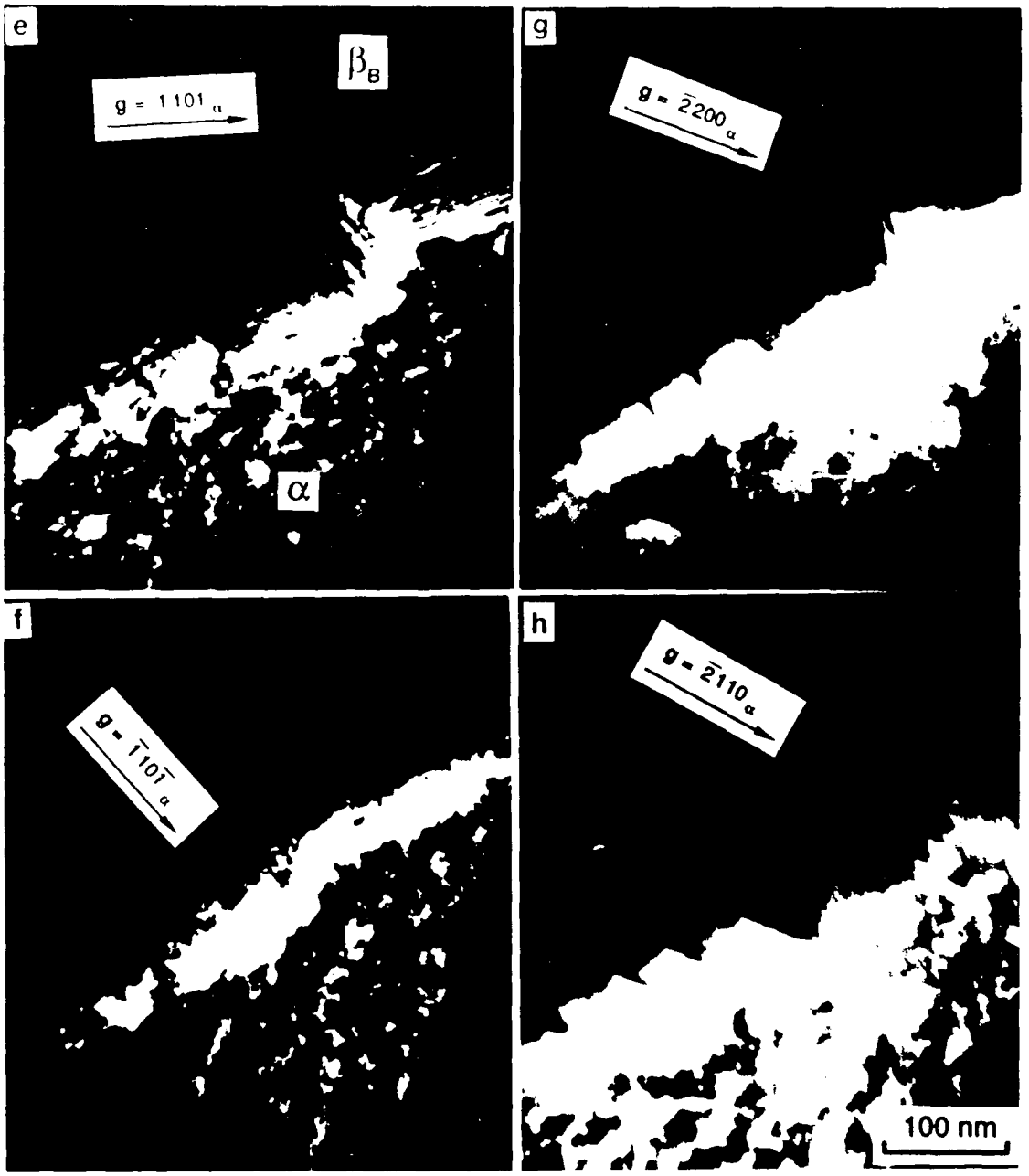

Figure 17
Continued

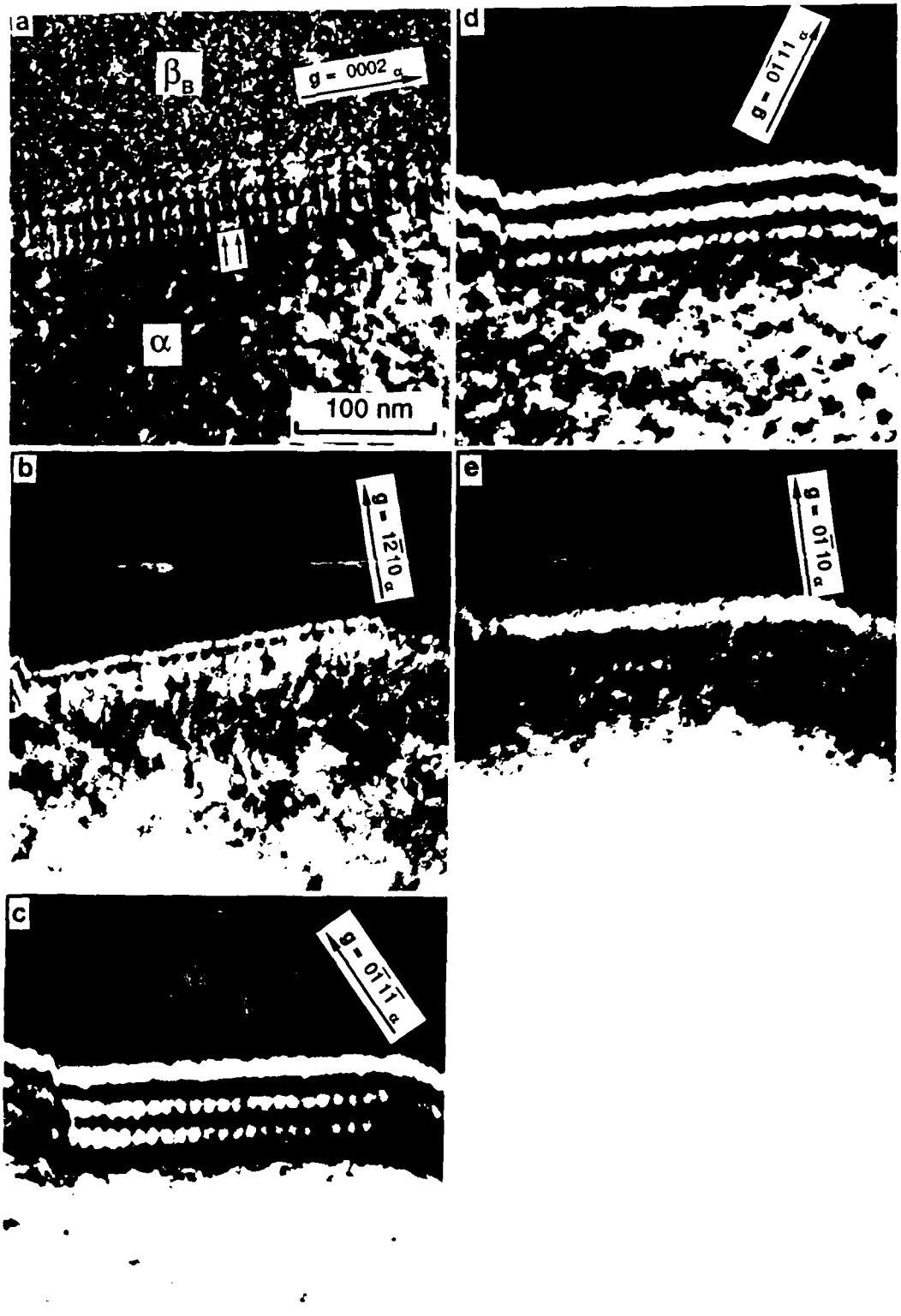
a
β_B
g = 0002 α
α
100 nm
b
g = 12$\bar{1}$0 α
c
g = 01$\bar{1}$1 α
d
g = 0$\bar{1}$11 α
e
g = 01$\bar{1}$0 α

Figure 18

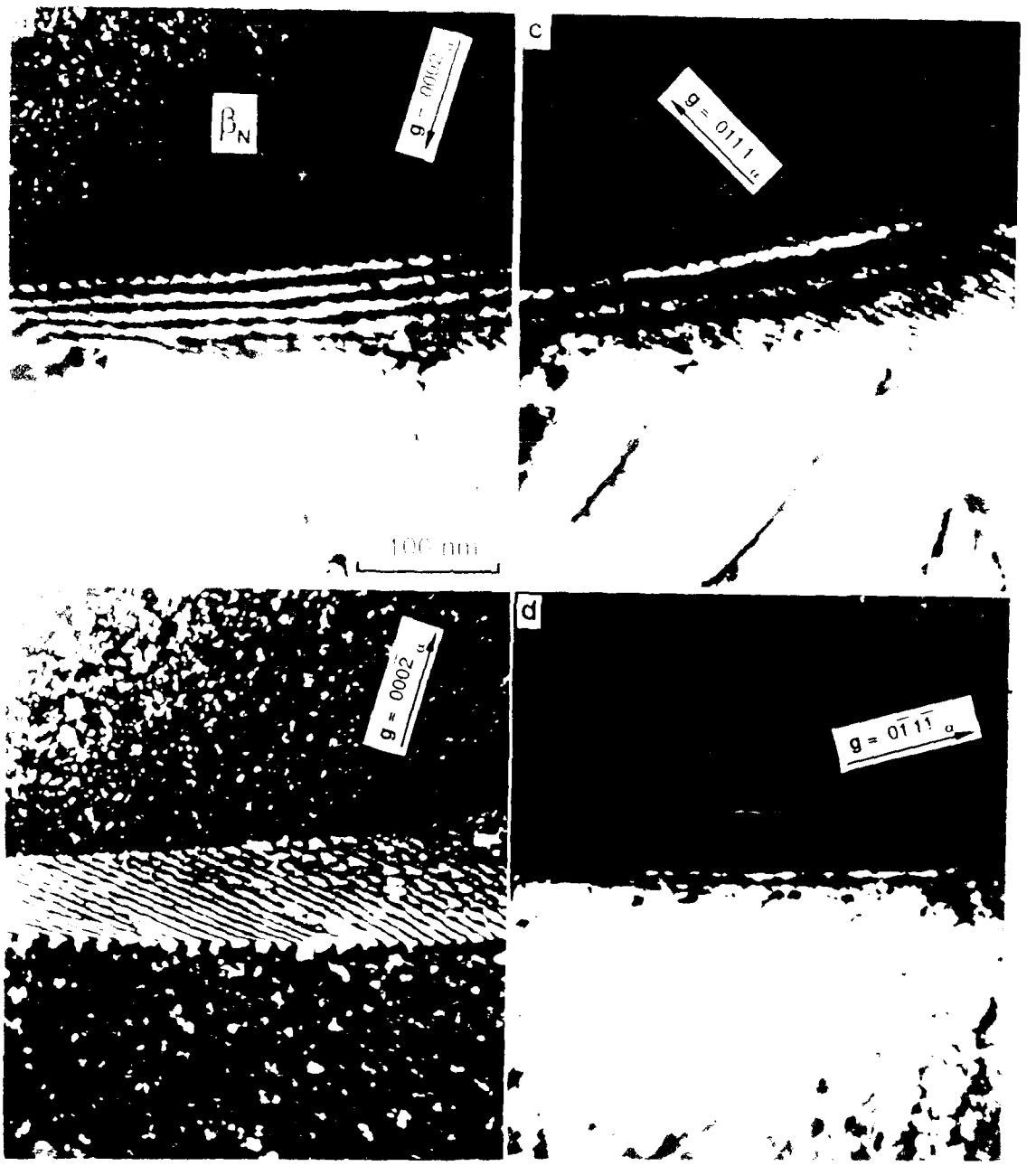
β_N
g = 0002 $_\alpha$
c
g = 0111 $_\alpha$
100 nm
g = 0002 $_\alpha$
d
g = $0\bar{1}\bar{1}\bar{1}_\alpha$

Figure 10

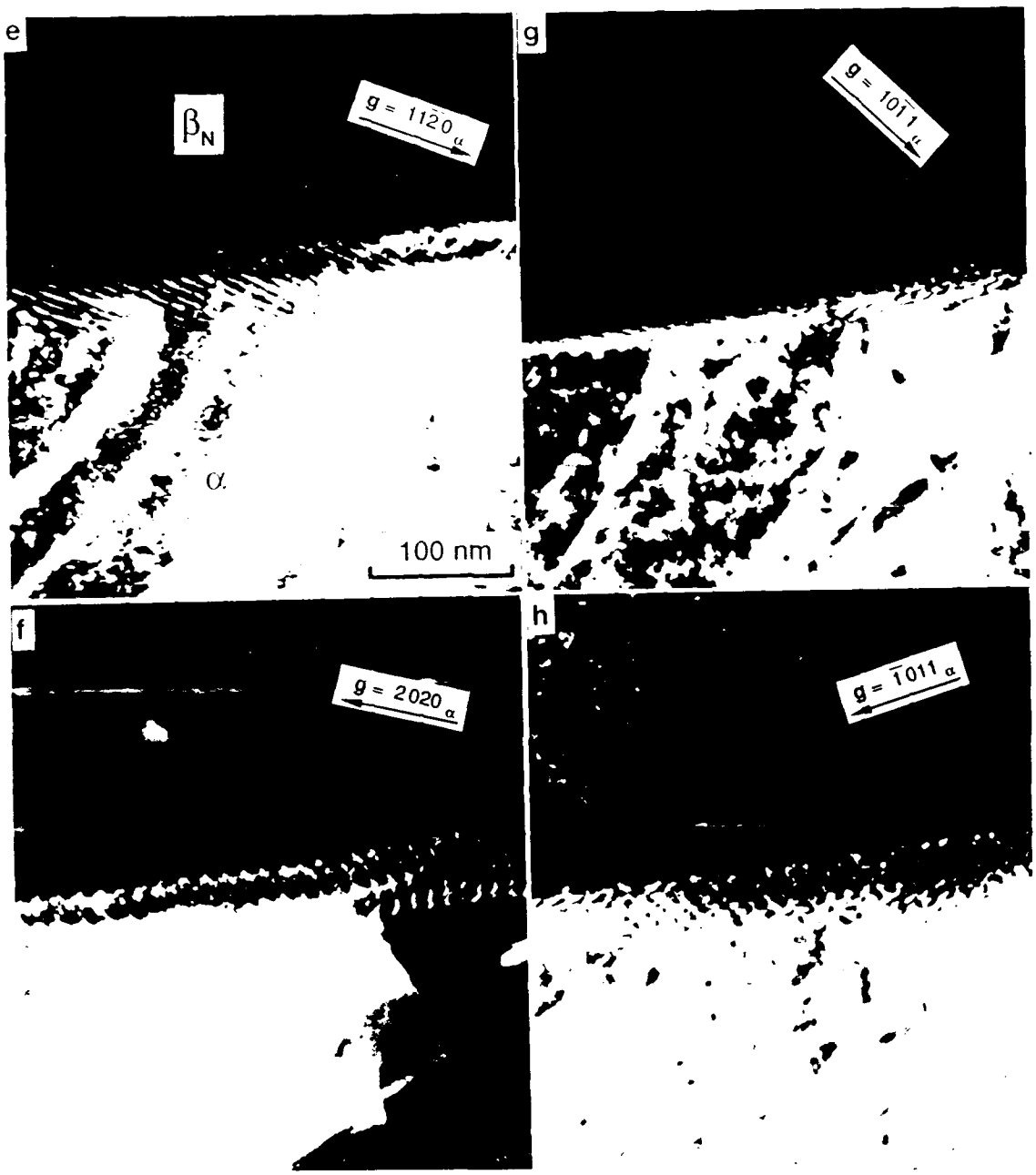

Figure 19
Continued

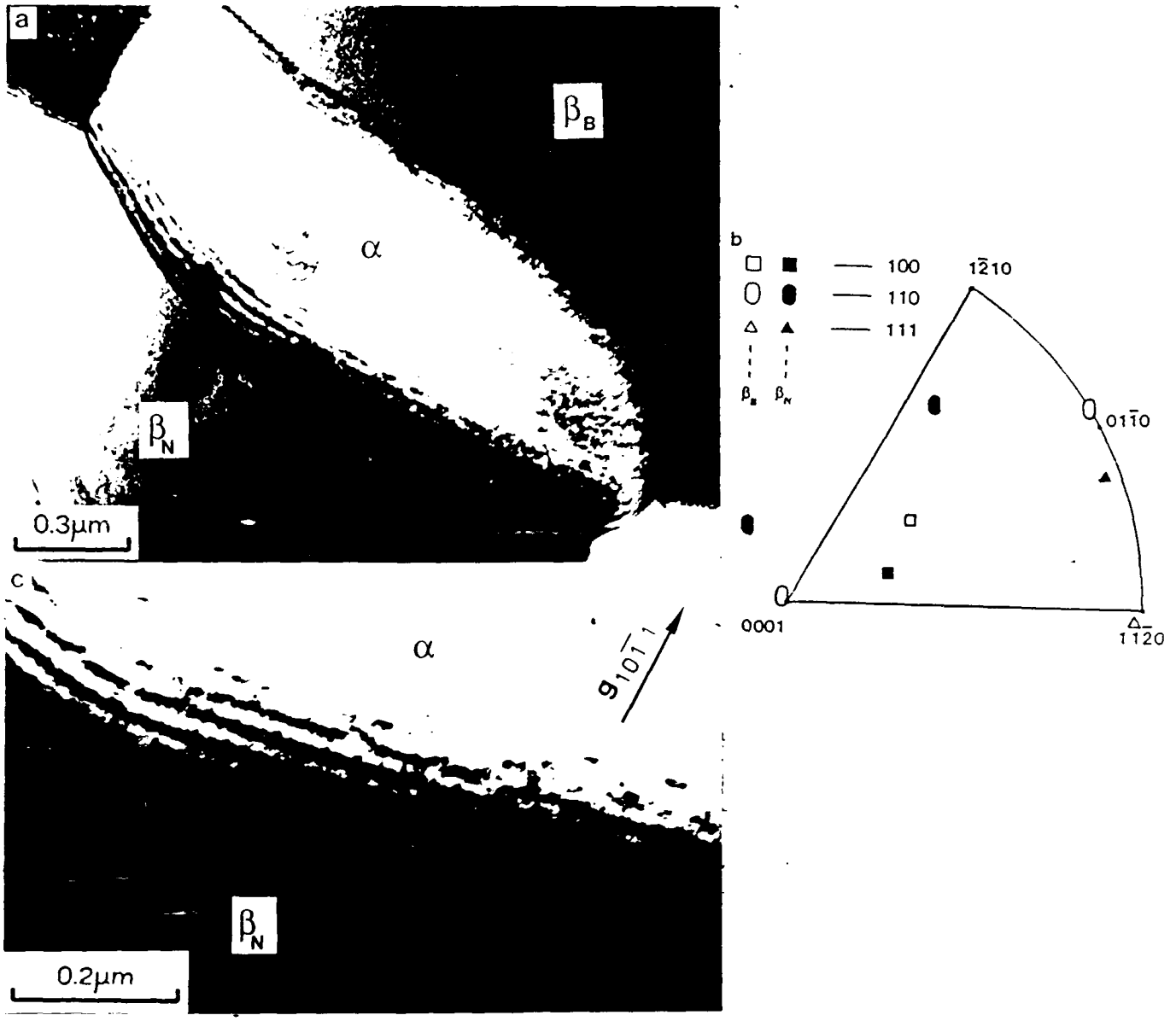
a
β_B
α
β_N
0.3μm
b
100
110
111
β_B
β_N
$1\bar{2}10$
$01\bar{1}0$
0001
$\bar{1}\bar{1}20$
c
α
$g_{10\bar{1}1}$
β_N
0.2μm

Figure 20

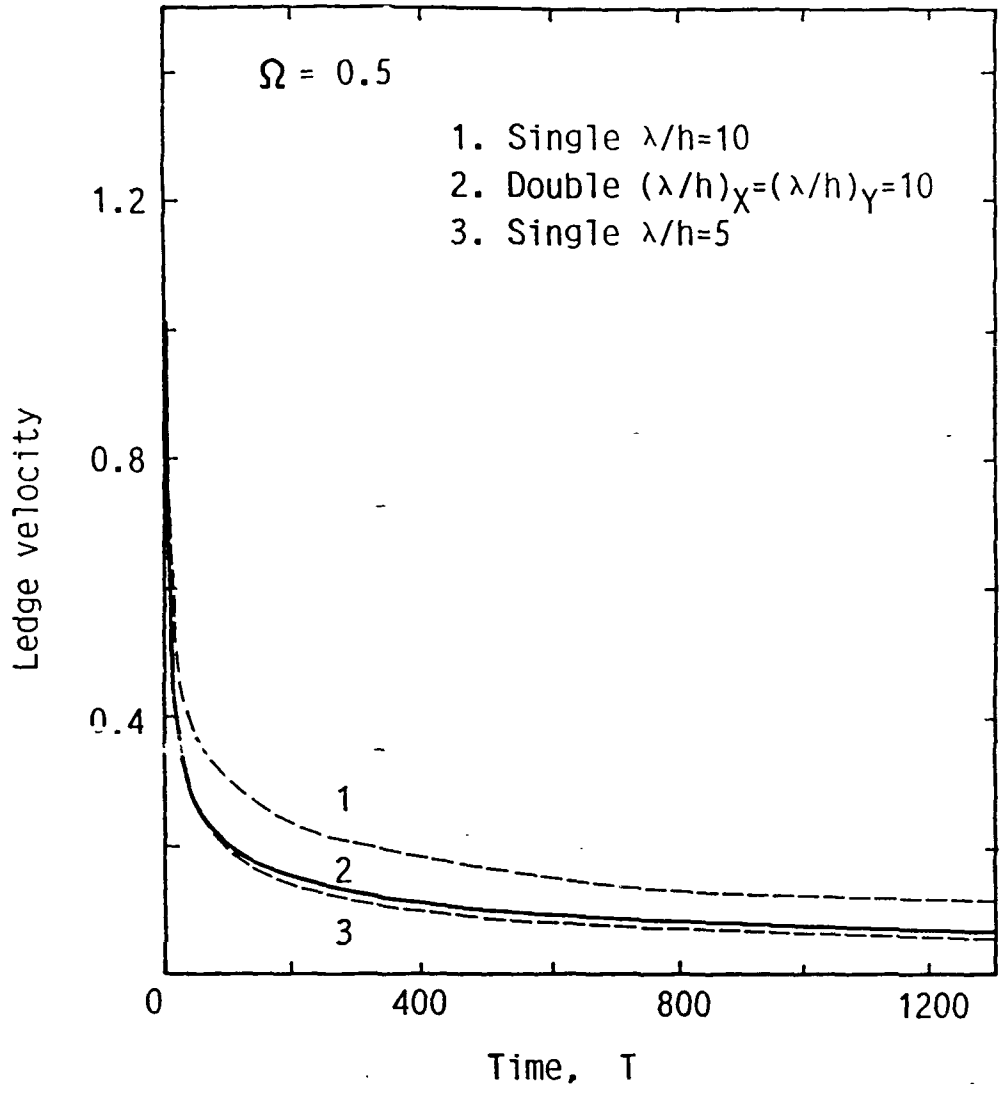
Ω = 0.5
1. Single λ/h=10
2. Double (λ/h)X=(λ/h)Y=10
3. Single λ/h=5
Ledge velocity
1.2
0.8
0.4
0
400
800
1200
Time, T
1
2
3

Figure 21

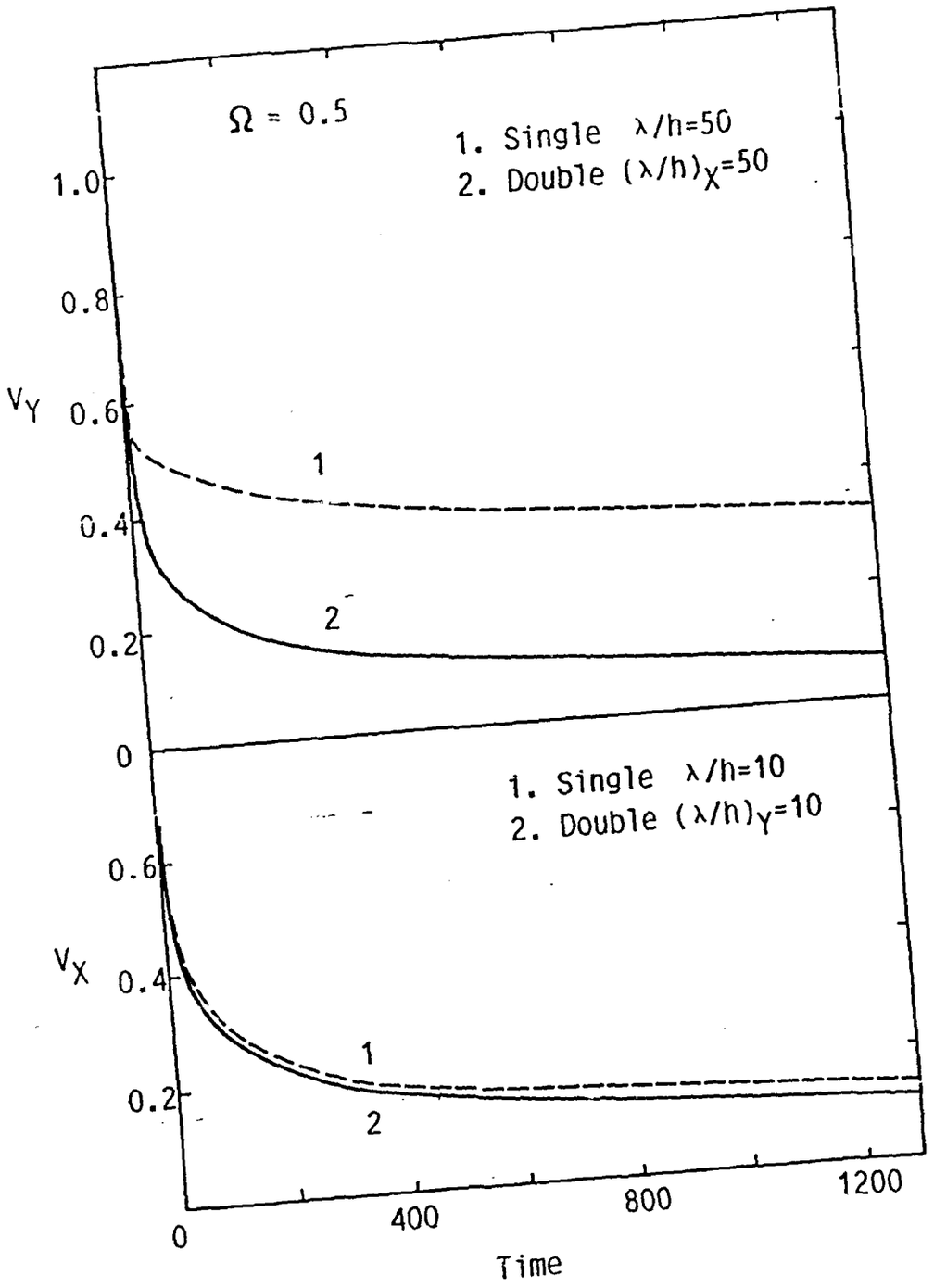
Ω = 0.5
1. Single λ/h=50
2. Double (λ/h)X=50
1.0
0.8
VY 0.6
0.4
0.2
0
1
2
1. Single λ/h=10
2. Double (λ/h)Y=10
0.6
VX 0.4
0.2
1
2
0
400
800
1200
Time

Figure 22

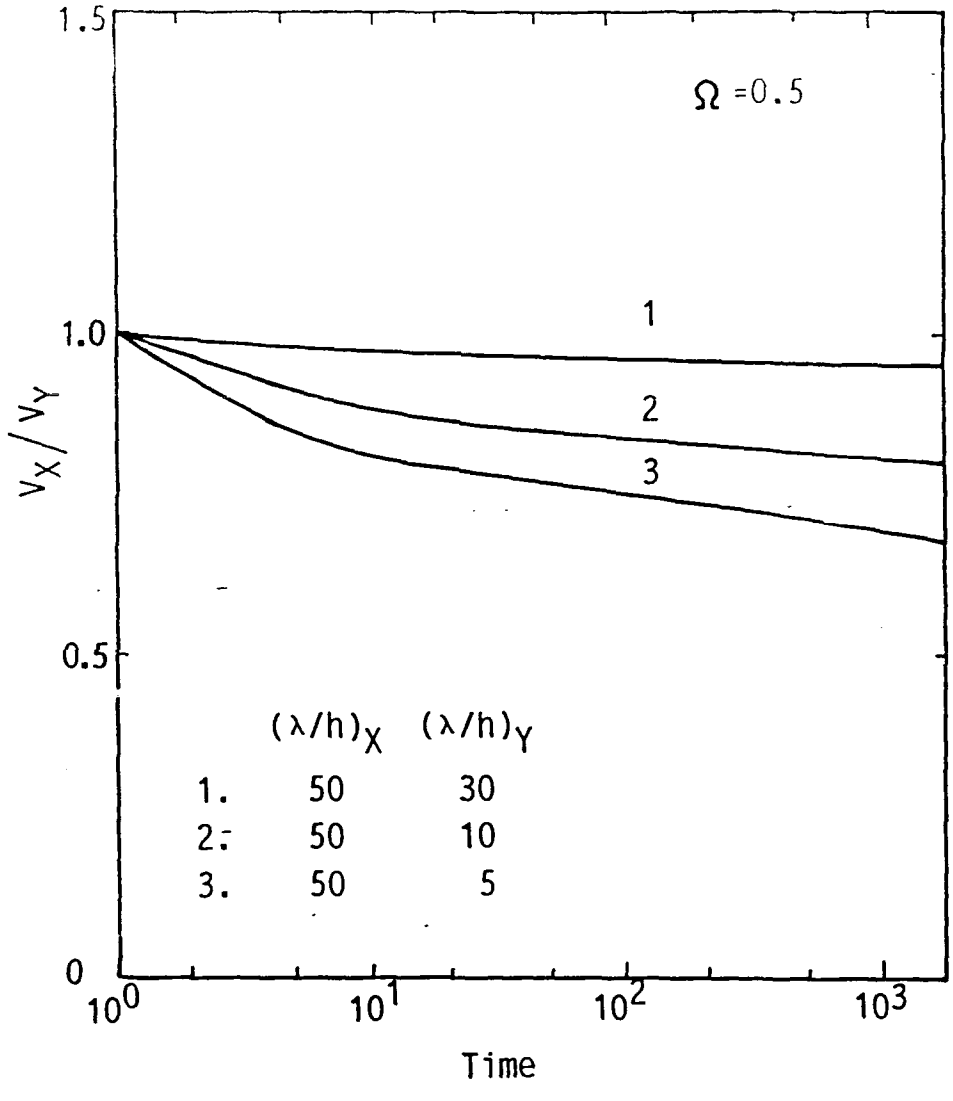
1.5
1.0
0.5
0
V_X / V_Y
Ω =0.5
1
2
3
$(\lambda/h)_X$ $(\lambda/h)_Y$
1. 50 30
2. 50 10
3. 50 5
10^0
10^1
10^2
10^3
Time

Figure 23

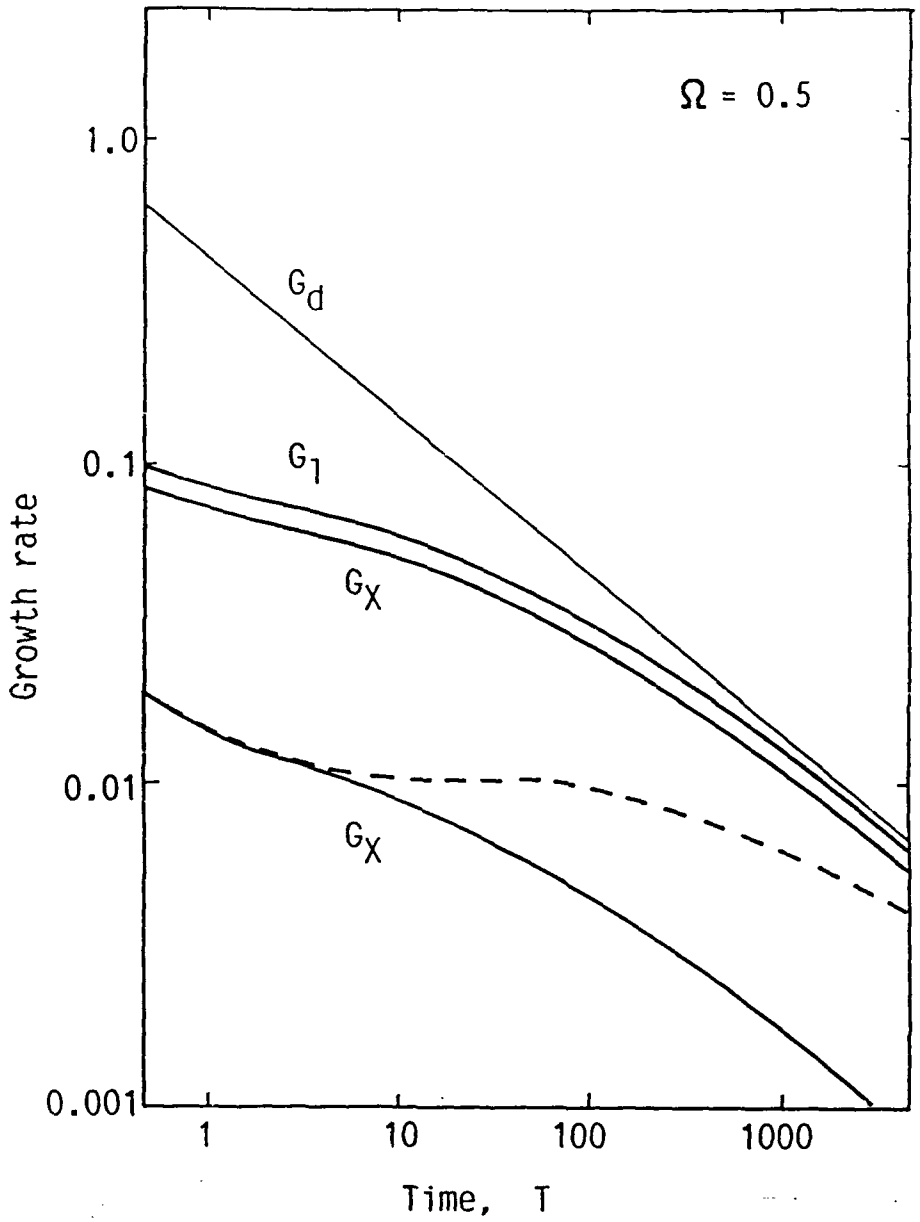

Figure 24

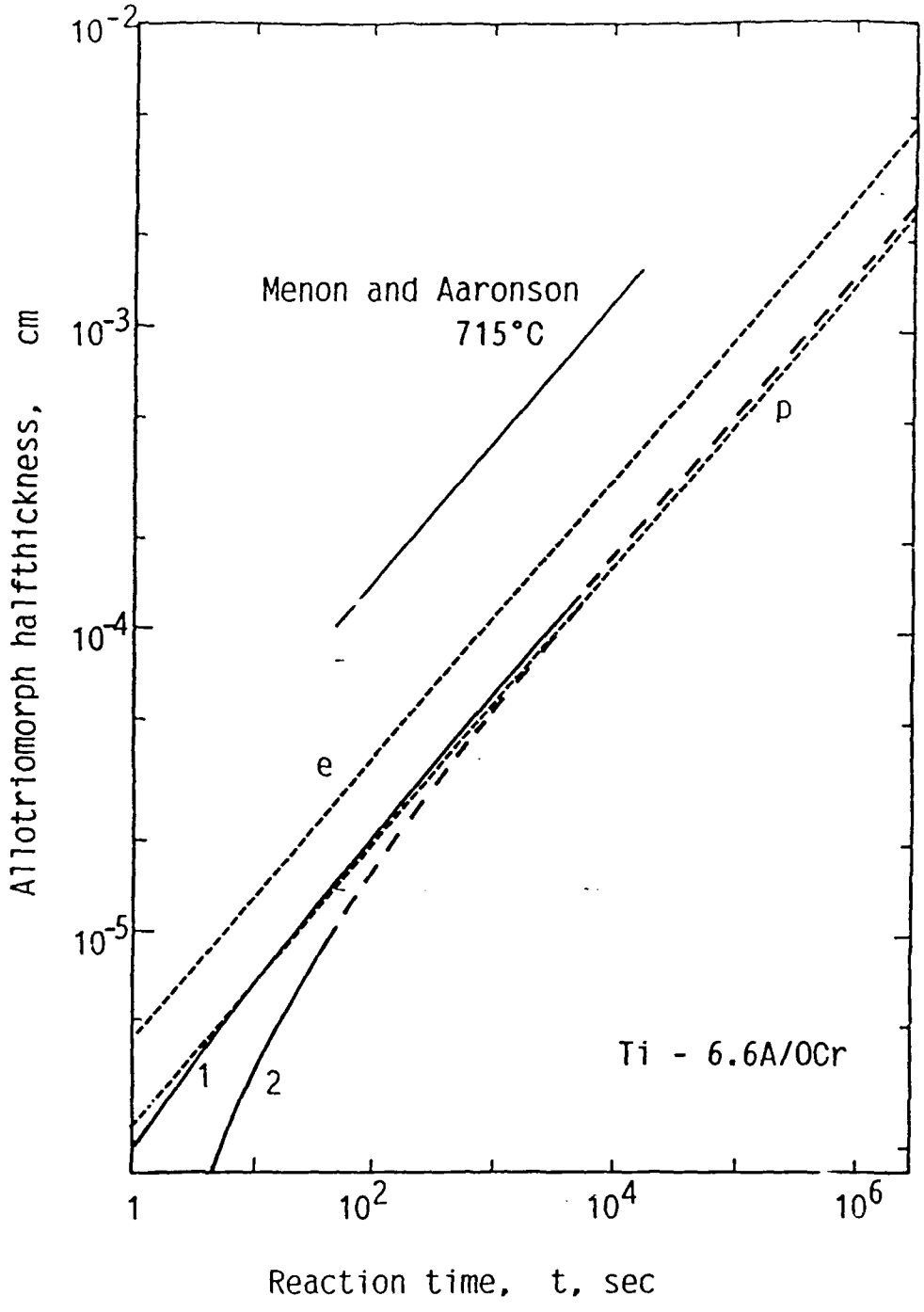
Allotriomorph halfthickness, cm
10^{-2}
10^{-3}
10^{-4}
10^{-5}
Menon and Aaronson
715°C
e
p
1
2
Ti - 6.6A/OCr
1
10^2
10^4
10^6
Reaction time, t, sec

Figure 25

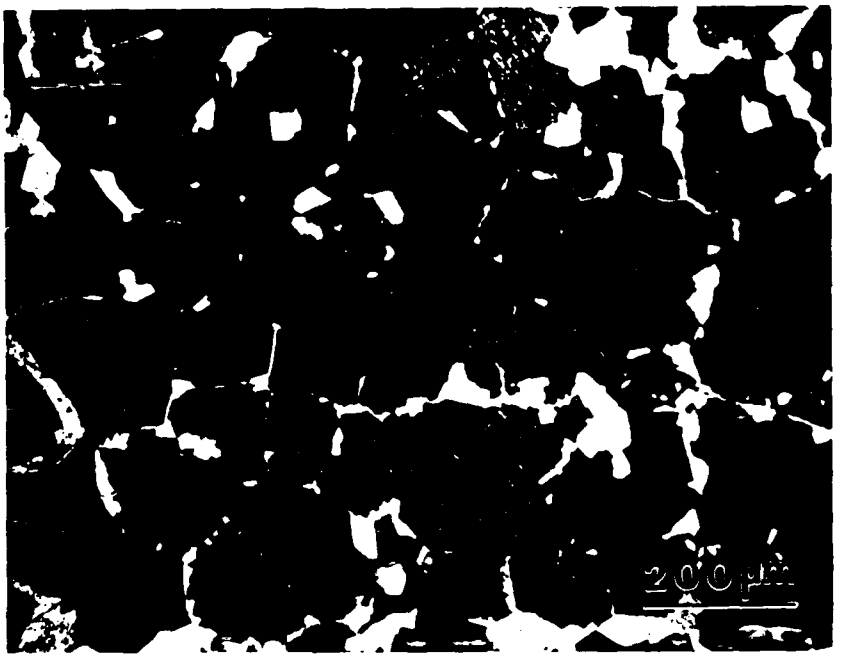

Figure 26

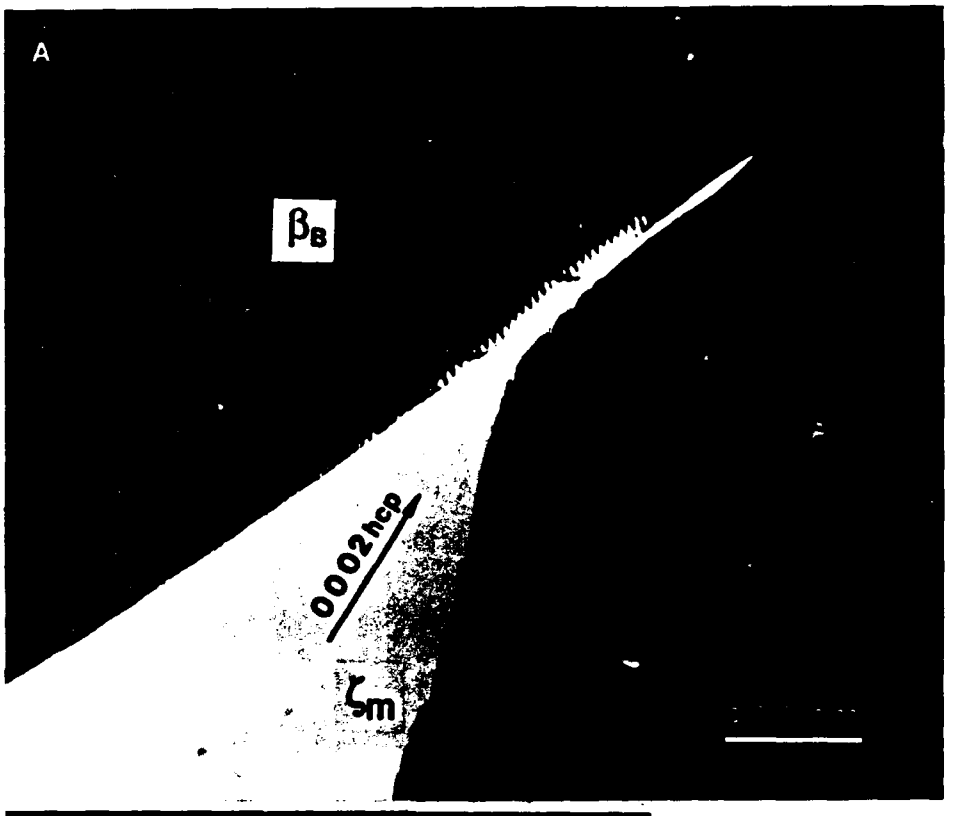

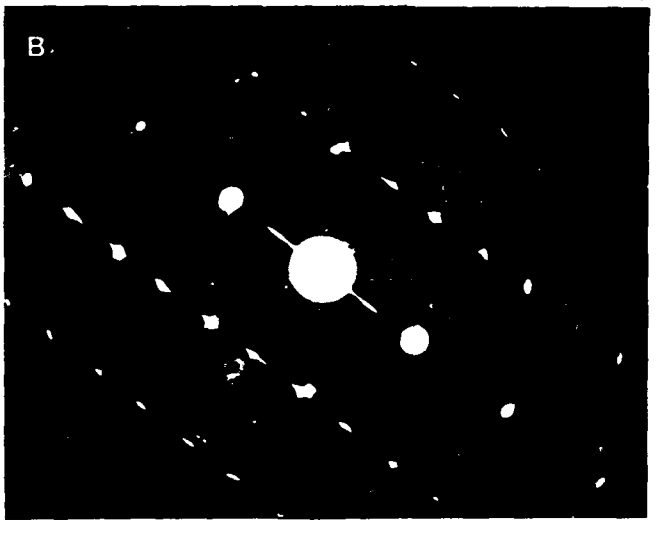

Burgers OR

ζ_m β

$(1\bar{2}10)//(11\bar{1})$

$(0001)//(\bar{1}10)$

$(\bar{1}010)//(\bar{1}\bar{1}2)$

Figure 27

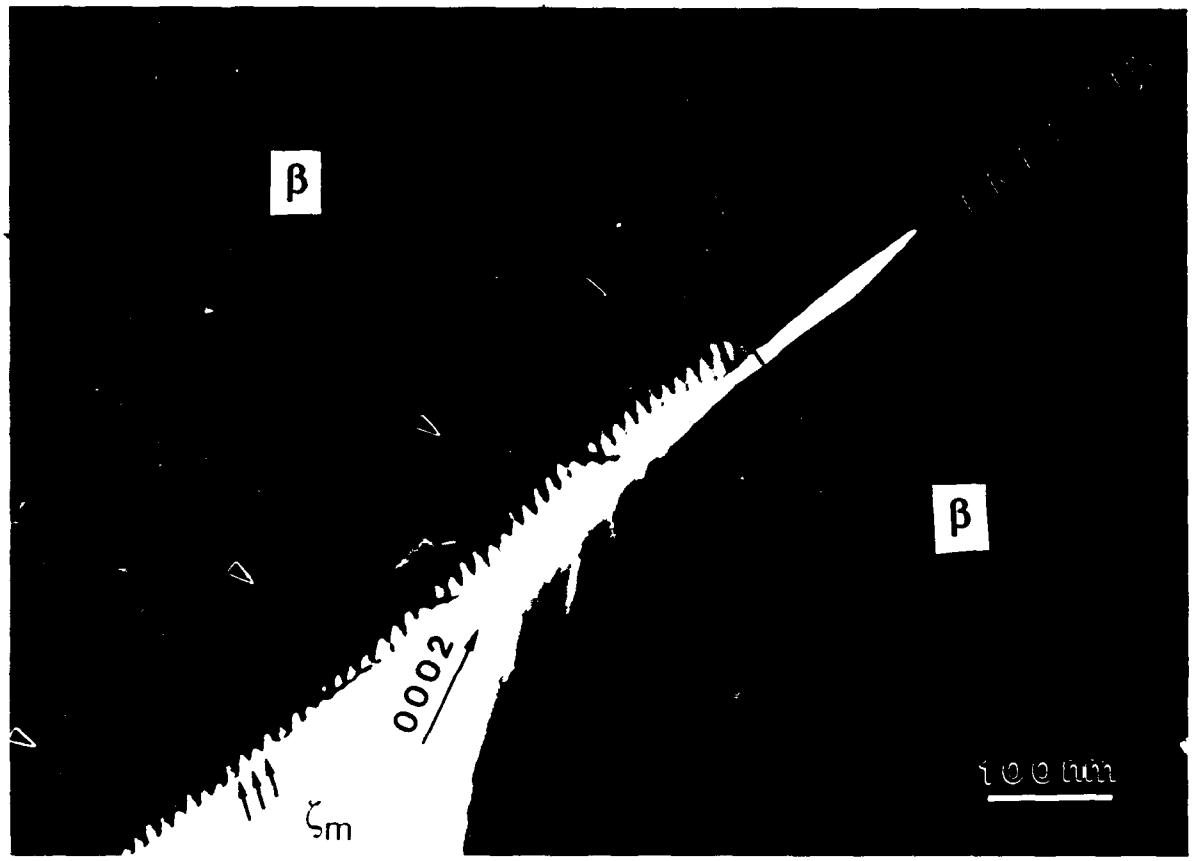

Figure 28

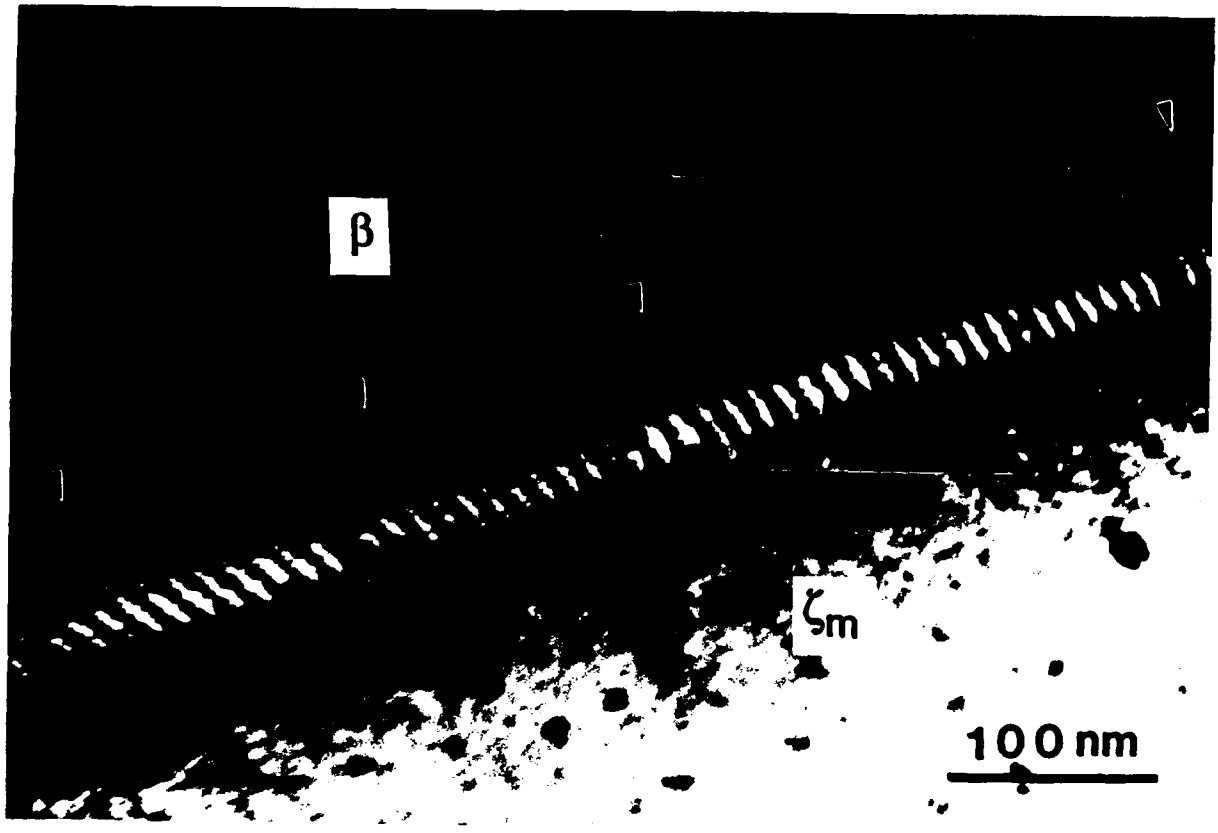

Figure 29

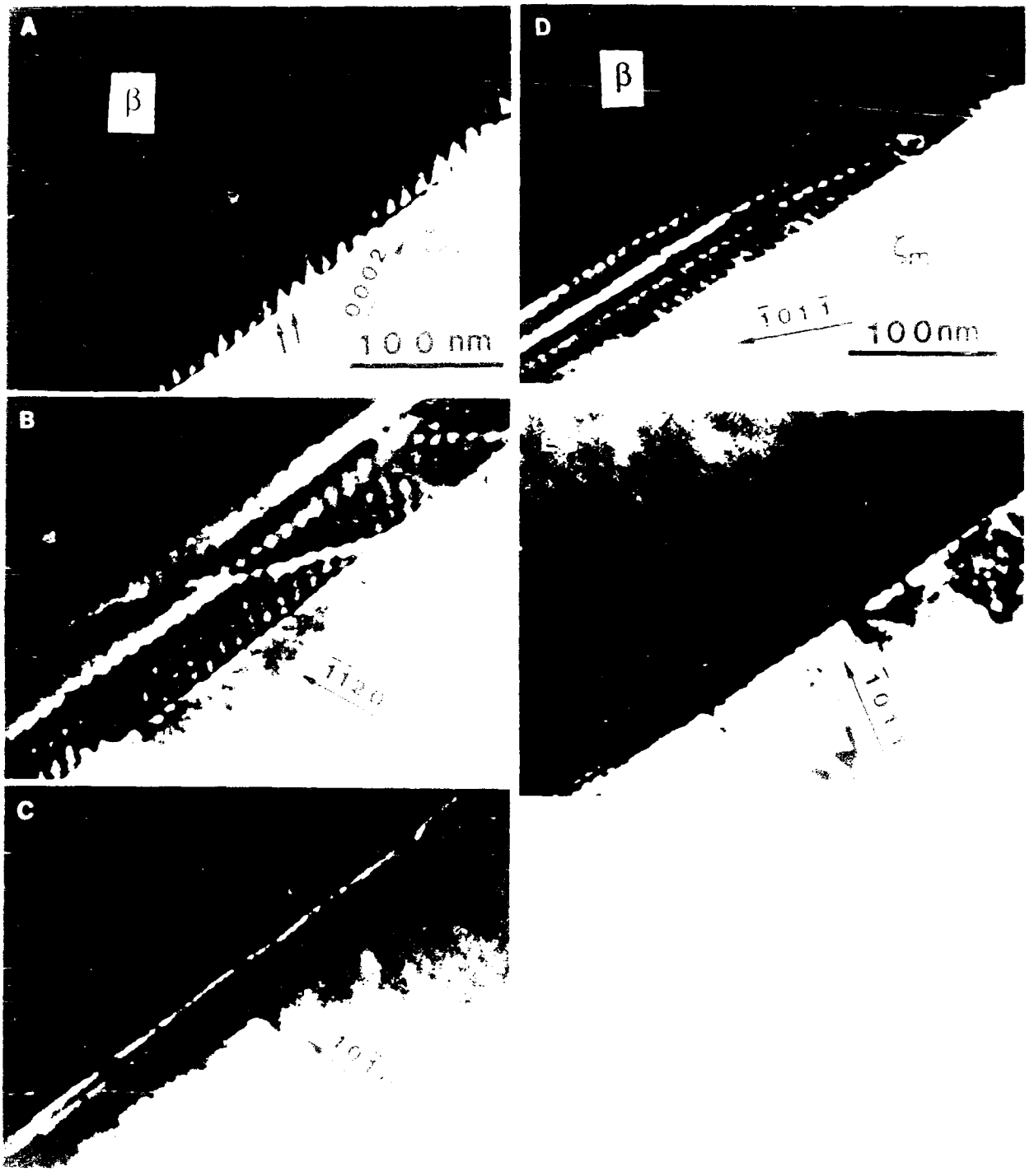
A
β
100 nm
D
β
100nm
B
C

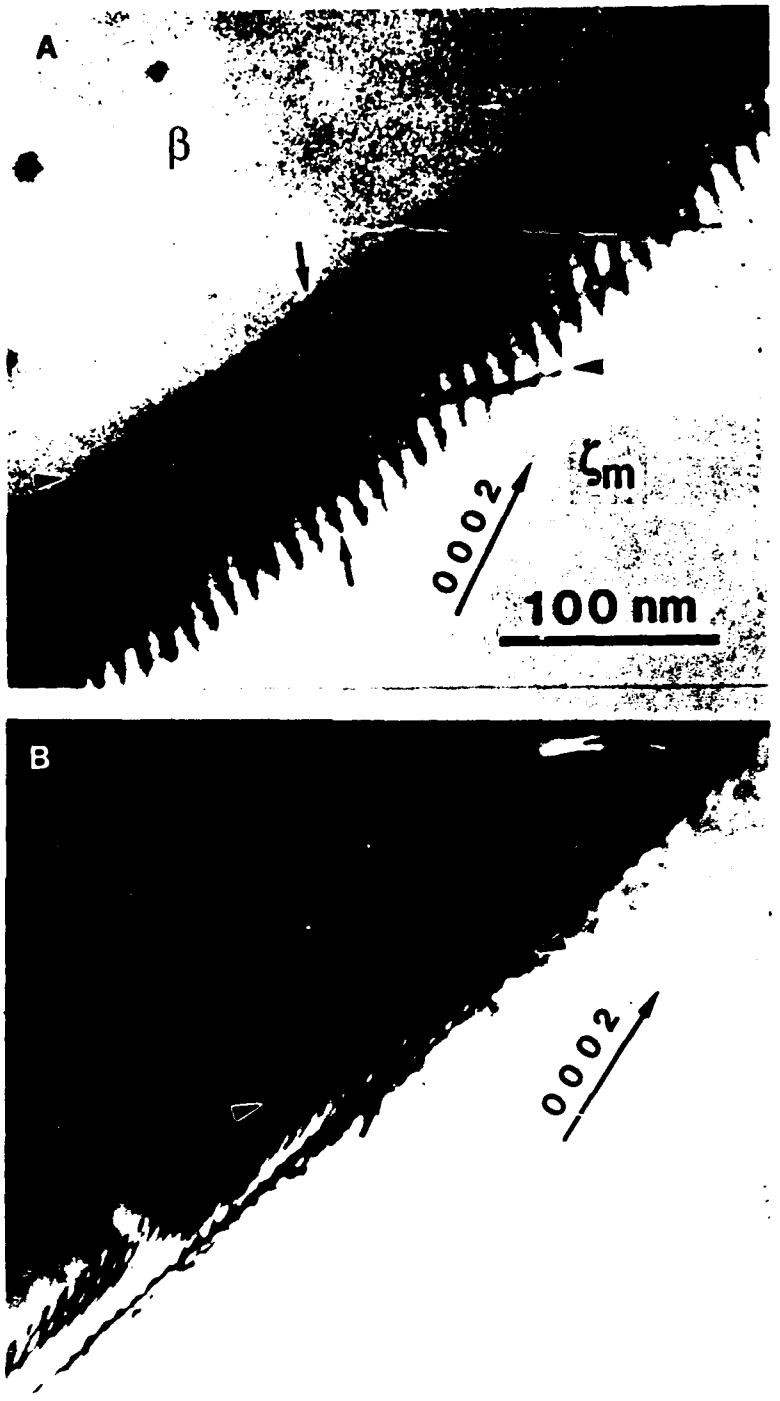

Figure 31

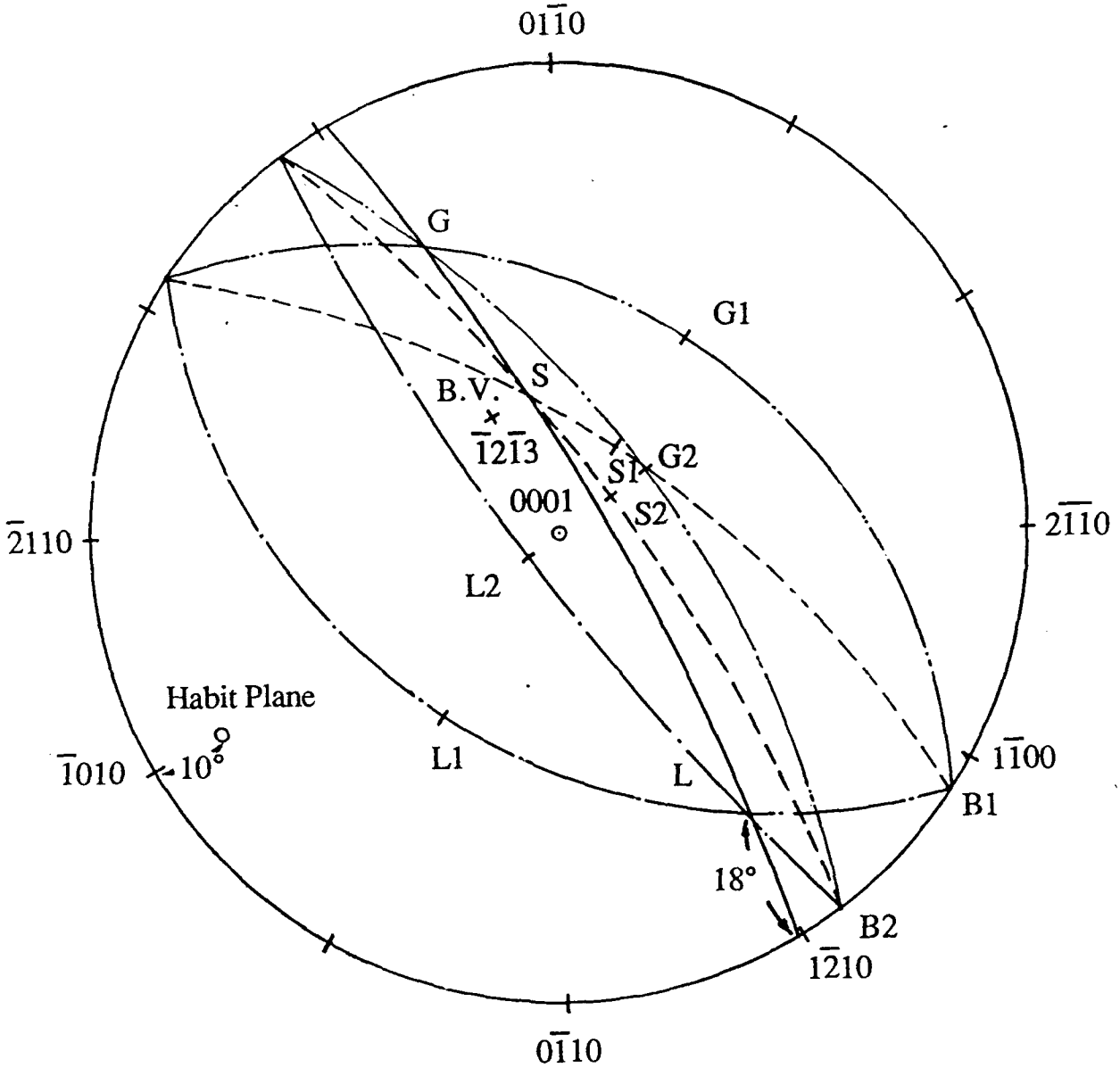
$01\bar{1}0$
G
G1
S
B.V.
$\bar{1}2\bar{1}3$
S1
G2
0001
S2
$\bar{2}110$
$2\bar{1}10$
L2
Habit Plane
$\bar{1}010$
10°
L1
L
$1\bar{1}00$
B1
18°
B2
$1\bar{2}10$
$0\bar{1}10$

Figure 32

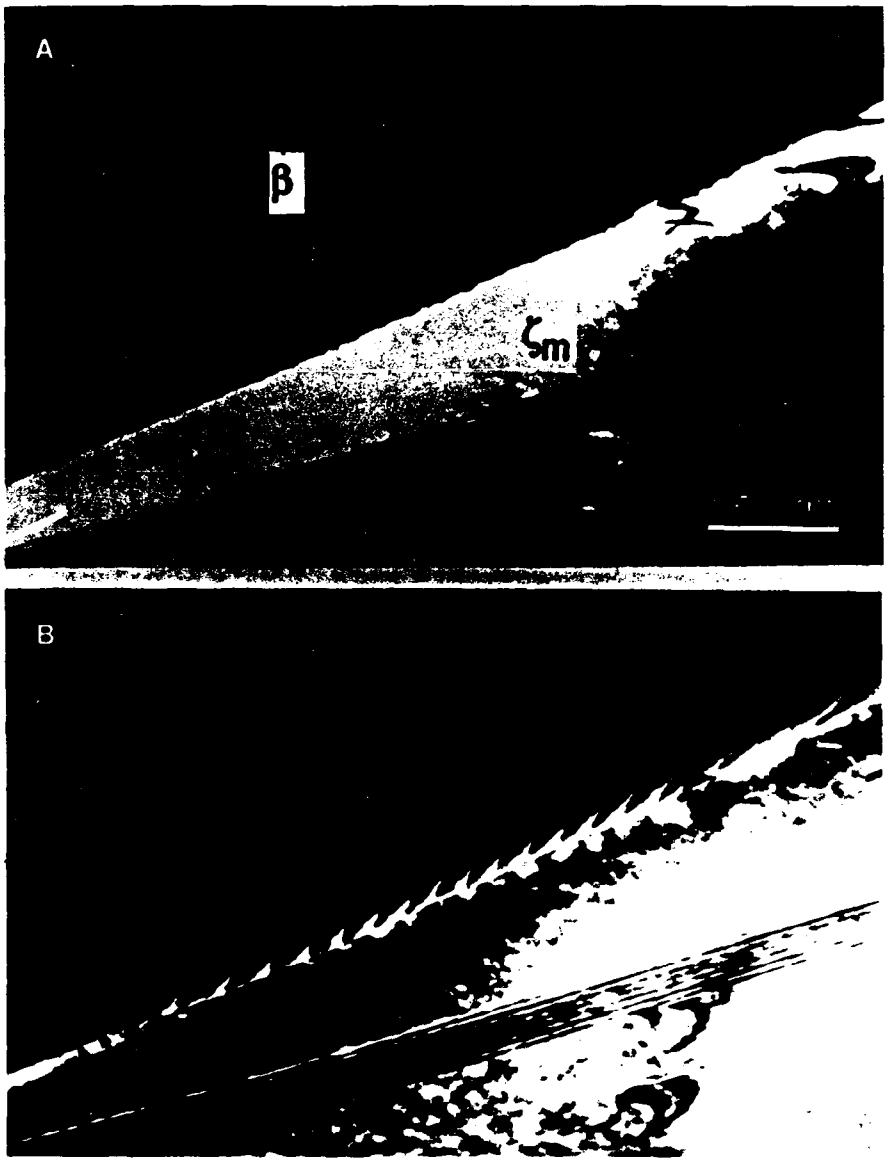

Figure 33

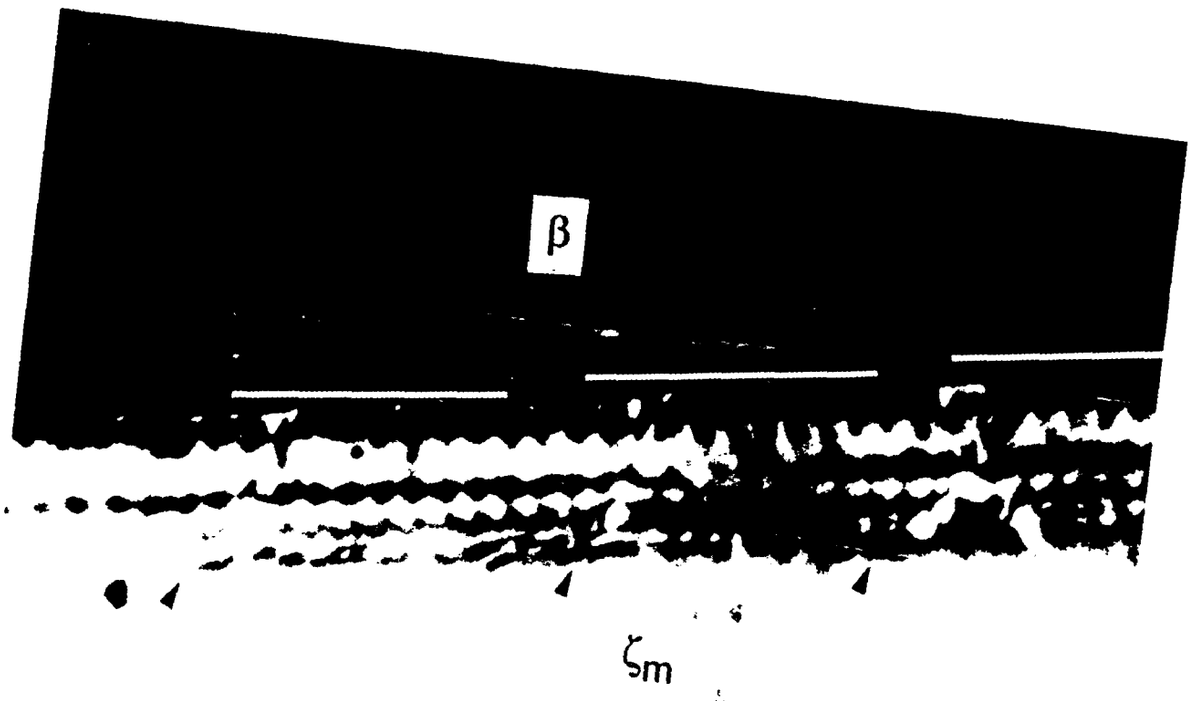

Figure 34

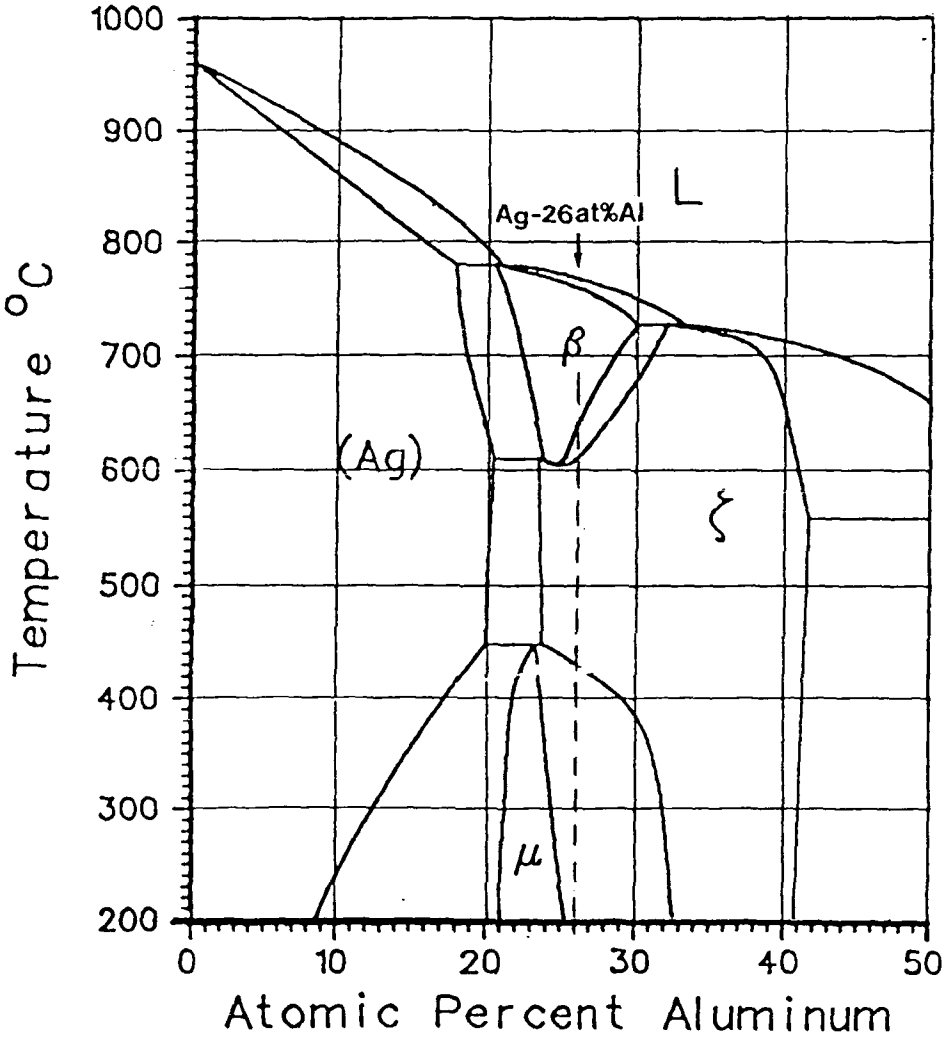
1000
900
800
700
600
500
400
300
200
Temperature °C
0
10
20
30
40
50
Atomic Percent Aluminum
Ag-26at%Al
L
β
(Ag)
ζ
μ

Figure 35

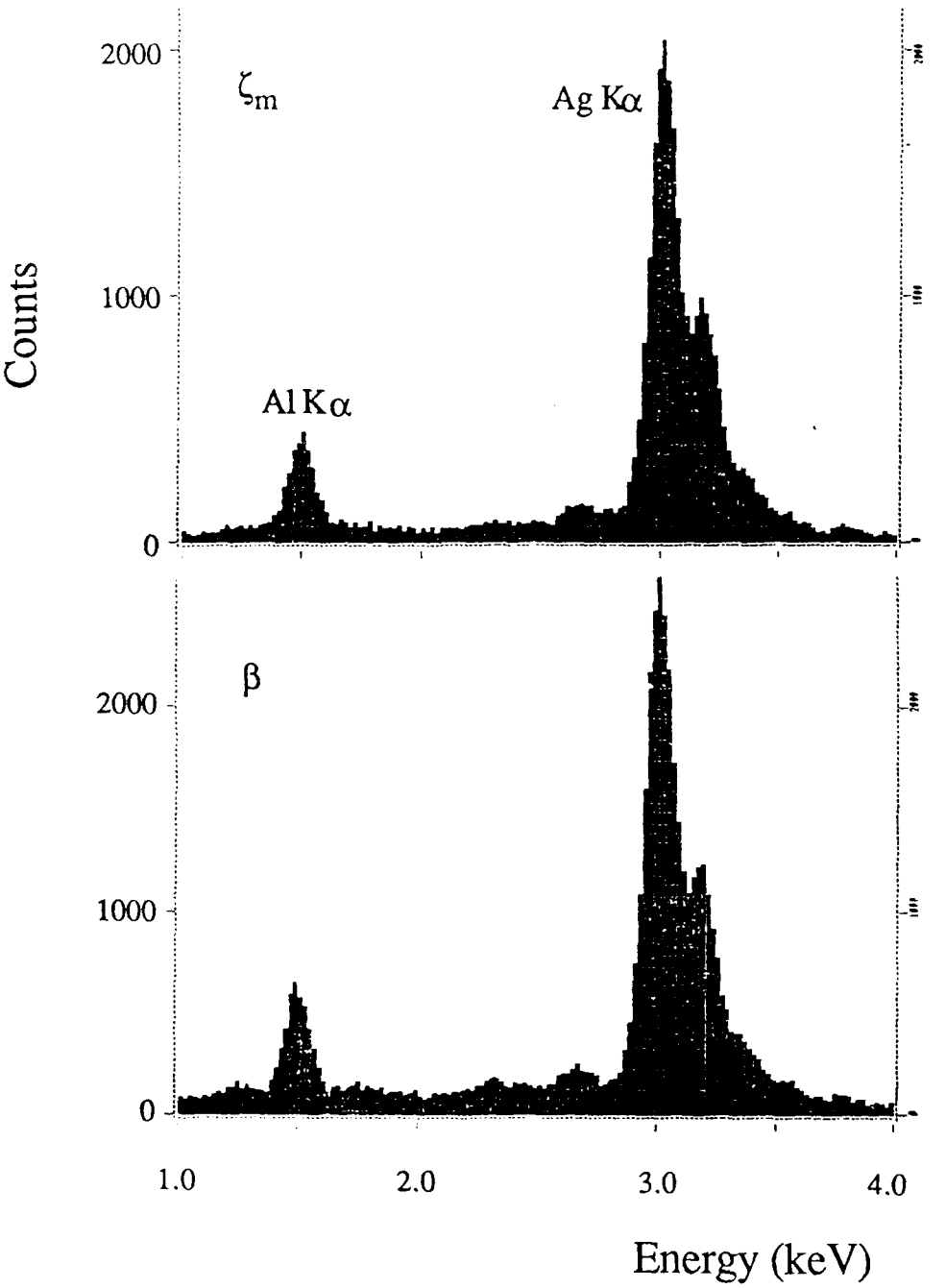
2000
1000
0
ζ_m
Ag Kα
Al Kα
Counts
2000
1000
0
β
1.0
2.0
3.0
4.0
Energy (keV)

Figure 36

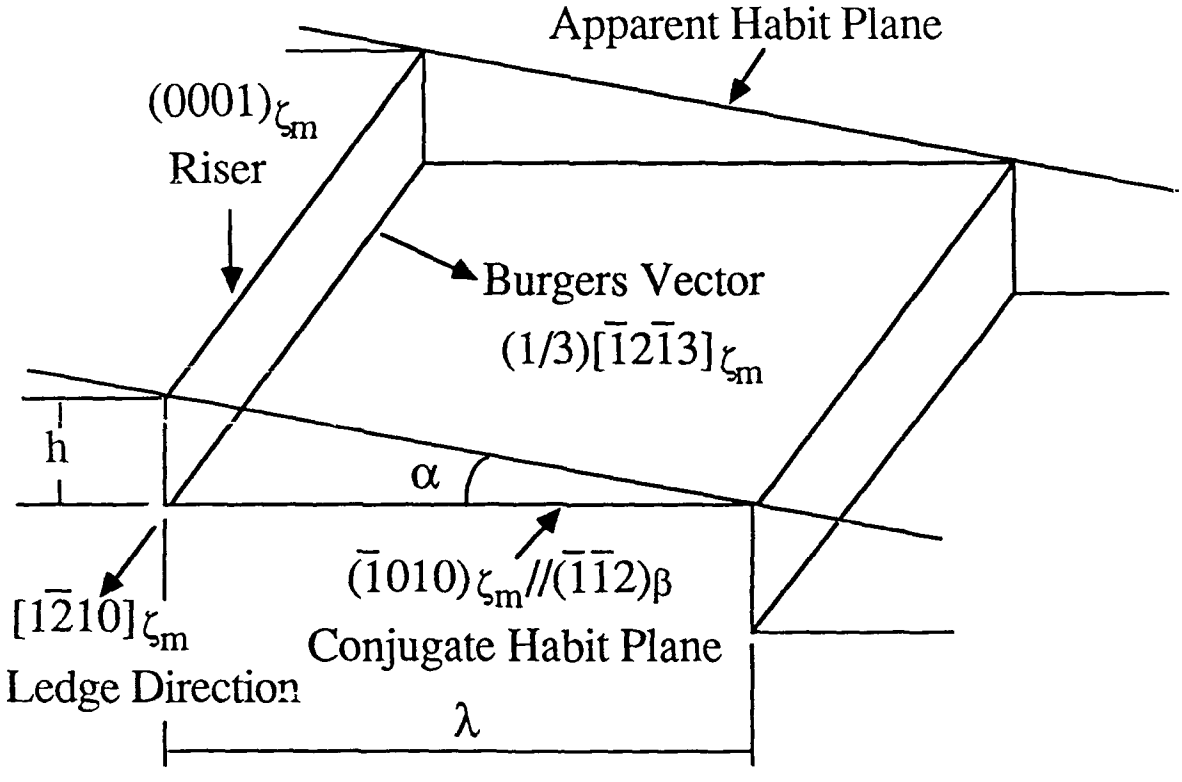
Apparent Habit Plane
$(0001)\zeta_m$
Riser
Burgers Vector
$(1/3)[\bar{1}2\bar{1}3]\zeta_m$
h
α
$(\bar{1}010)\zeta_m//(\bar{1}\bar{1}2)\beta$
$[1\bar{2}10]\zeta_m$
Conjugate Habit Plane
Ledge Direction
λ

Figure 37